Elongated T cell expansion by utilizing IL7 and IL15 leads to increased T cell yield while preserving Tcm/Tscm characteristics feasible for adoptive T cell therapy

Inaugural-Dissertation
to obtain the academic degree
Doctor rerum naturalium (Dr. rer. nat.)

Submitted to the Department of Biology, Chemistry, Pharmacy
of Freie Universität Berlin

by

Andreas Heimann

2020

Die Arbeit wurde im Zeitraum November 2015 bis Januar 2020 in der Abteilung Angewandte Transplantation Immunologie (Arbeitsgruppenleiterin Frau Prof. Dr. Il-Kang Na) am Experimental and Clinical Research Center (ECRC) in Berlin Buch angefertigt.

1. Gutachterin: Frau Prof. Dr. Il-Kang Na

2. Gutachter: Herr Prof. Dr. Oliver Daumke

Disputation in Berlin am 5.6.2020

Hiermit versichere ich, dass meine Dissertation selbstständig verfasst und keine anderen als die angegebenen Hilfsmittel genutzt habe. Alle inhaltlich übernommenen Stellen habe ich als solche gekennzeichnet.

Teile dieser Arbeit wurden aus dem sich in Submission befindenden Manuskript mit dem Titel

Extended expansion with IL-7/IL-15 increases T cell yield with preserved Tcm/Tscm properties for adoptive T cell therapy

übernommen.

Berlin, der 13.2.2020 — Andreas Heimann

Ort, Datum — Unterschrift

Danksagung

Während meiner etwa fünf Jahre andauernden Promotionsphase, deren Ergebnis die vorliegende Arbeit ist, habe ich zahlreiche, persönliche Reifungs- und Wandlungsphasen durchlebt, die mich nachhaltig geprägt haben. Meine Arbeit, im Besonderen aber auch mein persönliches soziales Umfeld, hatten großen Einfluss auf die vielfältigen positiven Entwicklungen der vergangenen Jahre.

Mein Dank soll zunächst Frau Professor Il-Kang Na gelten, die es mir ermöglicht hat, in ihrer Arbeitsgruppe meine Forschungsprojekte zu verfolgen und diese auch international präsentieren zu dürfen und so maßgeblich zur erfolgreichen Vervollständigung dieser Dissertation beigetragen hat.

Herrn Professor Oliver Daumke möchte ich dafür danken, dass er mir bei Fragen zu meinem Projekt und der Thesis stets bereitwillig geholfen und sich bereit erklärt hat, meine Arbeit als Zweitgutachter zu bewerten.

Darüber hinaus möchte ich mich bei Frau PD Dr. Uta E. Höpken für ihre effizienten und punktuellen Ratschläge zu meinen Fragen und ihrer Mitwirkung in meinem MDC-Komitee bedanken.

Ebenfalls möchte ich noch weiteren talentierten Wissenschaftlerinnen und Wissenschaftlern danken, mit denen ich zusammenarbeiten durfte. Zu nennen sind dabei insbesondere Frau Corinna Friedrich und Herr Dr. Philipp Mertins aus der Proteomics Facility des MDCs, Herr Dr. Benedikt Obermayer und Herr Dr. Dieter Beule aus der Core Unit Bioinformatics (CUBI) des BIH, Herr Dr. Hans-Peter Rahn und Frau Kirsten Rautenberg aus der FACS Facility des MDC und mein BIH-Koordinator Herr Dr. Iwan Meij.

Die Arbeit vor Ort haben mir meine lieben und herzlichen Kollegen und Ex-Kollegen versüßt. Besonderer Dank gilt deshalb Frau Josefine Ruß, Frau Stefanie Althoff, Frau Monique Butze, Herrn Daniele D‘Abundo und Herrn Martin Szyska, für die viele, in Gemeinschaft verbrachte Zeit – und die *kurzen* Kaffeepausen.

Besonders bedanken möchte ich mich darüber hinaus auch bei Frau Dr. Stefanie Herda, welche mir als Mentorin viel Expertise und Menschlichkeit vermittelt hat und dafür, dass sie das Lektorat für meine Dissertation übernommen hat.

Die Zeit und die Arbeit abseits des Labors haben mir meine privaten Freunde bereichert. Diese hatten stets ein offenes Ohr für mich und der Austausch mit ihnen stellte einen großen Gewinn für mich dar. In diesem Zusammenhang möchte ich mich vor allem bei Hans Gartmann, Malte Hilsch, Christiane Hartfeldt, Adel Antar, Stanislav Kulik, Danilo De Giorgi, Vassil Richter, Christoph Clouser, Willi Jahncke und Lisa-Michelle Dietz bedanken.

Vor und während der Zeit meiner Promotion habe ich ebenfalls viel Freizeit in den gemeinnützigen Verein der biotechnologischen Studenteninitiative e.V. investiert. Das Ehrenamt hat mir viel Aufschluss über meine Zukunft gegeben und es war mir eine besondere Freude so tolle Freunde und ein einzigartiges Netzwerk aufzubauen. Besonderer Dank hierbei gebührt meinen Freunden und Mitstreitern in den zwei Bundesvorstandsteams, von denen ich Teil sein durfte.

Danken möchte ich außerdem meinem Freund Darius Krutzek, der sich die Mühe gemacht hat meine (für ihn fachfremde) Arbeit zu lektorieren.

Ein großes Dankeschön geht darüber hinaus an Herrn Martin Rodden, welcher als *native English speaker* einen wichtigen Teil der sprachlichen Prüfung dieser Arbeit übernommen hat.

Im Rahmen der Schreibphase gilt ein besonderer Dank meinen Schwiegereltern, die mir die Möglichkeit geboten haben mich in Gänze auf meine Dissertation zu konzentrieren.

All dies wäre ohne den liebevollen, uneingeschränkten und vielfältigen Support meiner Familie nicht realisierbar gewesen. Meine Eltern haben mich stets bedingungslos unterstützt, meine Brüder Simon und Noah waren immer für mich erreichbar. Meine Ehefrau Michelle hat mir unentwegt den Rücken freigehalten und Mina – unsere gemeinsame Tochter – vermochte es, mir auch in schwierigen Phasen ein Lächeln ins Gesicht zu zaubern.

Grazie mille – vi amo!

1. INDEX

2. Introduction

2.1. Immune system

The immune system is a host defence system present in higher organisms, comprising many biological structures and processes within a host, which protects against potential disease. Potential adversaries include pathogenic microorganisms such as parasites, fungi, bacteria and viruses, which can damage or even kill the organism. In addition, the organism is surrounded by environmental influences, which can lead to pathogenic cell changes in the body. Usually these cell changes would lead to necrosis or apoptosis, but in rare cases they can degenerate and lead to cancer. The evolutionary outcome of these challenges led to development of the immune system [1].

In general, a distinction is made between two basic mechanisms of immune defence. The first mechanism is unspecific to the pathogen and only distinguishes between the body's own invaders and foreign threats. In this case, we speak of the *innate immune system*, which consists of anatomical and physiological protective mechanisms such as the skin, saliva with antimicrobial enzymes, different pH values and body temperature adaptation mechanisms. Furthermore, there are cell-based defence mechanisms in the form of monocytes, macrophages, granulocytes, natural killer cells, and dendritic cells. These use non-specific mechanisms against exogenous pathogens, recruit cells of the adaptive immune system by means of chemokine and cytokine secretion and present pathogen recognition features to the adaptive immune cells, leading to the formation of specific defence mechanisms. This immune response usually occurs after a few minutes and is the first hurdle for pathogenic invaders. The second mechanism is pathogen-specific, requires considerably more time and is able to form an immunological memory in order to react quickly and effectively to a renewed pathogen attack [2].

Furthermore, the adaptive immune system can be divided into B lymphocytes, which are responsible for humoral immunity, and T lymphocytes, which ensure the cell-mediated immune response. They differentiate from the common lymphoid progenitor cells and originate from the bone marrow. B cells evolve into mature B cells within the bone marrow, while simultaneously T cells migrate to the thymus, where they differentiate into mature T cells. Here they are selected across the tissue structure of the thymus, first positively and then negatively with regard to their reactivity and finally

develop into helper (CD4 positive) or cytotoxic (CD8 positive) T lymphocytes. After maturation to CD4 positive and CD8 positive T lymphocytes (CD4 and CD8 T cells), each T cell has an individual T cell receptor (TCR) capable of recognizing foreign peptides presented via a major histocompatibility complex (MHC). Class II MHC (MHCII) is expressed by antigen-presenting cells (APCs) such as dendritic cells, macrophages and B cells and presents endogenous or pathogen-related peptide snippets. CD4 T cells are subsequently enabled to interact with the MHCII on APCs via their CD4 receptor and the TCR and secrete cytokines that can induce or inhibit an immune response - depending on the origin of the presented peptide. A distinction is made between immunosupportive T helper cells and immunosuppressive regulatory T cells. However, CD8 T cells are generally cytotoxic T lymphocytes and recognize peptides presented by class I MHC (MHCI). MHCI is expressed on most cell surfaces of the body and displays peptide components of the cell. Since virally infected cells express viral peptides, these are also presented. The same applies to tumor cells that express neoantigens due to somatic mutations. Thus, MHCI proves to be an important recognition mechanism for viral infections and degenerated cells. Cytotoxic T lymphocytes with the appropriate TCR subsequently recognize the foreign peptides and eliminate the target cell by lysis via perforins and granzymes or induce apoptosis with Fas Ligand (FasL) [3, 4].

2.2. Immunotherapy

Immunotherapy, which makes use of the body's own immune system, is one of the most potent therapies in the field of cancer treatment, so much so that it was designated as a scientific breakthrough by Science magazine in 2013 [5]. Hundreds of clinical trials from all over the world have demonstrated the relevance of immunotherapy towards the promotion of clinical progress [6]. Its importance immunotherapy was acknowledged by the awarding Nobel prize for physiology or medicine in 2018 for the discovery of *cytotoxic T lymphocyte-associated protein* (CTLA-4) and *programmed cell death protein 1 / programmed cell death protein ligand 1* (PD-1/PDL-1) [7]. In general, cancer immunotherapies are categorized as immune checkpoint inhibitors (ICIs), adoptive T cell therapies (ATT) and tumor vaccines [8, 9]. ICI therapy has shown convincing clinical effects in melanoma and non-small cell lung cancer patients, but a large number still develop disease progression with these therapies [10, 11]. For decades, tumor vaccines were tested by immunizing recipients

with tumor peptides or tumor antigen presenting APCs, without a significant positive impact. Next-generation sequencing has revived the idea of tumor vaccination and the personalized analysis of tumor mutations provides the possibility of targeted antigen vaccination [12]. However, tumor vaccines often lack strong antigenic reactions, as they are tumor-associated antigens (TAA) and specific T cells are therefore eliminated in the host during maturation [13]. This might be an option for providing an additional treatment choice using ATT, as pioneered by Rosenberg and his colleagues at the National Institute of Health (Maryland, USA). Rosenberg established the idea of isolating murine tumor-infiltrating lymphocytes (TILs) from biopsies, expanding them and treating tumor-bearing mice with these tumor-derived lymphocytes [14]. One year later, the extensive trial led to the first described effective treatment option for patients with refractory metastatic melanoma [15]. This happened over 30 years ago – today, there are three different T cell sources for ATT-treatment: TILs, as mentioned above, T cell receptor- (TCR) engineered T cells with a TAA specific TCR and chimeric antigen receptor- (CAR) T cells, which express an artificial receptor composed of a single-chain variable fragment (svFv) and different co-stimulatory protein (Figure 1).

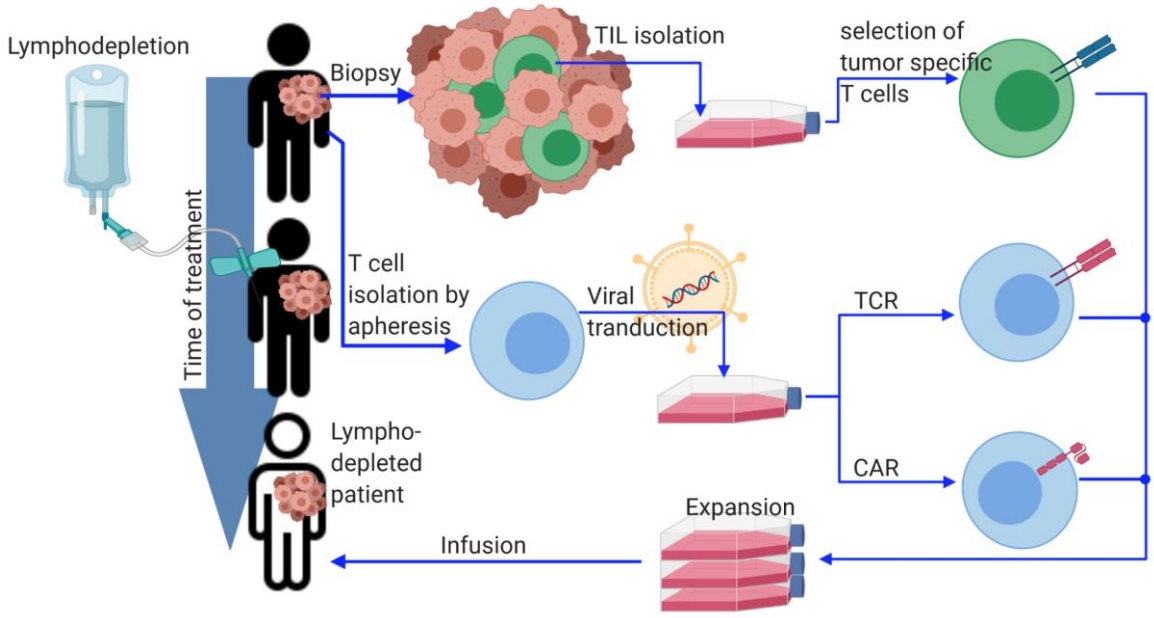

Figure 1. Schema of different strategies for adoptive T cell therapy TIL = Tumor infiltrating lymphocytes; TCR = T cell receptor; CAR = Chimeric antigen receptor. TILs were isolated from tumor biopsy, enriched by clonal proliferation and tested by in vitro assays for their tumor reactivity (top arrow). TCRs and CARs are developed using T cells isolated by apheresis. These cells are then transferred by viral transduction with a desired TCR or CAR and subsequently expanded (middle arrow). Both TILS and TCRs or CARs are administered to a lymphocyte depleted patient after successful expansion.

2.2.1. Adoptive T cell therapy

As mentioned before, Rosenberg proved to be a pioneer in the field of ATT. For his first approach, Rosenberg harvested murine TILs from MCA-105 sarcomas and applied the first documented beneficial ATT of TILs, curing murine colon adenocarcinoma [16]. Two years later, Rosenberg and his research group treated patients suffering from metastatic melanoma with TIL ATT, combined with Interleukin 2 (IL2) administration, and subsequently observed an objective regression in 9 of 15 patients [15]. One year later, Gideon Gross developed the first CAR, starting a ground breaking success story in the treatment of haematological malignancies [17]. However, for the next decade, this clinical approach remained exclusively for TIL. Dudley et al. improved the ATT of TILs by administration of lymphodepletion before TIL infusion, which offers more space for clonal expansion of tumor specific T cells [18]. In parallel, the team of Michel Sadelain developed the first effective CAR T cell (second generation) targeting prostate-specific membrane antigen (PSMA) [19]. In a follow-up study, Renier Brentjens, a member of this team, demonstrated the successful elimination of leukaemia in mice by human CD19-CAR T cells [20]. The first clinical trial with a MART-1 melanoma antigen specific TCR was performed in 2006, revealing a regression of metastatic melanoma in two patients and a durable engraftment of adoptively transferred T cell in all treated patients [21]. It took four more years of development until the first clinical trial to treat advanced B cell lymphoma with CD19 CAR T cells [22], followed by clinical studies against follicular lymphoma, large-cell lymphomas, chronic lymphocyte leukaemia and acute lymphocyte leukaemia (ALL) [23-26]. In parallel, a new TCR therapy with the freshly discovered new tumor antigen – *New York esophageal squamous cell carcinoma-1* (NY-ESO-1) was tested for the treatment of synovial sarcoma, resulting in an objective response rate of 67% [27]. A new benchmark of scientific pacing was established in 2012 by the research alliance established between University of Pennsylvania, represented by the Coley Award recipient Carl June, and the private sector investigating the CD19 CAR Prototype *CTL019* [28]. As of today, one of the most significant milestones has been the approval of the CTL019 CAR by the U.S. Food and Drug Administration (FDA) for treating children and young adults suffering from refractory ALL, which is now produced commercially by Novartis as Tisagenlecleucel [29]. So far, there has been an abundant number of clinical trials for TILs against cancer types other than melanoma [30],

different tumor antigen specific TCRs [31-33] as well as for several CAR-T cell targets [34], moving ATT to the next promising cancer treatment (Summarized in Figure 2).

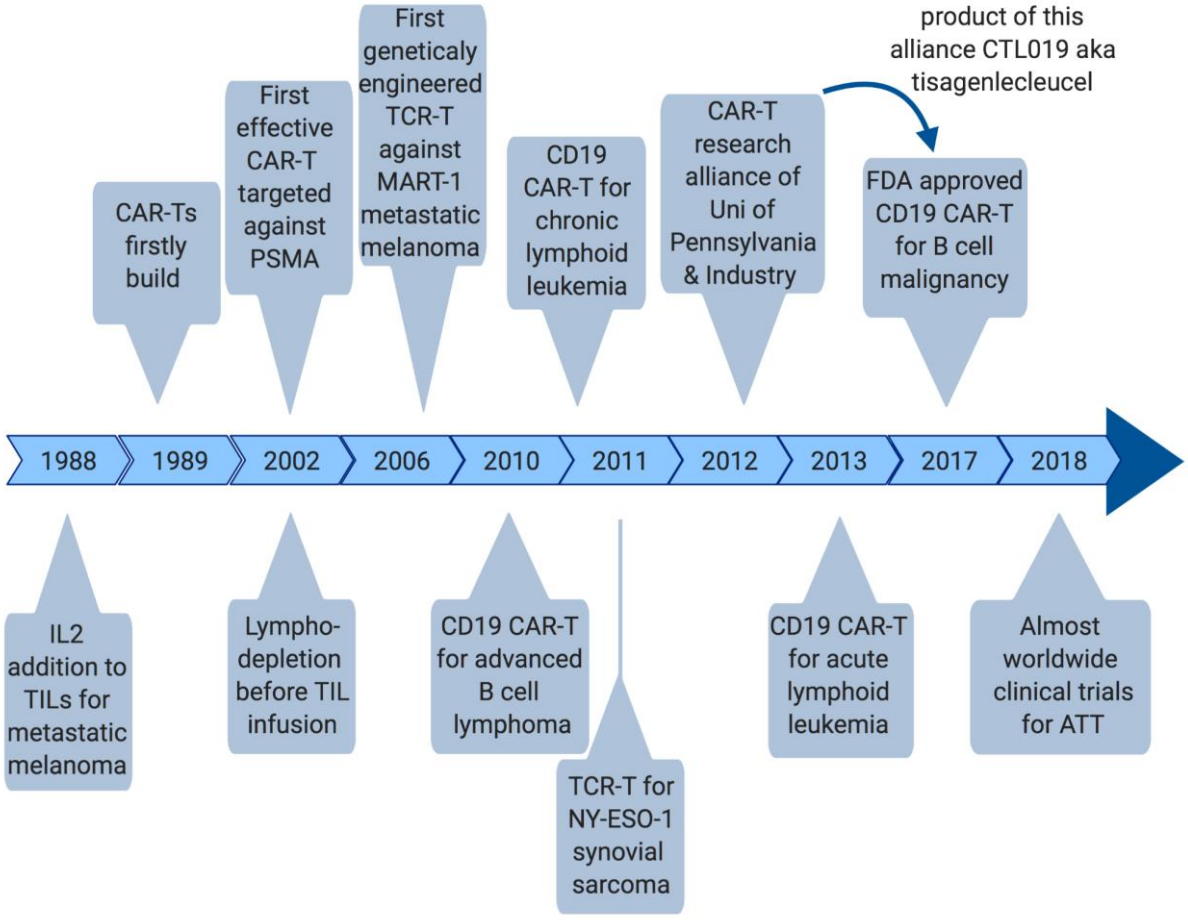

Figure 2. A brief history of ATT. The scheme outlines key events in the development of ATT in the treatment of cancer from 1988 to 2018. TIL = Tumor infiltrating lymphocytes; TCR = T cell receptor; CAR = Chimeric antigen receptor. Adapted and added figure with information and idea from Jiang et al. 2019.

Each of these findings focused on CD8 T cells, but the impact of CD4 T cells in the ATT for tumor patients did not go unnoticed. For example, it was shown that ATT with CD4 T cells was able to eradicate large established melanoma or B16 tumors in mice [35, 36]. In light of this animal experimental research, clinical studies for anti-tumor therapy with adoptively transferred CD4 T cells were carried out with promising results [37-39]. Despite these promising findings, ATT remains challenging in both T cell expansion, toxicity issues and successful response rates.

2.2.2. Toxicity and other pitfalls

Like any other form of treatment, ATT has its own limits and side effects. Beside the beneficial impact of ATT with TILs, TCRs or CARs and their increasing potency, limitations become evident. According to current data, TILs are listed as a safe

treatment method (as other forms of autologous cellular therapy without gene-editing) and arising toxicity is predominantly caused by lymphodepleting preparative regimens, which result in febrile neutropenia and pancytopenia [40-42]. However, these side effects are associated with TCR and CAR T cell therapy as well [27, 43]. Further side effects due to IL2 infusion can be controlled by means of supporting measures [44]. Despite the manageable side effects, TIL therapy occasionally fails due to methodological hurdles. Because of a lacking availability of bioptic specimens, limited TIL exhibition or failure to reach sufficient expansion of tumor specific T cells, clinical cell expansion is not trivial and remains a general hurdle of ATT [45-47]. Still, ATT is a feasible and effective way to treat melanoma with durable and complete cancer regression, though further treated tumor entities (as ovarian, breast, colon, cervical, sarcoma and renal tumor) showed only moderate clinical responses with TIL-based ATT [48-52]. One well observed general side effect of ATT is cytokine release syndrome (CRS), which is a non-antigen related toxicity occurring when widespread inflammation is induced by T cells recognizing their antigens [53]. Although this could also occur in TIL-based ATT, it has not yet been reported in clinical trials including TILs. However, CRS has been reported as a common side effect for TCR and CAR T cell treatment [54, 55].

Specific pitfalls for genetically engineered TCR T cells include reported cross-reactivity. TCRs recognizing the target antigen, could potentially also bind similar peptide structures expressed on host tissue, as described for MART-1 or MAGE-A3 [56, 57]. To address this problem an increasing focus has been placed on neoantigens during the last five years. Neoantigens are tumor-specific antigens resulting from somatic mutations; due to improved access to next-generation sequencing it is becoming increasingly feasible to find personalized neoantigens exclusively in tumor tissue and to generate corresponding TCR T cells [4]. Furthermore, TCR T cells are MHC I restricted, hence only able to recognize peptide structures exhibited on MHC I complexes. As a consequence, tumor cells that down-regulate the MHC complex can no longer be recognized and eliminated by the TCR T cells, which is a well-known escape mechanism [58]. For overcoming this escape mechanism, CAR T cells, which recognize surface peptides, independent of the MHC complex, constitute a good alternative. However, clinical trials with CD19 CARs showed an outgrowth of CD19-negative tumor cells [59-61]. Unfortunately, the targeting of surface molecules leads to a higher risk of “on-target, off-tumor“ toxicity [62]. Nevertheless, this is not a pitfall

exclusive to CAR T cell therapy as it also occurs in TCR T cells [63, 64]. In addition neurotoxicity - as yet unexplained - with occasionally lethal outcomes has been observed with CD19-specific CAR T cells [60]. Still, CAR T cell therapy remains a potent treatment option for haematological malignancies (rightly received FDA approval for a CD19-CAR). However, CAR T cells have as yet exhibited only a negligible effect in the treatment of solid tumors [62] (The main side effects and hurdles are summarized in Figure 3)

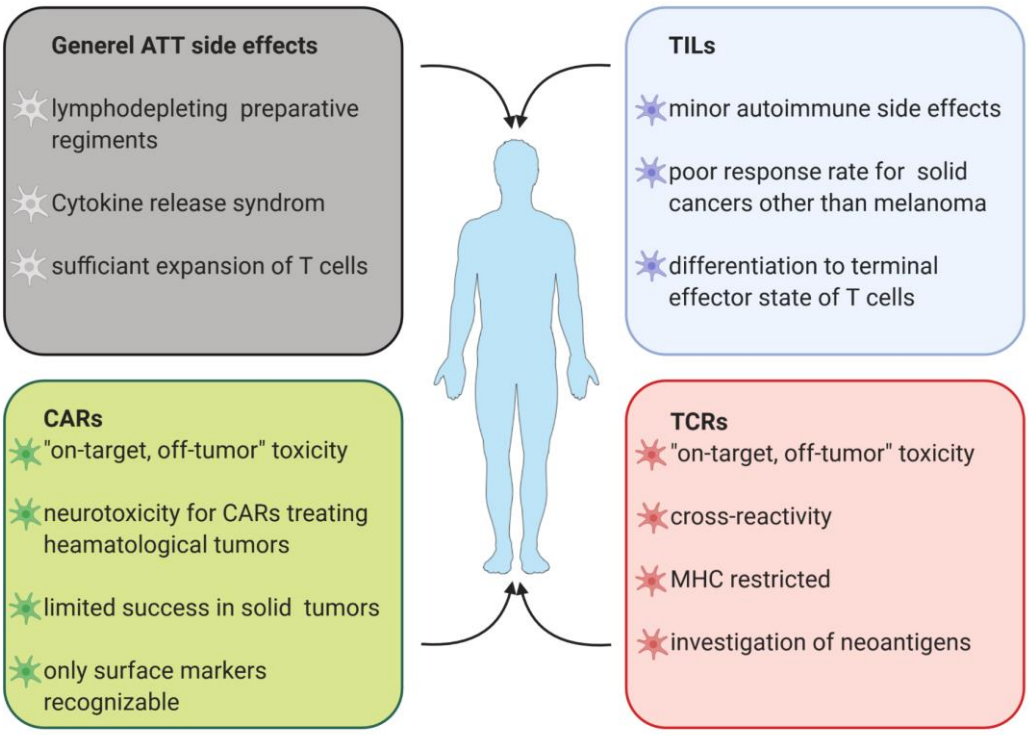

Figure 3. Overview of main side effects and hurdles of ATT treatment TIL = Tumor infiltrating lymphocytes; TCR = T cell receptor; CAR = Chimeric antigen receptor

2.2.2.1. Sufficient T cell expansion

In 1976, the first T cell-specific expansion was described, using a conditioned medium obtained from phytohemagglutinin-stimulated human blood lymphocytes [65]. Over the following years, it became clear that the growth factor IL2 was the main contributor in the medium [66]. Rosenberg based his preparation and outgrowth of TILs out of tumor biopsies on T cell culture with added IL2 [15]. The classic TIL expansion protocol includes an outgrowth of TILs from tumor biopsies of about 6-8 weeks, followed by REP, together with higher IL2 doses for 10-14 days [45]. This manufacturing protocol often leads to a successful rate of T cell numbers, although not always. The prosperous

growth of viable TILs achieved in the past clinical trials failed in a mean range of 7-38 %. In 2014, Svane et al. reported, that failure to expand (sufficient numbers of) TILs for treatment makes up 30 % of the general dropout rate [45, 46, 67-69]. Even though the total number of CAR T cells used for infusion varies between 10^8-10^9 only, failure to manufacture adequate CD19-CAR T cell numbers is reported for 6-24 %, something especially observed in older patients or those in which heavily pre-treated diffuse large B cell lymphoma (DLBCL) is present [70-72]. Clinical trials with TCR T cell products have not explicitly described expansion dropouts so far, but an appropriate cell count seems to be crucial [73]. In a study with MART-1-specific TCR T cells, the average expanded amount of cells within the 6 (out of 20) patients who demonstrated a partial tumor response was 2.15 x 10^{10}, whereas the range of expanded T cells was 3.8-48 x 10^9 [64, 73]. Similar discrepancies between the achieved individual cell count and the higher mean cell count of successfully treated patients can be found in the treatment with NY-ESO-1 specific TCR transduced T cells [27, 73]. For gene modified T cells like TCRs and CARs, only the long procedure of outgrowth is not needed, and direct use of REP is possible (e.g. [26, 74, 75]). This short expansion period is crucial due to expansive clinical grade manufacturing costs and the guided differentiation to the final effector phenotype [76, 77]. Several current studies show feasible T cell culture with IL7 and IL15, deriving transduced TCR or CAR-T cells to a less differentiated phenotype [78-80], though as of yet limited data on culture duration are available. In addition, the short duration of T cell expansion prevents the option to expand even more T cells when needed or to treat patients with a potential second donor lymphocyte infusion, which has been shown to be beneficial [60]. The knowledge gained on T cell differentiation and the homeostatic potential mediated by IL7/IL15 culture might give us the possibility to elucidate the T cell expansion even beyond two weeks. However, improving T cell expansion for ATT remains a desirable goal.

2.2.2.2. "On-target, off-tumor"-toxicity

Prior to current ATT studies and therapies, the performance of allogeneic (non-self) hematopoietic stem cell transplantation (allo-HSCT) had been a clinically common practice, as continues to be the case [81]. Since 1997, it has become evident that adoptive transferred allogeneic T cells within the transplant can induce complete remission with chronic myeloid leukemia [82]. However, one major side effect of allo-HSCT is graft-versus-host disease (GvHD), which develops when donor T cells encounter host antigen and can become lethal, with strong immunopathology

appearing in lymph nodes, bone marrow, lungs, skin, liver, brain and the gastrointestinal tract [83]. Although the treatment with allo-HSCT and the prevention of side effects have improved, GvHD remains lethal and limits the application [84]. One reason for the development of GvHD, despite genomic tissue typing and human leucocyte antigen (HLA) accordance, is the genetic differences that lie outside the HLA loci – referred to as minor histocompatibility antigens [85].

Now, in the course of emerging ATT treatments with specific expanded T cells against viral infection [86-88] or tumor burden [18, 89] and based on evidence that the likelihood of GvHD occurring is dramatically decreased this might be an option to avoid GvHD burden without lacking graft-versus-tumor (GvT). Even so, there is no exclusive MHC-linked antigen or surface molecule so far. This means that CAR or TCR T cells also have cytotoxic effects against normal tissue that share the same epitope as the aimed target cells, a phenomenon which is thus referred to as “off-tumor, on-target” toxicity [63]. For TCR T cells targeting melanoma differentiation antigens such as gp100 or MART-1, this is known to cause severe skin rash, ototoxicity and uveitis due to expression of the mentioned antigens on normal tissues [64]. CAR T cells therapy has shown similar toxicity [90, 91], whereas for CD19-CAR therapy, B cell aplasia is one expected side effect and can be treated with intravenous immunoglobulin [23]. Developing strategies to improve safety of TCR or CAR T cell therapy is still a challenging field and needs further investigation.

2.2.3. BLITC-mouse as model system

Recently, our research group published a dual-luciferase reporter mouse, called bioluminescence imaging of T cells (BLITC) [92]. The reporter system consists of a constitutive Renilla luciferase (Rluc), which enables the observation of the process of migration and expansion of the isolated T cells, and a *nuclear factor activated T cells* dependent click beetle luciferase (NFAT-CBR). This enables us to observe specific T cell activation (Figure 4). The system was transferred into two tumor models which were both used for this work.

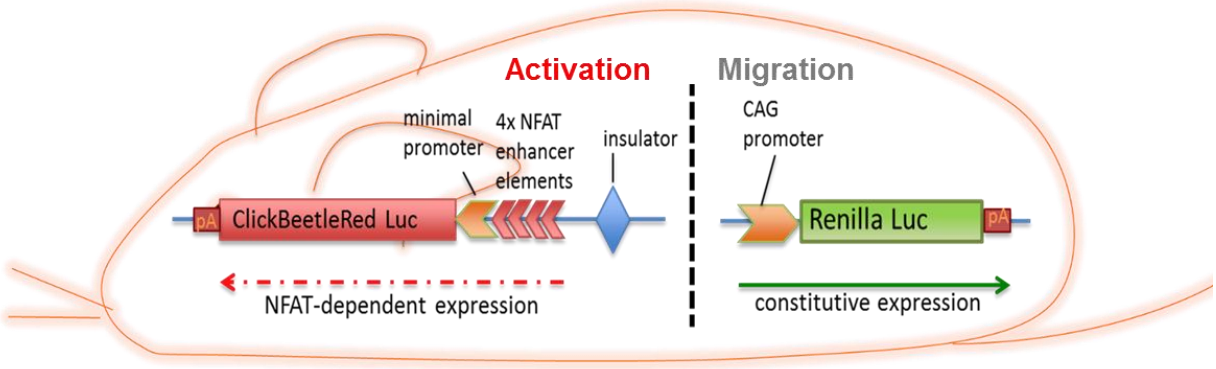

Figure 4. Schema of contained gene constructs of the dual-luciferase reporter BLITC-mouse. On the left is the NFAT-dependent ClickBeetleRed luciferase construct, consisting of four NFAT enhancer connected in a series. The right side shows the constitutive Renilla luciferase construct consisting of one CAG promoter and the luciferase, which leads to a constitutive expression.

In order to obtain an appropriate mouse model for clinical questions, we utilized the well-described minor histocompatibility antigen H-Y transplantation model [93]. This model was chosen because it is MHC-restricted and endogenous to mimic non-artificial TCR ATT and has been involved in clinically significant graft-versus-tumor- (GvT) and GvHD-effects/"on-target, off-tumor" toxicity [94, 95]. Therefore, BLITC mice were cross-bred with H-Y TCR-transgenic Marilyn (ML) mice that generate CD4 T cells and MataHari (MH) mice that generate CD8 T cells, to obtain TCR-transgenic reporter mice called ML-BLITC and MH-BLITC [92, 96, 97]. This H-Y related model involves two different approaches: Firstly, transferring H-Y TCR-transgenic T cells into male recipients with ubiquitous H-Y expression on male tissue, enabling us to imitate a strong "on-target, off-tumor" toxicity. Adding an H-Y tumor to the recipients allows to sound out the balance between "on-target, off-tumor" toxicity and GvT. Secondly, using female tumor bearing recipients mimics tumor specific TCR ATT in order to investigate optimisation possibilities without "on-target, off-tumor" toxicity.

Performing typical genetical engineering as is customary in the clinic required the selection of an appropriate model. For this reason, the well-known simian virus 40 (SV40) large tumor antigen (Tag)-driven tumor model was used [98, 99]. With TAg-specific TCR (TCR-I) retrovirally transduced WT-BLITC CD8 T cells were processed

as needed and followed by ATT into TAg-positive tumor (200.09ΔLuc) bearing mice [92] (Figure 5).

Combining the BLITC reporter system with these 2 antigen encounter models enables investigation of different treatment approaches for ameliorating ATT.

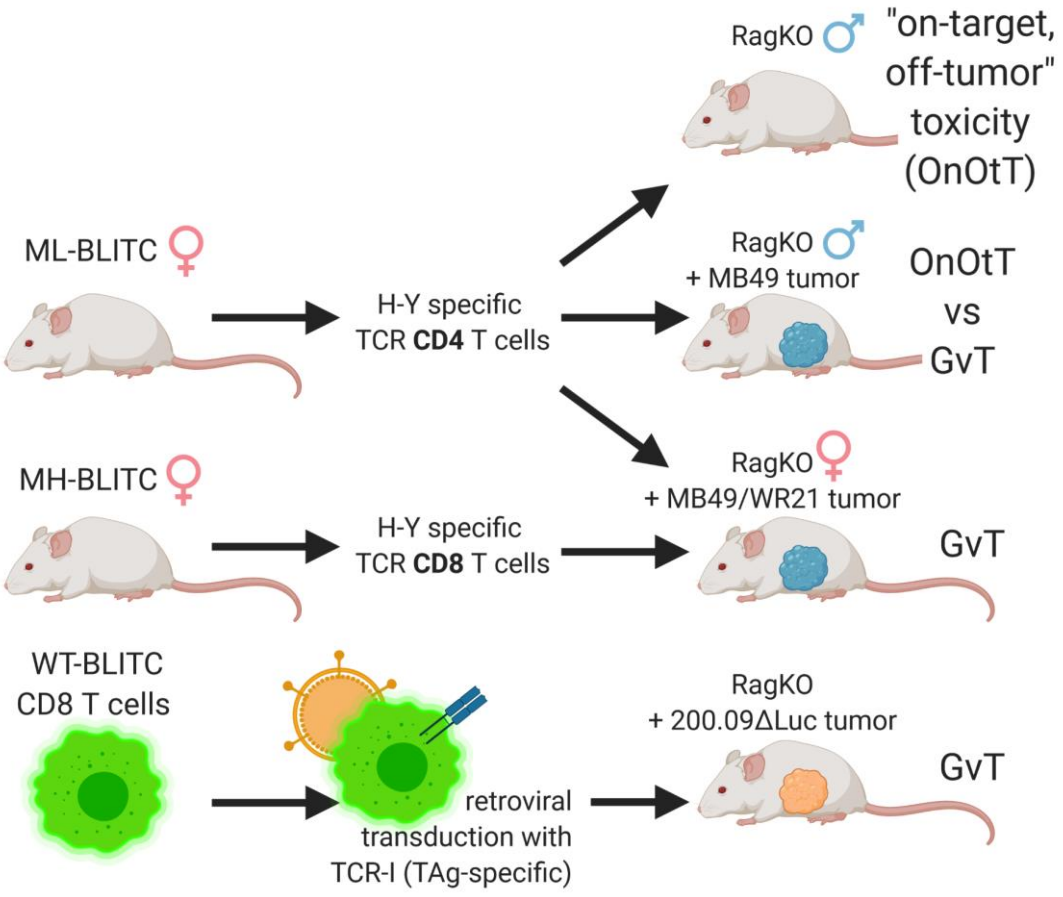

Figure 5. Schema of utilized mouse models in order to analyze and treat "on-target, off-tumor" toxicity (OnOtT), graft-versus-tumor (GvT) or to attenuate GVHD while maintaining GvT. T cells from female ML-BLITC mice lead to OnOtT in male recipients, but can also achieve GvT in HY-tumor bearing (male or female). T cells from female MH-BLITC mice are used to investigate GvT. WT-BLITC CD8 T cells (female and male) were retrovirally transduced with TAg-specific TCR (TCR-I) and used for investigation of GvT in TAg-tumor bearing mice.

2.3. Integrins as target for lymphocyte blocking

Integrins are heterodimeric transmembrane adhesion receptors found on all nucleated cells. In their cell-cell adhesion and also bidirectional signalling across the cell membrane, they mediate the regulation of cell proliferation, migration, activation and homeostasis [100]. Consisting of two different receptor peptides divided into α- and β-subunit, 18 α- and 8 β-subunits yield a total of 24 possible and currently known integrins in vertebrates [100, 101]. The importance of several integrins has become evident in mice experiments lacking different subunits. Knockout of the α4 subunit

shows impaired cardiac development and α6 knockout mice develop severe skin lesions [102, 103]. Alongside their crucial role in organ development, they have been described as being involved in the process of cancer development, wound healing and immune responses against infection and autoimmune disease. To date there have been reports on 12 integrins, which are expressed in several types of leucocytes (summarized in [104]). Demonstrating this immunological impact, the targeting of specific integrins promotes a new potential as therapeutic option. For instance, the antibody targeting αL-subunit has turned out to be effective in the treatment of plaque psoriasis [105] and the low-molecular weight tetrahydroisoquinoline antagonist of αLβ2 has been shown to block the T cell invasion of the conjunctiva and suppresses local inflammation [106]. Raab-Westpahl et al. has described further treatment options, targeting integrins, while this work continues to address the blocking of α4β7 [107].

2.3.1. Lymphocyte Peyer's patch adhesion molecule (LPAM-1)

The integrin α4β7 was first introduced in 1989. At this time, it was only known as *activated lymphocyte Peyer's patch adhesion molecule* (LPAM-1), which serves as a homing receptor to the mucosal site [108, 109]. Further studies established that LPAM-1 consists of two subunits as α4β7 integrin and specifically binds *Mucosal Addressin Cell Adhesion Molecule-1* (MAdCAM-1) which is exclusively present on intestinal endothelial cells of high endothelial venules [110] (Figure 6). Hamann et al. demonstrated, that LPAM-1 plays a key role in murine lymphocyte migration to the mucosal site [111]. A subsequent study by Erle et al. showed that LPAM-1 is expressed on human lymphocytes (T and B cells, NK cells), stimulated monocytes macrophages and eosinophils [112]. LPAM-1 has become interesting as a relevant homing molecule for two reasons: Firstly, it has been shown that LPAM-1 is important for T cell invasion into the gut that induces GvHD in mice. Secondly, both an allogeneic bone marrow transplantation model with LPAM-1 depleted donor T cells, and allo-HSCT with β7 knockout mice, demonstrated less GvHD [113, 114]. In clinical practice it is a well-known fact that the gut is a significant GvHD target [115]. Hence, using the blocking antibody against LPAM-1, could prove to be a promising technique for the future, as will be further explained in the following.

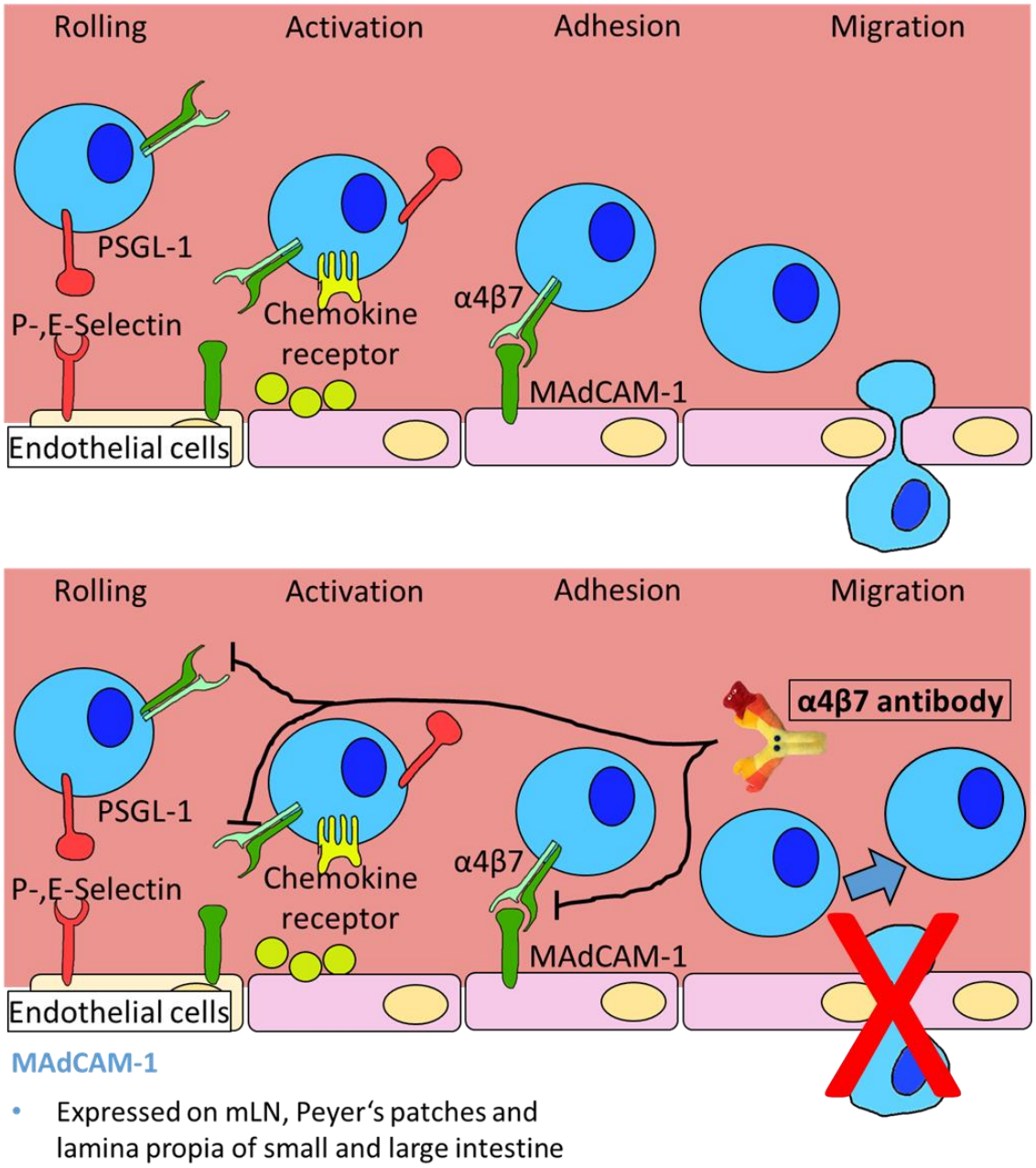

Figure 6. Schema of lymphocyte rolling and adhesion process on mucosal endothelial cells. Migration of T cells to the target tissue occurs in several steps. Chemokines are often used to guide cells to the target tissue by a gradient. First, the cells slow down and roll due to selectins. Afterwards, down-stream activation takes place, which can be triggered by chemokine receptors, and integrins are activated. Activated integrins are used for adhesion. The cells then migrate into the tissue. The LPAM-1 integrin-blocking antibody is intended to prevent the strong adhesion of the cell to the mesenteric tissue.

2.3.2. LPAM-1 antibody

In order to investigate the homing role of LPAM-1, Hamann et al. developed a blocking antibody against murine LPAM-1 in the hybridoma clone DATK32 [111], following work from Andrew et al. and Katayama et al. that demonstrated in different experiments the binding and blocking potential of DATK32 [116, 117]. The first clinical approach was

the humanization of DATK32 and application within a chronic colitis mouse model [118]. In parallel the development of an antibody effective against the α4 subunit moved forward and targeted encephalomyelitis and multiple sclerosis (MS) as treatment indication by blocking α4β1 and α4β7 [119, 120]. The resulting clinical antibody *Natalizumab* was approved by the FDA for MS and Crohn's disease, but showed progressive multifocal leukoencephalopathy (PML) as a severe side effect [121, 122]. On the other hand, *Vedolizumab,* an antibody against human α4β7, was established in clinical practice. This antagonistically binds specific human LPAM-1 and thereby inhibits the migration of T cells into intestinal tissue, which did not show severe side effects as *Natalizumab*. FDA-approval was given for the treatment of Crohn's disease and ulcerative colitis in 2014 [123-125]. Furthermore, the first clinical trial with *Vedolizumab* in six steroid-refractory intestinal GvHD patients showed promising clinical responses [126]. It might be of interest to target LPAM-1 in order to block T cell homing to gut after ATT, leading to less GvHD or "on-target, off-tumor" toxicity and potentially promoting GvT retaining more donor T cells in circulation.

2.4. T cell culture and their cytokines

As mentioned above, the implementation of isolated T cell culture took place more than 40 years ago. It involves adding the growth factor IL2 into culture media [65, 66]. The isolation and expansion of TILs was established by Rosenberg et al. and to this day T cells of all ATT types are expanded for therapies and clinical trials via expansion with IL2 [15, 26, 74, 127]. In recent years, though, it has become apparent that T cell culture with IL2 promotes terminal effector differentiation [76, 77, 128]. This is accompanied by lower potential of self-renewal and engraftment potential *in vivo* [129-131]. With the establishment of a preceding lymphodepletion for ATT, both treatment response and persistence improved [18, 34]. Gattinoni et al. determined that one reason for the ATT enhancement was a cellular sink, which provided more space for T cell expansion and fewer cells intercepting homeostatic cytokines like IL7 and IL15 [132]. Based on these findings, a variety of investigations were performed to analyze the potential of priming T cells even before T cell infusion. Using IL15 instead of IL2 promotes a T cell phenotype described as central memory T cells (Tcm), whereas IL2 culture leads to an effector memory T cell (Tem) phenotype [133]. Studies by Cieri, Zoon and Cha et al. compared T cell development by IL2 to IL7/IL15 culture. For IL7/IL15, they demonstrated a tendency towards Tcm cells with high self-renewal potential and anti-

tumor capacity, whereby IL2 culture promotes a more effector T cell-like phenotype lacking anti-tumor elimination potential [78, 134, 135]. In 2011, the option of treating tumor bearing mice with different cytokines such as IL7, IL15 and IL21 after ATT was introduced by Klebanoff et al., showing a dose-dependent beneficial anti-tumor effect mediated by adoptively transferred CD8 T cells [136]. The promoting impact of IL7/IL15 T cell culture towards Tcm left Gomez-Eerland et al. to establish the first clinical trial protocol in which IL7/IL15 was applied for a transgenic TCR T cell product [137]. This was confirmed in relation to human CAR T cells *in vitro* and with T cell samples from ALL patients [72, 138]. The achievement of striking Tcm populations via IL7/15 culture is one way to enhance a desired T cell product. Another way is to affect development and differentiation pathways via small molecular weight compounds such as glycogen synthase kinase 3 beta (GSK3β) inhibitor TWS119 or Delta-like 1 protein (DL1), which promote the generation of Tcm / stem Tcm (Tscm) with improved ATT properties [139-142]. Although there has been a lot of research investigating the effects of Tcm/Tscm cells and their cultivation, there is still potential for improvement regarding efficacy of expansion and functionality.

2.4.1. Interleukin 7

The discovery of Interleukin 7 (IL7), which has been categorized as member of the IL2 superfamily, was made over 30 years ago [143, 144]. The associated IL7 receptor is a heterodimer and consists of IL-7Rα, which is also part of the thymic stromal lymphopoietin (TSLP) receptor, and the common γ chain, which is shared by the receptors for IL2, IL4, IL9, IL15 and IL21 [145, 146]. The IL7 receptor is expressed on CD4 and CD8 T cells, for instance, and plays a major role for homeostasis of T cells [147]. It has also been shown, that IL7 has a crucial role in T cell development, as patients with congenital immunodeficiency lacking IL7 receptor do not have T cells, but still B cells, unlike mice [148, 149]. For IL7 it is well-known that human IL7 is functional in both the human and the murine environment, and vice versa [150, 151]. The down-stream signalling caused by IL7 receptor binding leads to phosphorylation of JAK1 and JAK3, which further activate signal transducers and transcription activators (STAT1, STAT3 and STAT5) [152, 153]. Another important cross-talk pathway arising from IL7 binding, is the PI3K-Akt pathway, which is associated with several signal transduction networks regulating cell survival [154]. Additionally, IL7 promotes anti-apoptotic signals

like Mcl-1 and Bcl-2 and retains telomerase length in T cells [155, 156]. It can thus be concluded that IL7 seems to play an essential role as T cell survival factor [157].

2.4.2. Interleukin 15

In 1994, two different teams discovered the growth factor Interleukin 15 (IL15) [158, 159]. Like IL7, IL15 belongs to the four α-helix bundle family and as with IL7 receptor, the heterodimeric IL15 receptor also shares the common γ chain [160]. The second receptor branch is the β chain and is shared with the IL2 receptor [161]. Additionally, the IL15 receptor complex has a unique α subunit (IL15Rα) [162]. IL15Rα usually appears as membrane-bound *trans*-presenting IL15, forming an immunological synapse [163]. This is believed to be in order to limit exposure to circulating IL15, restricting aberrant immune stimulation and decreasing the risk of autoimmunity from uncontrolled IL-15 exposure [164]. However, the soluble *cis*-presenting IL15-IL15Rα complex can also trigger the IL15 receptor signaling cascade [165]. Similar to the signal transduction of IL7, IL15 receptor signaling induces activation of JAK1, JAK3 and subsequently STAT3 and STAT5 with further activation of the PI3K-Akt pathway [157]. Although the similar signal cascade, IL7 or IL15 knockout mice show different phenotypes with a T cell (and B cell, natural killer (NK) cell, NKT cell and intraepithelial lymphocytes (IEL)) deficiency in IL7 knockout mice or a specific lack of memory CD8 T cells (and NK cells and IELs) in IL15 knockout mice [166, 167]. On the other hand, it has been shown that administration of IL15 leads to a robust expansion of memory CD8 T cells *in vivo* [168, 169]. For memory CD4 T cells, similar results were demonstrated by observation of reduced antigen specific memory CD4 T cells in IL15 knockout mice [170]. This underlines the characteristics as a survival factor for IL7 and growth factor for IL15.

2.4.3. Interleukin 27

IL27 is a heterodimeric cytokine, consisting of the p28 and Epstein-Barr virus inducible protein 3 (EBI3) subunits. It belongs to the cytokine family of IL6 and IL12 and shares the same heterodimeric receptor [171]. Stimulation of IL27 has been shown to arouse different complexes of STAT1 and STAT3, which in turn has shown that the ability to activate both transcription factors, regulates diverse lymphocyte-based functions [172, 173]. Pflanz et al. discovered IL27 and described a mediated Interferon γ (IFNγ) expression of naïve CD4 T cells [174]. Additionally, it has been shown to be required during viral infection to maintain CD4 T cell persistence [175, 176]. For CD8 T cells, it

is reported to promote granzyme secretion *in vitro* [177] and human CD8 T cells showed enhanced proliferation and effector function [178]. Interestingly, IL27 demonstrated also enriched CD8 Tcm cells following subunit vaccination or tumor challenge [179, 180], but not vaccinia virus vaccination, while influenza virus-specific CD8 Tcm cells seem to even lose responsiveness to IL-27 [181]. Moreover, enhancement of CD8 functionality against cancer by IL27 was observed [182, 183]; whereas detailed gene analysis attributed induction of an inhibitory gene program in CD8 T cells to IL27 [184]. This contradictory data on IL27 illustrate how complex the mechanism of IL27 function is and that this field needs more investigation. Nevertheless, IL27 seems to be an attractive cytokine for T cell culture with the potential to enhance effector function, maintain Tcm phenotype of T cells and it might promote CD4 T cell expansion.

2.5. Aim of the project

Allo-HSCT can cure hematological malignancies due to the GvT effect mediated by alloreactive donor T cells [185]. The importance of transplanted T cells for cancer control has emphasized the relevance of ATT. However, transplanted donor T cells also tend to attack non-malignant host tissues as organ tissues feature, even if donor and recipient are MHC-matched, differences in minor antigens causing GvHD. Similar side effects could occur in ATT with gene modified T cell products because of arising "on-target, off-tumor" toxicity that leads to similar damage on tissue with expression of the same targeted antigen.

"On-target, off-tumor" toxicity and GvT are both impacted by the principal parameters of the migration and activation of donor T cells. T cells act locally on target tissue by secreting cytotoxic agents such as perforins and granzymes [186, 187] as well as inflammatory cytokines like IFNγ and *tumor necrosis factor* α (TNFα) [188-190]. T cells have to migrate to the site of action to fulfilling their effector function. Whereas in the microenvironment of solid tumors T cells are frequently found suppressed or lacking, large amounts of infiltrating and activated T cells are found in organs with "on-target, off-tumor" targets.

The aim of the thesis is to investigate the therapeutic potential of three approaches to skew the immune response of donor T cells from "on-target, off-tumor" toxicity towards tumor rejection. The fate of adoptively transferred T cells was monitored by our bioluminescence-reporter system, which is suitable for the longitudinal visualization of migration and activation of transferred T cells *in vivo*.

The first aim was selective inhibition of T cell migration into intestinal tissues by targeting α4β7-integrin (LPAM-1). It has been suggested that circulation of adoptive transferred CD4 T cells will increase by blocking migration into mucosal site and anchor on tumor tissue. The LPAM-1 antibody is already FDA-approved and has clinical relevance for Crohn's disease, ulcerative colitis and most recently also for GvHD treatment [123, 124, 126]. The mouse analogue demonstrated specific blocking potential of LPAM-1 [111, 116]; thus the goal was to investigate the therapeutic potential of LPAM-1 antibody in order to mitigate "on-target, off-tumor" toxicity within the gut and maintain or improve GvT.

The second aim was to modify the properties of adoptive transferred T cells by a novel expansion condition. Previous work has shown that mainly naïve T cells cause GVHD [191]. Although there are contradictory data about Tcm causing GvHD, it is certain that they induce less GvHD than naïve T cells [191, 192]. Recent studies may show that CD8 T cell culture with IL7/IL15 leads to a Tcm or Tscm cell phenotype [78, 134, 135]. However, CD4 T cell culture has not been focused on. Culturing T cells with IL27 has been demonstrated to promote CD8 Tcm development, to play an important role in CD4 persistence *in vivo*, and to enhance granzyme secretion [175, 177, 179, 180, 193]. Hence it was of value to investigate IL27 in combination with homeostatic cytokines such as IL7 and IL15 in order to obtain an optimized T cell culture protocol feasible for ATT.

The third aim was to prolong the expansion of T cells while keeping them functional and reactive for ATT. The current duration of T cell expansion protocols followed by transfusion of enriched T cell product is 10-14 days [45]. This duration is intended to provide cost-efficiency and to avoid terminal differentiation of T cells [76, 77, 194]. However, several treatment dropouts occur due to insufficient T cell expansion [69]. Using IL7/IL15 culture or a potential novel cytokine condition, Tcm/Tscm cell phenotype is likely to be mediated, and elongated expansion might increase the yield of desired T cell product, providing the option for a second donor lymphocyte infusion. This option had to be analyzed in detail.

3. Material

3.1. Antibodies

Murine

Antigen	Clone	Fluorochrome	Company
CD3	145-2C11	PerCP Cy5.5	Biolegend
	145-2C11	No	BD Bioscience
CD4	RM4-5	BV510	Biolegend
CD8	53-6.7	APC-Cy7	Biolegend
CD28	37.51	No	BD Bioscience
CD44	IM7	PE-Cy7	Biolegend
CD62L	MEL-14	APC	Biolegend
LAG3	C9B7W	BV 421	Biolegend
TIM3	RMT3-23	PE-Cy7	Biolegend
PD1	HA2-7B1	PE	Biolegend
CTLA-4	UC10-4B9	APC	Biolegend
Granzyme A	368.5	PE	Biolegend
Granzyme B	GB11	Alexa Fluor 647	Biolegend
IFNγ	XMG1.2	APC	Biolegend
TNFα	MP6-XT22	BV510	Biolegend
IL10	JES5-16E3	PE-Cy7	Biolegend
IL2	JES6-5H4	PE	Biolegend
Bcl-2	BCL/10C4	PE	BD Biosciences
Sca-1	D7	Alexa Fluor 647	Biolegend
CD122	TM-BETA1	BD Horizon	BD Biosciences
CXCR3	CXCR3-173	APC	Biolegend
CD16/CD32	93	No	Biolegend
LPAM-1	DATK32	No	DRFZ Facility
LPAM-1	DATK32	No	BioXcell
Vβ7	TR310	FITC	Biolegend

Human

Antigen	Clone	Fluorochrome	Company
CD3	UCHT1	Alexa Fluor 700	Biolegend
	OKT3	No	Miltenyi Biotec
CD4	RPA-T4	PerCP Cy5.5	Biolegend
CD8	RPA-T8	BV 650	Biolegend
CD28	15E8	No	Miltenyi Biotec
CCR7	FAB197F-100	FITC	R&D Systems
CD45RO	UCHL1	BV510	Biolegend
CD45RA	HI100	BV650	
LAG3	REA351	Vio Blue	Miltenyi Biotec
TIM3	F38-2E2	APC	Miltenyi Biotec
PD1	PD1.3.1.3	PE	Miltenyi Biotec
IFNγ	45-15	PE Vio770	Miltenyi Biotec
TNFα	cA2	APC Vio770	Miltenyi Biotec
IL2	MQ1-17H12	BV 605	Biolegend

3.2. Buffer

Buffer	Ingredients
10 X PBS	10.588 mM KH_2PO_4 1.5517 M NaCl 29.664 mM Na_2HPO_4 (Gibco™; Cat. number: 70013032)
1 X PBA	1 X PBS 0,5 % BSA
MACS-Buffer	1 X PBA 2mM EDTA
10X Red Blood Cell Lysis Buffer (1 L)	89.9 g NH_4Cl 10 g $KHCO_3$ 370 mg tetrasodium EDTA pH 7.3

3.3. Cell culture media

Media name	Media basis	Additives
cDMEM	DMEM, High Glucose GlutaMAX™ (Thermo Fisher	10 % FCS 1 mM sodium pyruvate 100 mM MEM nonessential aa

	Scientific; Cat. number: 10566016)	5 mM HEPES 100 U/mL penicillin 100 mg/mL streptamycin
RPMI +	RPMI 1640 Medium (Thermo Fisher Scientific; Cat. number: 11875093)	10 % FCS 100 U/mL penicillin 100 mg/mL streptomycin
RPMI Dox	RPMI 1640 Medium (Thermo Fisher Scientific; Cat. number: 11875093)	RPMI + 0.5 µg/mL Doxycyclin (Dox)
T cell media (TCM)	RPMI 1640 Medium (Thermo Fisher Scientific; Cat. number: 11875093)	10 % FCS 1 mM sodium pyruvate 100 mM MEM nonessential aa 50 mmol/L β-Mercaptoethanol 2 mmol/L L-glutamine 100 U/mL penicillin 100 mg/mL streptamycin
Plat-E Media	DMEM, High Glucose GlutaMAX™ (Thermo Fisher Scientific; Cat. number: 10566016)	10 % FCS 1 mM sodium pyruvate 100 mM MEM nonessential aa 5 mM HEPES 100 U/mL penicillin 100 mg/mL streptamycin 10 µg/mL Blasticidin 1 µg/mL Puromycin

3.4. Cell lines

- DATK32-hybridoma (ATCC)
- TK-1 (Alf Hamann, DRFZ, Berlin)
- Plat-E (ATCC)
- 200.09**Δ**Luc (Martin Szyska)
- MB49 (Tomas Blankenstein, MDC, Berlin)
- WR21 (ATCC)

3.5. Chemicals

Chemical	Company	Order number
≥ 99.5 % Ph. Eur., reinst EtOH	Carl-Roth	5054.4
2-Propanol, ≥ 99.5 %	Carl-Roth	9866.5
50 X TAE (Rotiphorese)	Carl-Roth	CL86.1
Agar	Carl-Roth	2266.3
Annexin V APC	Biolegend	640920
Annexin V Binding Buffer	Biolegend	422201

Biocoll	Merck (Biochrom)	L6113
Blasticidin	Thermo Fisher Scientific	R210-01
BSA	Merck (Sigma-Aldrich)	B6768-500G
CFSE	Merck (Sigma-Aldrich)	21888-25MG-F
Chemical	Company	Cat. number
Coelenterazin	Biosynth	C-7002
DAPI	Thermo Fisher Scientific	D1306
D-luciferin	P.J.K.	102132
DMSO	Carl-Roth	4720.2
Doxycyclin	AppliChem	A2951.0025
EDTA	Merck (Sigma-Aldrich)	E5391-250G
FCS	Gibco	10500-064
Fixation buffer	Biolegend	420801
IL15	Peptrotech	200-15
IL2	Peptrotech	200-02
IL27	Peptrotech	200-38
IL7	Peptrotech	217-17
Isofluran	A3Apotheke (Baxter)	7253744
KH_2PO_4	Merck (Sigma-Aldrich)	P5655-500G
$KHCO_3$	Merck (Sigma-Aldrich)	237205-500G
L-glutamine	Merck (Sigma-Aldrich)	G7513-100ML
LPS (Escherichia coli O55:B5)	Merck (Sigma-Aldrich)	L6529-1MG
Matrigel	BD Biosciences	356234
MEM nonessential aa	Merck (Sigma-Aldrich)	M7145
NaCl	Merck (Sigma-Aldrich)	S3014-1KG
NH_4Cl	Merck (Sigma-Aldrich)	A8434-500G
Penicillin-streptamycin	Merck (Sigma-Aldrich)	P4333-100ML
Permeabilization buffer	Biolegend	421002
Puromycin	Thermo Fisher Scientific	A1113803
Retronectin	Takara (Clonetech)	T100A
sodium pyruvate	Merck (Sigma-Aldrich)	S8636-100ML
TransIT-LT1 Transfection Reagent	MoBiTec	MIR2300

Tripsin-EDTA	Gibco	R-001-100
TRIzol™	Thermo Fisher Scientific	15596018
β-Mercaptoethanol	Gibco	21985-023

3.6. Kits

- RNeasy Mini Kit (QIAGEN)
- Granzyme B Mouse uncoated ELISA Kit (Thermo Fisher Scientific)
- CD4+ and CD8+ isolation kit (Miltenyi Biotec)

3.7. Enzymes

- SuperScript™ II Reverse Transcriptase (#18064014; Thermo Fisher Scientific)
- Phusion® High-Fidelity DNA Polymerase (#M0530L; NEB)

3.8. Primer

UTY	forward	5‘ GCTCACTTATATGAAACCCAGAGGAA 3‘
	reverse	5‘ CATATTATGGTGCATCCAACCTAACT 3‘
DBY	forward	5‘ CAATAGCAGCCGAAGTAGTGGTAGT 3‘
	reverse	5‘ AACTGCCTGGGAGTTATAATTTCCT 3‘
HPRT	forward	5‘ CAACGTAGGAGGACCCTTTAATGC 3‘
	reverse	5‘ CCACAGGACTAGAACACCTGCTAA 3‘

3.9. DNA vectors

Gratefully provided by Thomas Blankenstein: pMP71-TCR-1

3.10. Mice

- Albino B6 (C57BL/6(Cg)-Tyrc-2J)
- Albino Rag knockout (albino RagKO; B6129S6-Rag2tm1Fwa N12-Tyrc-2J)
- Matahari-BLITC (MataHari-TCR$^{+/+}$Rag2$^{-/-}$NFAT-CBR$^{+/+}$Rluc$^{+/+}$)
- Marilyn-BLITC (Marilyn-TCR$^{+/+}$Rag1$^{-/-}$NFAT-CBR$^{+/+}$Rluc$^{+/+}$)

3.11. Devices

- Cell sorting by FACS Aria II or Aria III (BD Biosciences)
- Flow cytometry by FACS Canto II (BD Biosciences) or CytoFLEX LX (Beckman Coulter)
- Irradiation by RS 2000 Biological System (RADSOURCE)
- Spectrophotometry by NanoPhotometer TM P300 (IMPLEN)
- Bioluminescent imaging by Xenogen IVIS 200 (PerkinElmer)

- Gel documentation by EAGLE EYE II (STRATAGENE)
- PCR by peQSTAR 2xGradient (peQlab)

3.12. Software

- Living Image 5.0 (Caliper LifeSciences; Waltham)
- Prism 7 and 8 (GraphPad Software; La Jolla)
- Office 2011/2019 – Mac and Windows (Microsoft; Redmond)
- FlowJo 10 (now Becton, Dickinson & Company; Ashland)
- Illustrator, Photoshop, Reader (Adobe; Munich)
- Endnote X9 (Clarivate Analytics; London)
- BioRender.com (Toronto)
- Magellan 5 (Tecan Traiding AG; Switzerland)
- SoftMax Pro 5 (Molecular Devices; San Jose)

4. Methods

4.1. Molecular biology methods

4.1.1. RNA isolation

Short-term and long-term expanded CD8 or CD4 T cells were sorted for $CD44^{+}CD62L^{+}$ (>97%). T cells were centrifuged (400 g, 5 min) and resuspended in RLT buffer (RNeasy Kit, QIAGEN), then stored at -80°C. After collection of all samples, further RNA isolation steps with RNeasy Kit (QIAGEN) were performed according the manufacturer's instructions. RNA concentration and quality were measured by spectrometry analysis with NanoPhotometer TM P300 (IMPLEN).

4.1.2. RNA isolation from tumor samples

Sacrificed mice with tumor outgrowth were dissected and the tumor tissue was prepared and removed as completely as possible. The obtained tumor tissue was then homogenized using pre-separation filters (30 µg; Miltenyi Biotec) and diluted with PBS up to 1 mL. For RNA isolation, 500 µL were centrifuged (400 g, 5 min) and the obtained cell pellet was resuspended in 500 µL TRIzol™ (Thermo Fisher Scientific). Further isolation steps were performed according to the manufacturer's protocol.

4.1.3. Reverse transcription PCR (RT-PCR)

To synthesis cDNA out of isolated RNA from tumor tissue, the RNA was reversed transcribed using SuperScript™ II Reverse Transcriptase (Thermo Fisher Scientific) according to the manufacturer's protocol.

4.1.4. Polymerase chain reaction (PCR)

Tumor cDNA was further amplified for gene analysis of DBY, UTY and HPRT. PCR was prepared using Phusion® HF DNA Polymerase with following master mix:

10 µl Phusion® HF Mastermix
x µl H2O
1 µl Primermix 10 µM (1:1 reverse vs. forward primer)
0,5 µg DNA

Specimens were then taken using the following PCR protocol:

Step	Temperature [°C]	Time [s]	
Heating lid	110°	120	
Initial denaturation	98°	30	
Denaturation	98°	10	38 cycles
Annealing	58°	30	
Elongation	72°	120	
Final elongation	72°	600	
Storage	10°	∞	

4.1.5. Agarose gels

The amplified DNA fragments were separated by size using 1% agarose gel. The agarose gel was prepared with TAE and gel-electrophoresis was performed by 120 V for 30 min.

4.1.6. RNA Sequencing

RNA samples were submitted to the BIH Genomic Facility (Berlin), where an RNA library was generated by using the NEBNext Ultra™ II Directional RNA Library Prep Kit for Illumina® (NEB). Illumina sequencing was performed with NextSeq® 500/550 High Output Kit v2 (Illumina).

4.1.7. Bioinformatic Analysis

RNA-seq expression data were normalized and log-transformed as log2 (1+TPM) (TPM: transcripts per million) for our own data and GSE80306 [195]. Microarray data was downloaded from GEO using the R package GEOquery (v2.46.15) for GSE92381 [195], GSE61697 [196], GSE23321 [139], GSE93211 [140] and GSE80306 [195] or directly extracted from cell files using the packages affy (v1.56), affydata (v1.26) and limma (v.3.34.9) for GSE41909 [134] and GSE68003 [141], with rma background correction, quantile normalization and avgdiff summarization. Datasets were summarized over gene names, mapping mouse and human gene names onto each other using orthologues from MGI (HOM_MouseHumanSequence.rpt), and then combined after removing the bottom 5% of expressed genes, quantile normalization and batch correction with respect to assay using ComBat (package sva, v3.26.0). Clustering and PCA was performed using row z-scores for the gene set of Gattinoni et al. [139]. Differential expression analysis was performed using DESeq2 [197] and GO term analysis with topGO (v2.30.1).

4.2. Biochemical methods

4.2.1. Liquid chromatography-mass spectrometry (LCMS) analyses

Digestion buffer (8M urea, 75 mM NaCl, 50 mM Tris pH 8, 1 mM EDTA) was added to the samples for 15 minutes at 4°C. Proteins were reduced with 5 mM dithiothreitol for 1h at 37°C and alkylated with 10 mM iodoacetamide for 45 minutes in the dark at room temperature. Endopeptidase LysC (Wako, Japan) and sequence grade trypsin (Promega) were added with an enzyme: substrate ratio of 1:50, and samples were digested over-night at 37°C. Samples were acidified with formic acid (final concentration 1%) and peptides were desalted using the StageTips protocol [198].

Peptides from 3 replicates for each antibody were measured on a Q Exactive HF-X instrument (Thermo). 100 ng peptides were injected per sample and separated on a 20 cm reversed-phase column (ReproSil-Pur C18-AQ; Dr. Maisch GmbH) using a 60 min gradient with a 250 nL/min flow rate of increasing Buffer B concentration (from 2% to 60%) on an easy nLC1200 High Performance Liquid Chromatography (HPLC) system (ThermoScientific). The mass spectrometer was operated in the data dependent mode with a 60K resolution, 3×10^6 ion count target and maximum injection time 10 ms for the full scan, followed by top 20 MS2 scans with 15K resolution, 1×10^5 ion count target and maximum injection time of 22ms.

Raw data were analyzed using the MaxQuant software (v1.5.2.8) as described [199]. The internal Andromeda search engine was used to search MS2 spectra against a decoy UniProt database for rats (downloaded 05/2018) containing forward and reverse sequences. The search included variable modifications of oxidation (M) and N-terminal acetylation, deamidation (N and Q) and fixed modification of carbamidomethyl cysteine. Minimal peptide length was set to 7 amino acids and a maximum of two missed cleavages was allowed. The FDR was set to 0.01 for peptide and protein identifications. Unique and razor peptides were considered for quantification. Retention times were recalibrated based on the built-in nonlinear time-rescaling.

4.3. Cell culture methods

4.3.1. Murine T cell culture

T cells harvested from the spleens of donor mice were enriched by using CD4 or CD8 isolation Kit (Miltenyi Biotec). T cells were cultured in T cell medium (TCM). For activation, T cells were activated *in vitro* for 18 hours (Marilyn and MataHari mice) or 72 hours (albino B6 mice) in TCM plus IL2 (1 ng/mL; PeproTech) in 6-well or 24-well culture plates coated over night at 4°C with anti-CD3/CD28 (anti-CD3 3 mg/mL; anti-CD28 2 mg/mL). T cells were than expanded by using TCM containing recombinant human IL15 (50 ng/mL) and recombinant human IL7 (10 ng/mL) or IL15 and recombinant human IL27 (50 ng/mL). The medium was refreshed every third or fourth day.

4.3.2. Human T cell culture

PBMC were isolated by density gradient centrifugation (Biocoll; Merck) from fresh heparinized blood samples from healthy donors. PBMC were stimulated in vitro for 72 hours in TCM plus recombinant human IL2 (1 ng/mL) in 6-well culture plates coated over night at 4°C with anti-CD3/CD28 (3 mg/mL anti-CD3; 2 mg/mL anti-CD28). Afterwards, T cells were expanded using TCM containing recombinant human IL15 (50 ng/mL) and recombinant human IL27 (50 ng/mL) or recombinant human IL7 (10 ng/mL). The medium was refreshed every third or fourth day.

4.3.3. Activation assay

T cells from cell culture were harvested and adjusted to 2e6 cells/mL. Cells were plated (100 µL/well) into flat 96-well plates coated with anti-CD3/CD28 in the presence of human IL2 (1 ng/mL) and Brefeldin A (10 µg/mL) and incubated for 4 hours on 37°C. After activation cells were harvested and proceed by intracellular Flow Cytometry Staining Protocol (Biolegend) for granzyme A and B or INFγ (Biolegend).

4.3.4. Annexin/DAPI assay

Expanded T cells were harvested, adjusted, plated and re-stimulated as described in section 4.3.3., but without Brefeldin A. After activation cells were harvested and surface staining was performed, followed by Annexin V staining protocol (Biolegend) with AnnexinV-APC and AnnexinV binding buffer. Before measurement via flow cytometry, DAPI was added (final concentration 1 ng/mL DAPI).

4.3.5. T cell inhibiting receptor (TIR) assay

ST and LT expanded T cells were harvested, adjusted, plated and re-stimulated as described in section 4.3.4., but the utilized wells were previously coated with less anti-CD3/CD28 (1 mg/mL anti-CD3; 0,66 mg/mL anti-CD28). The T cells rested for a period of 10 days at 37°C. The medium was refreshed every third or fourth day. On day 10 T cells were harvested, and the surface stained with CD3, CD4, CD8, PD-1, LAG3 and TIM3. Mean fluorescence intensity was measured via flow cytometry.

4.3.6. *In vitro* proliferation assay

Expanded T cells from albino B6 mice were adjusted to 1e6/mL and labelled with 10 µM CFSE (Sigma-Aldrich) for 10 minutes at room temperature. Afterwards, cells were washed twice with TCM and then plated (1e5 cells/well) into flat 96-well plates coated with anti-CD3/CD28 for 11 days. CFSE dilution was then measured by flow cytometry.

4.4. Immunological methods

4.4.1. Flow cytometry

Surface staining was performed according to standard staining protocols and recommended antibody diluents. Intracellular staining for IFNγ, TNFα, IL2, IL10 and Bcl-2 was done with fixation/permeabilization buffer (Biolegend), according to the manufacturer's instructions. To detect apoptosis, cells were stained by DAPI (Thermo Fisher Scientific) and AnnexinV-APC using Annexin V Binding Buffer (Biolegend). Samples were acquired on a FACS Canto II (BD Biosciences) or CytoFLEX LX (Beckman Coulter), and all analyses were performed using FlowJo software (Becton, Dickinson & Company).

4.4.2. Cell sorting

Surface staining of splenocytes or expanded T cells was executed according Flow cytometry (see section 4.4.1.). The subsequent cell sorting was performed using a FACS Aria II, Aria III or Aria F (BD Biosciences).

4.4.3. Enzyme-linked immunosorbent assay (ELISA)

T cells from cell culture were harvested and adjusted to 2e6 cells/mL. Cells were plated (100 µL/well) into flat 96-well plates coated with anti-CD3/CD28 in the presence of human IL2 (1 ng/mL) and incubated for 4 hours at 37°C. After activation supernatant was harvested and stored at -20°C. Granzyme B secretion within supernatant was analyzed with a granzyme B Mouse Uncoated ELISA Kit (Thermo Fisher Scientific),

according to the manufacturer's protocol. The final enzyme reaction was then stopped with H_2PO_4 and light absorbance measured at 450 nm with Magellan 5 (Tecan Trading). Granzyme B concentration was calculated with SoftMax Pro 5 (Molecular Devices).

4.4.4. T cell transduction

The utilized retroviral vector pMP71-TCR-I that bears the alpha and beta-chain of a TCR specific for the H-2D^b (MHCI)-restricted epitope I of SV40-Tag, was built on the pMP71 backbone (Engels, cam et al. 2003). The subsequent retroviruses were produced by PlatE cells that were transfected with pMP71-TCR-I using TransIT (Mirus Bio). Meanwhile, freshly isolated splenocytes from BLITC mice were enriched for CD8 T cells using a CD8 MACS isolation kit (Miltenyi Biotec) and activated as described in section 4.3.1. Two days after transfection, activated CD8 T cells (5e5 cells/well) were spinoculated on a RetroNectin® coated 24-well plate (coated with 20 µg/mL RetroNectin over-night, 4°C) for 30 min at 32°C in PlatE supernatant containing retroviral particles. After spinoculation the plate rested in the incubator (37°C) over a period of three days. T cells were than washed and further expanded short-term or long-term as described in section 4.3.1. until the day of ATT. ATT was performed with ST or LT CD8 BLITC T cells sorted for Vβ7$^+$ TCR.

4.5. In vivo experimental methods

4.5.1. Bioluminescent imaging

For *in vivo* bioluminescence measurement, the IVIS 200 were used after mice were anaesthetized with isoflurane (Baxter) in an XGI-8 anesthesia system (PerkinElmer). 3 minutes before Rluc acquisition, native coelenterazine (Biosynth) was dissolved in 10 µL DMSO, diluted in 100 mL PBS, and immediately injected iv into anaesthetized mice (100 mg native coelenterazine per mouse). BLI acquisition was performed for 5 minutes at small binning. Bioluminescent data were acquired, analyzed, and visualized using Living Image software (PerkinElmer). BLI quantification was performed by digitally setting regions of interest (ROI) around abdomen region, prospective or visible tumor areas and computing respective total flux values.

4.5.2. *In vivo* "on-target, off-tumor" toxicity treatment with LPAM-1 antibody

Freshly isolated splenocytes from Marilyn-BLITC mice were sorted for CD3$^+$CD4$^+$ (>97%) and injected intravenously into sublethally irradiated (tumor bearing) male

albino RagKO mice. The treated group received a daily LPAM-1 antibody injection (iv) over a period of 6 to 10 days. The control group obtained PBS injections. The “on-target, off-tumor” toxicity was observed daily and evaluated by a score sheet rating fur, posture, skin, activity/vitality and weight.

4.5.3. Lypopolysaccharide (LPS) injection

Freshly isolated splenocytes from Marilyn-BLITC mice were sorted for $CD3^+CD4^+$ (>97%) and injected intravenously into sublethally irradiated tumor bearing male albino RagKO mice. Mice received a daily injection of LPAM-1 antibody (200 µg), LPAM-1 antibody plus LPS (0.5 µg) or LPS only. Evaluation of toxicity was performed as described in section 4.5.2.

4.5.4. *In vivo* proliferation assay

To analyze *in vivo* proliferation, expanded T cells from female BLITC mice (MataHari or albino B6) were sorted via FACS cell sort for $CD44^+CD62L^+$ (>97%) and labeled with CFSE as described in section 4.3.6. Labeled cells were then transferred into male albino RagKO mice (1e6 cells/mouse). 3 and 10 days later, Rluc signals were measured via bioluminescent imaging.

4.5.5. *In vivo* kill

Expanded T cells from MataHari-BLITC mice were sorted for $CD44^+CD62L^+$ (>97%) and 1e6 cells per mouse injected intravenously into female albino RagKO. Male splenocytes from albino B6 mice were used as targets and female splenocytes as an internal negative control. Male and female splenocytes were labeled with CFSE at 10 mM and 1 mM, respectively. A 1:1 mixture of male and female splenocytes (5e6 total cells/mouse) was injected into transplanted mice 2 hours after T cell transfer. Spleens were harvested 20 hours after injection of target cells. Ratios between male target ($CFSE^{high}$) and female target ($CFSE^{low}$) were calculated for each sample (R). The mean ratio measured in female albino RagKO without effector T cells was used as a control (meanRc) to normalize samples. The killing percentage was obtained using the formula: 100-100*(R/meanRc). Mean killing frequencies of control mice that did not receive MataHari T cells were subtracted from killing frequencies of mice that did receive ST and LT expanded MataHari T cells.

4.5.6. Tumor challenge

For tumor challenge, three different tumor cell lines were used, depending on experimental setup: The urothelial carcinoma cell line MB49 [200], the TAg-expressing

gastric carcinoma cell line Tag$^+$200ΔLuc [92] or the male-derived submandibular salivary gland carcinoma cell line WR21 [201]. MB49 and WR21 were grown in RPMI+; Tag$^+$200ΔLuc was grown in DMEM Dox. MB49 and WR21 cells were adjusted to 2e5 cells/mL, Tag$^+$200ΔLuc were adjusted to 1e8 cells/mL in PBS, mixed 1:1 with matrigel (BD Biosciences), and kept on ice until subcutaneous injection of 100 mL into the hind flank of recipient mice using 1 mL insulin syringes (Omnican-Braun). The tumor was set 10-13 days (WR21 and MB49) or 45 days (Tag$^+$200ΔLuc) before ATT.

4.5.7. *In vivo* engraftment and persistence assay

Expanded T cells from BLITC mice or Matahari-BLITC mice were sorted for CD44$^+$CD62L$^+$ (>97%) and 1e6 cells per mouse injected intravenously into albino RagKO mice. Matahari-BLITC cells were injected into male albino RagKO mice. Rluc signals of transferred T cells were measured weekly for the first month, then monthly by bioluminescent imaging. Mice were sacrificed after one month for engraftment analysis or after 3 (CD4) or 6 months (CD8) for persistence analysis. Sacrificed mice were dissected and inguinal, mesenteric, cervical lymph knots and spleen were prepared and homogenised using pre-separation filters (30 µm; Miltenyi Biotec). Cell surface was stained with CD3, CD4, CD8, CD44 and CD62L antibodies in the presence of Fc-blocking antibodies (anti-CD16/32). Quantification of T cell numbers in secondary lymphoid organs was carried out using flow cytometry.

4.5.8. H-Y anti-tumor assay

Albino RagKO mice were challenged with MB49 or WR21 tumor as described in section 4.5.6. After 10-13 days tumor was established. Animals bearing MB49 tumor received intravenously 5e5 ST or LT expanded T cells from Marilyn BLITC mice, that were sorted for CD44$^+$CD62L$^+$ (>97%) on day of ATT. Animals bearing WR21 tumor received intravenously ST and LT expanded T cells from Matahari BLITC mice as described for above for Marilyn BLITC T cells. Mean tumor diameter was determined every two days by calliper measurement and tumor size was calculated as length * width * weight/2. Mice were killed if tumor volume reached 1500 mm^3.

4.5.9. SV40 anti-tumor assay

Albino RagKO mice were challenged with Tag$^+$200ΔLuc as described in (tumor challenge). After 45 days, tumor was established. Meanwhile T cells from BLITC mice were transduced with TCR-I as described in section 4.4.4. and ST or LT expanded. T cells were sorted for Vβ7$^+$ TCR (>97%) and injected intravenously into tumor bearing

mice (1e5 cells/mouse). Mean tumor diameter was determined every two days by calliper measurement and tumor size was calculated as length * width * weight/2. Mice were killed if tumor volume reached 1500 mm^3.

4.6. Statistics

Statistical analysis was performed using the two-tailed t-test for in vivo experiments and two-tailed paired t-test for in vitro experiments. Analyses were carried out by GraphPad Prism 7.0 software (GraphPad Software). P values < 0.05 were considered statistically significant.

4.7. Figures

Figures were designed with PowerPoint (Microsoft) or under a paid subscription with BioRender.com. Graphs and diagrams were created with Prism 8 (GraphPad). FACS Dotplots were obtained using FlowJo 10 (Becton, Dickinson and Company).

5. Results

5.1. Blocking the integrin LPAM-1

5.1.1. Selective inhibition of T cell migration into intestinal tissues by targeting LPAM-1

T cells migrate into the gut via interaction of LPAM-1 (α4β7-integrin) with adhesion molecules present on intestinal endothelial cells of high endothelial venules [113, 114]. The aim of this study was to investigate the therapeutic potential of the LPAM-1 antibody to mitigate gut “on-target, off-tumor” toxicity. During the period of this PhD project, research was published showing that the humanized LPAM-1 antibody shows amelioration in GvHD suffering patients [126]. However, investigation for the therapeutic potential of LPAM-1 antibody regarding the balance between “on-target, off-tumor” toxicity and GvT is still needed. Thus, the administration of LPAM-1 antibody was carried out in tumor bearing mice (Figure 7). For this purpose, our transplantation model consisting of T cell receptor (TCR) transgenic CD4 T cells specific for the minor histocompatibility DBY antigen was used, which is exclusively expressed by all cells in male individuals. Furthermore, the T cells transgenic for an NFAT (nuclear factor of activated T cell)-inducible click-beetle luciferase and a renilla luciferase, in order to allow their activation and migration *in vivo* to be detected simultaneously. These T cells are called Marilyn(ML)-BLITC [92].

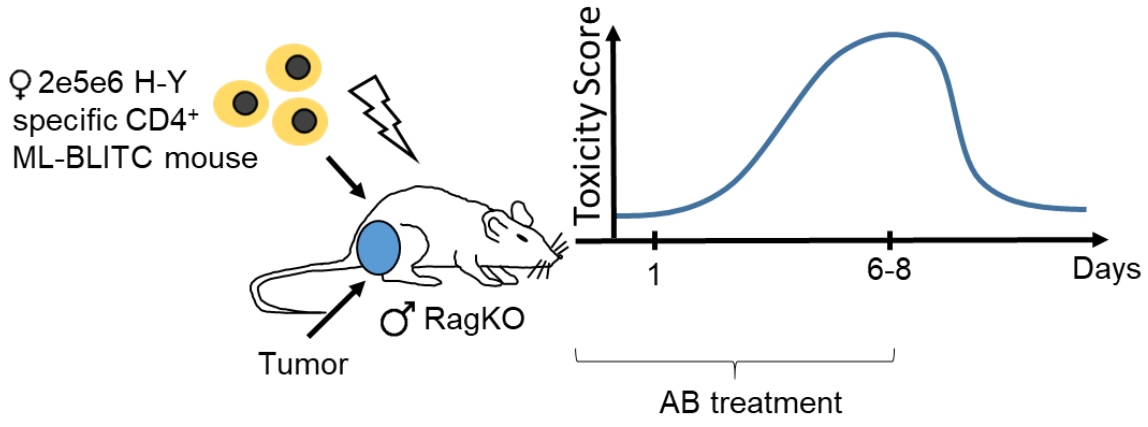

Figure 7. Schema of the experimental setup. HY-tumor bearing mice receive HY-specific CD4 ML-BLITC T cells after sublethal irradiation. After adoptive T cell transfer (ATT), the treated group received a daily injection of LPAM-1 antibody. The mice developed symptoms of severe “on-target, off-tumor” toxicity during the period of 10-12 days, peaking between day 6-8. Toxicity scores were monitored each day.

5.1.2. LPAM-1 antibody treatment diminishes GvHD burden correlating with lower T cell expansion

First of all, the therapeutic potential of the LPAM-1 antibody was analyzed by provoking GvHD in RagKO tumor-free mice. Thus, freshly isolated ML-BLITC cells were injected intravenously (iv) into sublethally irradiated male RagKO mice (see section 4.4.2 and 4.5.2). The first group was treated with a daily dose of 200 µg LPAM-1 antibody over a period of 6 days, whereas the second group received PBS only and the third group served as irradiation control and did not receive T cells. During disease peak (which took place between day 6 and 9 after ATT), less weight loss (Figure 8 A) and reduced GvHD score (Figure 8 B) were observed compared to the control group which received PBS (see section 4.5.2). The BLI measurements of the abdominal region of interest (ROI) showed signals indicating lower and delayed expansion of T cells in the LPAM-1 antibody treated group (Figure 8 C and D). These results demonstrate a diminished “on-target, off-tumor” toxicity burden and reduced T cell expansion associated with the LPAM-1 antibody treatment.

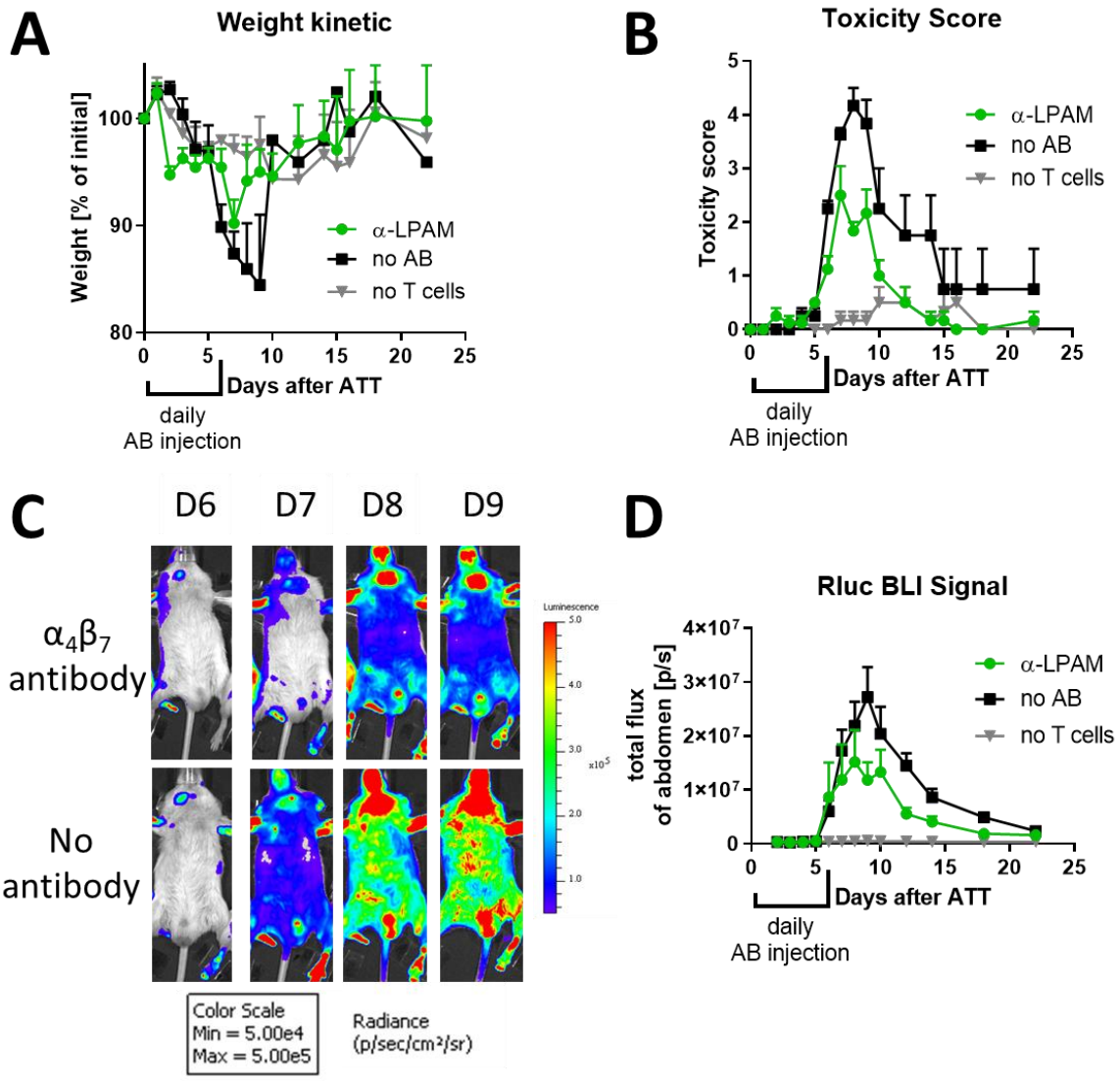

Figure 8. LPAM-1 antibody treatment diminishes "on-target, off-tumor" toxicity compared to non-treated mice. RagKO recipients received a sublethal irradiation followed by an ATT of 5e5 FACS sorted Marilyn cells. The groups were treated daily with 200 µg LPAM-1 antibody (green) or PBS (black) over 6 days or left untreated (gray). A) The graph shows weight loss after ATT over time; mean values ± SEM. B) The graph shows toxicity scores after ATT over time; mean values ± SEM. C) Representative mice of the antibody treated and non-treated group for day 6, 7, 8 and 9 after ATT. D) The graph shows total flux values of the abdomen after ATT over time; mean values ± SEM. Data were generated in 2 independent experiments with n = 3-4 mice. A two-tailed t-test was performed.

5.1.3. LPAM-1 antibody treatment seems to redirect T cell migration to the tumor site resulting in an increased anti-tumor response

Next, the potential of the LPAM-1 antibody was tested, with intent to support the anti-tumor response, which is potentially induced by a reduced gut T cell infiltration and higher intratumoral accumulation. For this purpose, MB49 tumor cells, expressing the DBY antigen, were injected into male recipients. After 10 days, the male tumor-bearing mice received naïve ML-BLITC cells (see section 4.4.2, 4.5.6 and 4.5.8). For these experiments, the treated subjects received daily LPAM-1 antibody injections over

7 days. Subsequently, less weight loss (Figure 9 A) and a reduced GvHD score (Figure 9 B) for the treated group compared to the untreated group was observed, confirming the impact of the LPAM-1 antibody at disease onset. Interestingly, in comparison, the tumor growth in antibody treated mice turned out slower, but tumors relapsed three days after antibody discontinuation (Figure 9 C). Also, a higher ML-BLITC/tumor cell ratio in the tumor tissue of antibody treated mice ensued (Figure 9 D), indicating an increased tumor infiltration (see section 4.4.1). In addition, higher BLI signals in the tumor region of the antibody treated mice compared to control mice were observed (Figure 9 E) (see section 4.5.1). This could be seen especially during the peak of "on-target, off-tumor" toxicity on day 6 and 7 (Figure 9 F) supporting the FACS data. Mice were sacrificed due to toxicity or tumor burden and T cell infiltration into lymph nodes and tumor tissue was analyzed. The frequency of ML-BLITC cells in antibody-treated mice was lower in mesenteric (mLN) and draining lymph nodes (dLN) in comparison to the control mice (Figure 9 G). The infiltration into tumor inguinal lymph nodes (iLN) was comparable in both groups (Figure 9 G). These results may support the hypothesis that specific antibody blocking of the gut-homing integrin $\alpha4\beta7$ reduces T cell infiltration into the intestines, ameliorates "on-target, off-tumor" toxicity and results in redirection of adoptively transferred T cells from the mLNs to the tumor tissue, reducing tumor burden in this minor mismatch model.

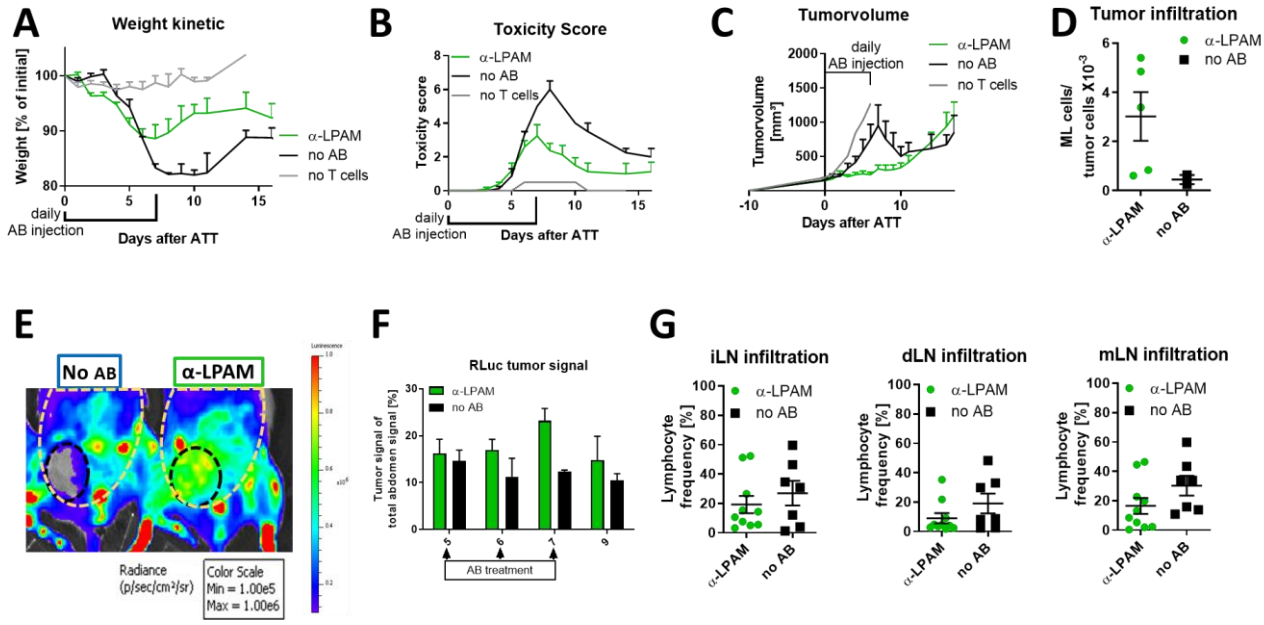

Figure 9. "on-target, off-tumor" toxicity vs. GvT. RagKO recipients got a sublethal irradiation followed by an ATT of 5e5 FACS sorted Marilyn cells. The groups were treated daily with 200 µg LPAM-1 antibody or PBS over 7 days. The groups consisted of LPAM-1 -antibody (green), PBS (black,) and control (gray). A) Showing the weight loss

after ATT over time; mean values ± SEM. B) Showing toxicity scores after ATT over time; mean values ± SEM. C) Showing the tumor growth after ATT over time; mean values ± SEM. D) Ratio of ML cell count and tumor cell count within tumor tissue; mean values ± SEM. E) Showing exemplary mice of the antibody treated and non-treated group. The tumor tissue is encircled. F) Quantification of the flux values of the total abdomen and tumor region. Showing the percentage of the tumor signal within the abdomen region. G) Showing lymphocyte frequencies of inguinal, draining and mesenteric lymph nodes at day of death. Combined data were generated in 2 independent experiments; a4b7-antibody n = 6-10; PBS n = 2-7. A two-tailed t-test was performed.

5.1.4. Previous data were not reproducible with purchased LPAM-1 antibody

In order to analyse the pharmacokinetics of the LPAM-1 antibody, experiments with higher antibody concentration were performed. In order to overcome delay of experiments due to time-intensive self-production of the antibody (thankfully done by the antibody-facility of the *Deutsches Rheuma-Forschungszentrum*, Berlin Germany), the LPAM-1 antibody was purchased from BioXcell (West Lebanon USA). Self-production and purchased antibodies were both produced from the same clone DATK32.

Unfortunately, the previous data were not replicable with the purchased antibody. Weight loss (Figure 10 A) and “on-target, off-tumor” toxicity (Figure 10 B) were not ameliorated compared to the non-treated group, even with doubled concentration. All animals suffered comparably from “on-target, off-tumor” toxicity, showed no tumoral T cell infiltration indicated by a lack of signal in BLI measurements (Figure 10 C) and consequently presented similar tumor outgrowth (Figure 10 D). These results were comparable in two independent experiments. In summary, these findings contradict the previous results, leading to the conclusion that there is a difference between the self-produced and the purchased antibody.

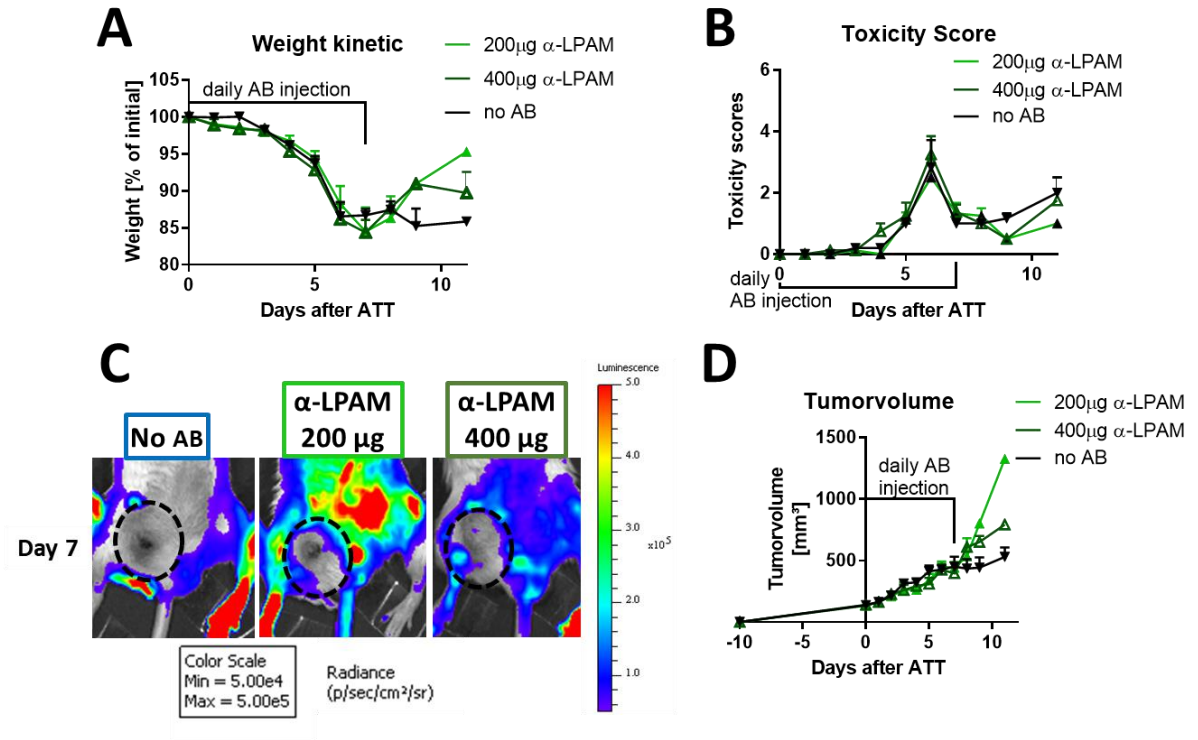

Figure 10. Previous "on-target, off-tumor" toxicity vs. GvT results were not reproducible with purchased LPAM-1 antibody. RagKO recipients received a sublethal irradiation followed by an ATT of 5e5 FACS sorted Marilyn cells. The groups were treated daily with 200 ug LPAM-1-antibody or PBS over a period of 10 days. LPAM-1-antibody 200 µg (green), of LPAM-1- antibody 400 µg (dark green), PBS (black). A) The graph shows weight loss after ATT over time; mean values ± SEM. B) The graph shows toxicity scores after ATT over time; mean values ± SEM. C) Exemplary Renilla luciferase signals of mice treated with antibody and non-treated group on day 7. D) The graph shows the tumor growth after ATT over time; mean values ± SEM. Data were generated in 2 independent experiments with n = 4-5 mice. A two-tailed t-test was performed.

5.1.5. Mass spectrometry analysis reveals same peptide constancy between purchased and self-produced LPAM-1 antibody

In cooperation with Dr. Philipp Mertins

The missing effect of the purchased LPAM-1 antibody compared to the self-produced equivalent may be due to different peptide sequences or composition. To investigate the peptide constancy between purchased and self-produced antibody, triplets of both samples were prepared and then submitted to the mass spectrometry facility (Dr. Philipp Mertins, *Max-Delbrück-Centrum für Molekulare Medizin*, Berlin Germany) (see section 4.2.1). After performing mass spectrometry analysis, a list of the contained peptides was obtained (see full list in appendix Table 2). Both antibodies contained overall the same peptides with only five exceptions (Table 1). These exceptions appeared only in the self-produced antibody and belong to different organisms like *sus scrofa* or *bos taurus*. Aside from that, the listed peptides were classified by the

mass spectrometry analysis as contamination, which is already deposited as known pollution of peptide analysis. These contaminations in the self-produced antibody might originate from hybridoma culture and less purification present in the industrially produced antibody, suggesting that these findings show no functional peptide difference between the purchased and the self-produced antibody.

Table 1. Summary of differently detected peptides by mass spectrometry analysis. Sample were prepared by Andreas Heimann (AH), mass spectrometric analysis was performed by Corinna Friedrich from Philipp Mertins Proteomic Facility.

Protein IDs	trivial name	Sequence coverage [%]	Mol. weight [kDa]	Intensity	bought alpha4beta7 antibody			self-produced antibody		
CON__P00761	Trypsin (Pig)	*19,5*	*24,409*	*3004000000*	*2553500000*	*0*	*0*	*131420000*	*46864000*	*272210000*
CON__ENSEMBL:ENSBTAP00000011227	Bos taurus protein	*15,3*	*14,629*	*485360000*	*0*	*0*	*0*	*215970000*	*166290000*	*103100000*
CON__Q95M17	Bos taurus protein	*3,2*	*52,129*	*301220000*	*0*	*0*	*0*	*132150000*	*57618000*	*111450000*
CON__P00978	AMBP Bos taurus	*3,4*	*39,234*	*120000000*	*0*	*0*	*0*	*49683000*	*46864000*	*23451000*
CON__P01030;CON__ENSEMBL:ENSBTAP00000007350	unknown	*1*	*192,79*	*39989000*	*0*	*0*	*0*	*21493000*	*11464000*	*7032800*

5.1.6. LPAM-1 antibody added with endotoxin and endotoxin only leads to diminished tumor growth and enhanced GvHD burden

Previous quality analysis of the self-produced antibody suggested endotoxin contaminations within the self-produced antibody. In order to test whether endotoxin level might have affected the ATT effect, mice were treated with low doses of endotoxin (Lypopolysaccharides, LPS) or in combination with purchased LPAM-1 antibody or only with the purchased antibody. Endotoxin treated mice showed an accelerated weight loss and earlier “on-target, off-tumor” toxicity symptoms upon first injection (Figure 11 A). This effect was also seen in some previous experiments with the self-produced antibody. Furthermore, endotoxin treated mice showed a plainly decreased tumor growth (Figure 11 B) and visualized by BLI a stronger T cell infiltration into tumor tissue (Figure 11 C-D) compared to the antibody group. There were no differences between endotoxin alone or the combination of LPAM-1 antibody and endotoxin. In summary, these results suggest that the previously described effects of the LPAM-1 antibody on ATT efficiency might have resulted from low doses of endotoxin in the self-produced antibody.

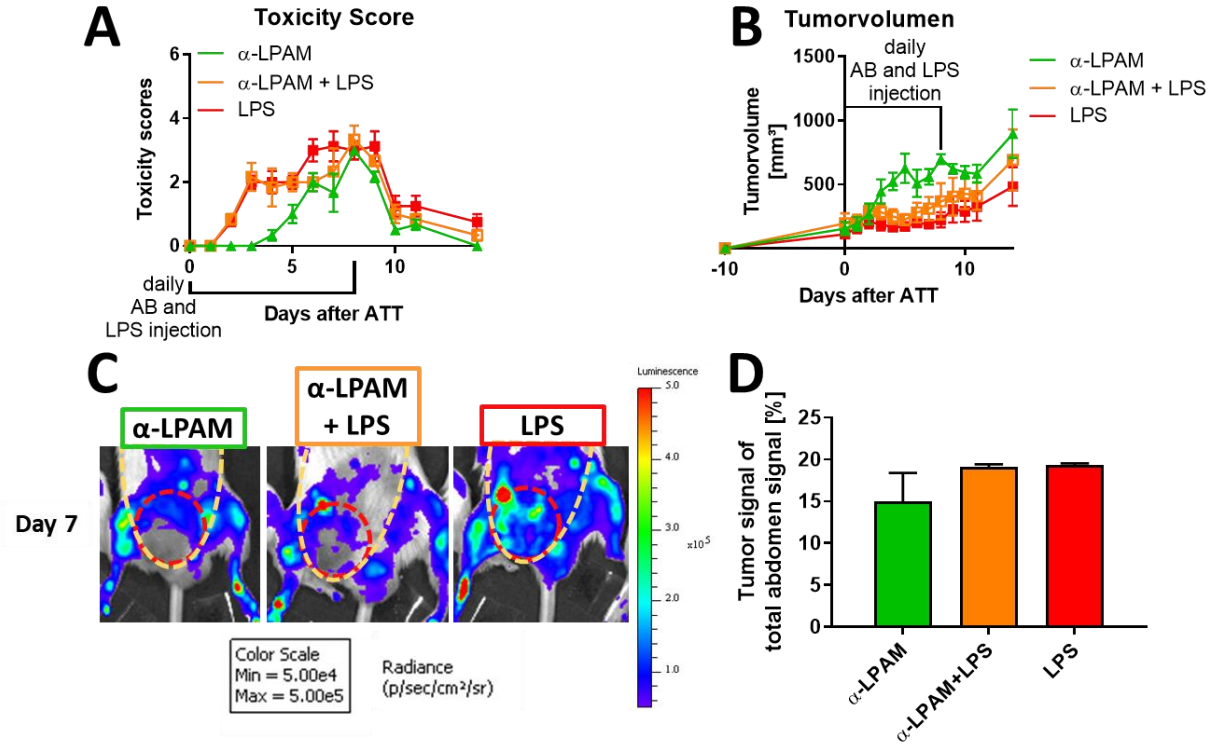

Figure 11. Treatment with endotoxin (LPS) leads to decelerated tumor growth independent of LPAM-1 antibody. RagKO recipients received a sublethal irradiation followed by an ATT of 5e5 FACS sorted Marilyn cells. The groups were treated daily with 200 µg LPAM-1- antibody, 200 µg LPAM-1- antibody + 0,5 µg LPS or 0,5 µg LPS only over 10 days. LPAM-1 antibody (green), of LPAM-1 antibody + LPS (orange), LPS (red). A) The graph shows toxicity scores after ATT over the time; mean values ± SEM. B) The graph shows the tumor growth after ATT over time; mean values ± SEM. C) Exemplary Renilla luciferase signals of mice treated with antibody and non-treated group on day 7. D) Quantification of the flux values of the total abdomen and tumor region, showing the percentage of the tumor signal within the abdomen region; mean values ± SEM. Data were generated of 1 experiment with n = 3. A two-tailed t-test was performed.

5.2. T cell expansion

5.2.1. Ameliorated ATT outcome by optimized T cell expansion

For ATT, manufacturing of T cells including expansion is necessary. Not every T cell culture is suitable for an ATT. Dropouts in the manufacturing process of T cells have been described. Optimization strategies for ATT outcome were implemented, which on the adaption of the needed T cell culture, promoting central memory T cells (Tcm) with high effector potential and longevity. In cooperation with Dr. Stefanie Herda the clinically established cytokine combination IL7/IL15 was thus compared with a new combination IL15/IL27 and expanded T cells for over four weeks (Figure 12) (see section 4.3.1).

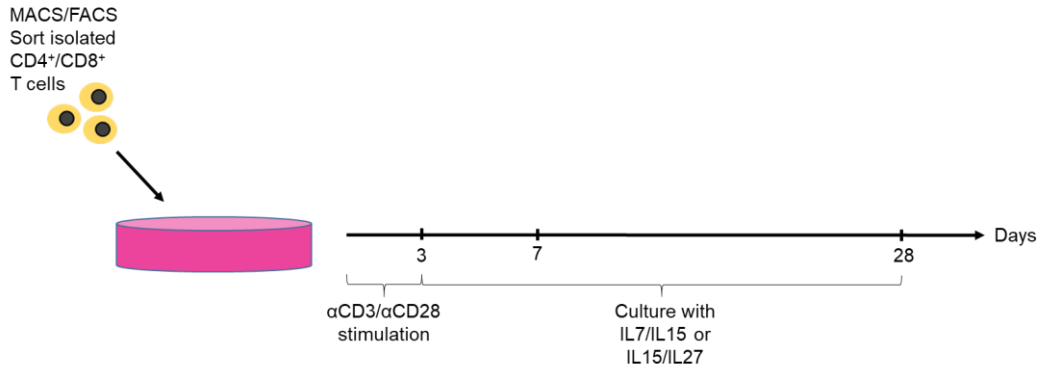

Figure 12. Overview schema of performed T cell culture. Isolated T cells (CD4 or CD8) were stimulated by incubation on an anti-CD3/CD28 coated 6-well plate for three days. Further T cell expansion was performed by expanding T cells with IL7/15 or IL15/27 over a period of four weeks.

5.2.2. A novel cytokine combination enhances granzyme A and B expression in CD8 T cells and improves T cell expansion of Tcm cells

Previous research suggests that IL27 enhances expression of granzyme B in CD8 T cells and promotes the early differentiation of CD4 T cells into TH1 [175, 177, 193]. To generate T cells with increased effector function for ATT, T cells were expanded in an initial experiment with IL-27, which lead to three times more granzyme B expression than with IL2 only (Figure 13 A). However, the T cells did not expand properly (Figure 13 A; Figure 14 A and D – gray line). To generate long-term surviving T cells with high effector potential and Tcm phenotype, IL27 was combined with IL15. IL15 promotes Tcm differentiation and is used with IL7 to generate memory stem T cells from naïve precursors [134]. Consequently, granzyme B expression of MACS sorted CD8 and

CD4 T cells was tested after one week of axpansion with IL7/IL15 or IL15/IL27 (see section 4.3.1 and 4.4.3). A tendency for a higher granzyme B expression in IL15/IL27 expanded CD8 T cells compared to IL7/IL15 expanded cells (Figure 13 B) became apparent but did not reach a significant level. This difference was not seen in CD4 T cells.

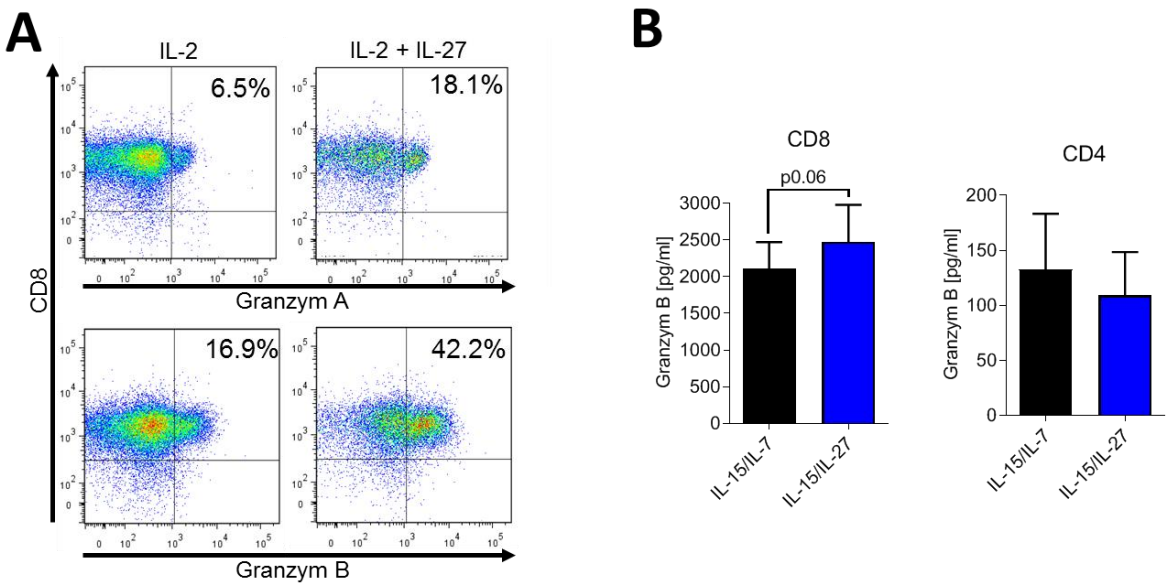

Figure 13. Slightly enriched granzyme B expression for IL15/IL27 expanded CD8 T cells compared to IL7/IL15 culture. Polyclonal CD8 or CD4 T cells (TC) were isolated from CB57BL/6J (WT) mice using MACS technology and activated via anti-CD3, anti-CD28 and IL2 for 72 hours. TCs were further cultured with the indicated cytokines. T cells were re-stimulated 5 days after initial stimulation with antiCD3 and antiCD28 for 4 hours. A) CD8 T cells were stained with intracellular granzyme A and B antibodies and detected via flow cytometry. Representative counter plots out of 2 independent experiments with n=2 performed by Stefanie Herda (SH) B) Granzyme B was measured via ELISA for CD8 by SH and CD4 T cells by AH. Mean data ± SEM from 5-8 independent experiments with pooled T cells of at least 2 mice. A two-tailed paired t-test was performed.

Furthermore, the growth kinetics and Tcm ratio were analyzed. IL2/IL7 expanded CD8 T cells served as negative control condition and failed to expand within the first weeks whereas IL7/IL15 and IL15/IL27 expanded CD8 T cells expanded massively, reaching a plateau after two-three weeks (Figure 14 A). Thereby, the IL15/IL27 expanded CD8 T cells multiplied the most resulting in significantly more T cells in comparison to IL7/IL15 and both conditions resulted in significantly more T cells after four weeks (Figure 14 B). The frequency of the favourable CD44+CD62L+ Tcm phenotype was comparable between both cytokine combinations after one week (Figure 14 C) and remained stable during culture period. In contrast to CD8 T cells, the CD4 T cells expanded with IL2/IL7 showed similar results as the IL7/IL15 culture. However, the IL15/IL27 expanded CD4 T cells showed improved expansion as seen in CD8 T cells,

while declining after three weeks of expansion (Figure 14 D). This results in comparable T cell numbers between day 7 and day 28 of T cell expansion for each culture condition (Figure 14 E). All culture conditions implemented a prominent CD4 Tcm phenotype, albeit less dominant compared to CD8 T cells (Figure 14 D).

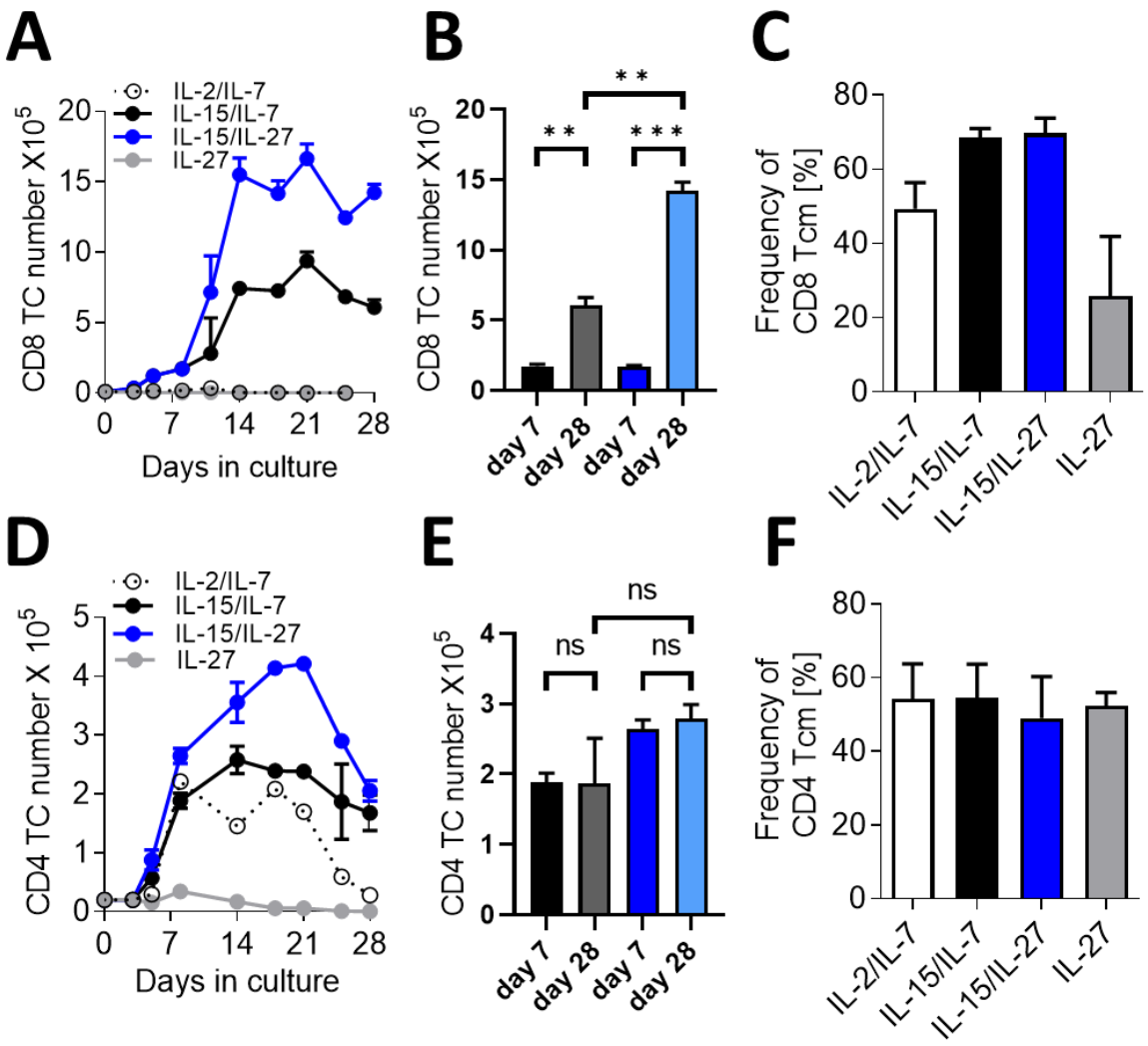

Figure 14. T cell number increases significantly more in IL15/IL27 culture compared to IL7/IL15 expansion. T cell expansion kinetics with different cytokine combinations. Polyclonal CD8 T cells (TC) were isolated from CB57BL/6J (WT) mice using MACS technology and activated via anti-CD3, anti-CD28 and IL2 for 72 hours. TCs were further expanded with the indicated cytokines. The quantification and phenotypical analysis were conducted by flow cytometry. A) Growth kinetics of CD8 TC are displayed in the line diagrams or B) total numbers on day 7 or day 28 as bar carts. CD4 and CD8 subpopulations were further characterized by CD44+ and CD62L+. C) CD8 Tcm frequency at culture-day 7-8 are illustrated in bar carts. D) Growth kinetics of CD4 TC as line diagrams or E) total numbers on day 7 or day 28 as bar carts. F) CD4 Tcm frequency at culture-day 7-8 as bar carts. Data generated by SH, data analysis performed by AH. Mean data ± SEM from 3-5 independent experiments with pooled T cells of at least 2 mice. ***$p < 0.001$, **$p < 0.01$, *$p < 0.05$ A two-tailed paired t-test was performed.

5.2.3. IL15/IL27 expanded T cells show similar central memory/memory stem cell like phenotype and *in vitro* cytokine expression

Each cytokine could induce an individual functional pathway with, for example, differences in developed phenotype or effector potential of T cells. Granzyme B expression was slightly increased by the IL15/IL27 culture in CD8 T cells, but regarding the impact upon the phenotype similar Tcm frequencies for CD8 and CD4 T cells were observed. To investigate the possible influence of IL15/IL27 on a memory stem cell like (Tscm) phenotype and further effector function, Tscm surface markers CD122, Sca1, Bcl-2 and CXCR3 or re-stimulated expanded T cells and their cytokine production via flow cytometry were analyzed [140, 202] (see section 4.3.1 and 4.4.1).

The development of the above-mentioned Tscm markers proved comparable between IL7/IL15 and IL15/IL27 expanded polyclonal CD8 T cells, except for Bcl-2, which turned out to be slightly higher expressed in IL15/IL27 expanded T cells (Figure 15 A). Next, after one week of culturing upon re-stimulation, the functional capacity of the differently expanded CD8 T cells were tested with anti-CD3 and anti-CD28 for four hours (see section 4.3.3). IL15/IL27 cultured CD8 T cells were significantly lower IFNγ and IL2 positive and significantly higher TNFα positive compared to IL7/IL15 expanded T cells. However, the differences were negligible (Figure 15 B and C).

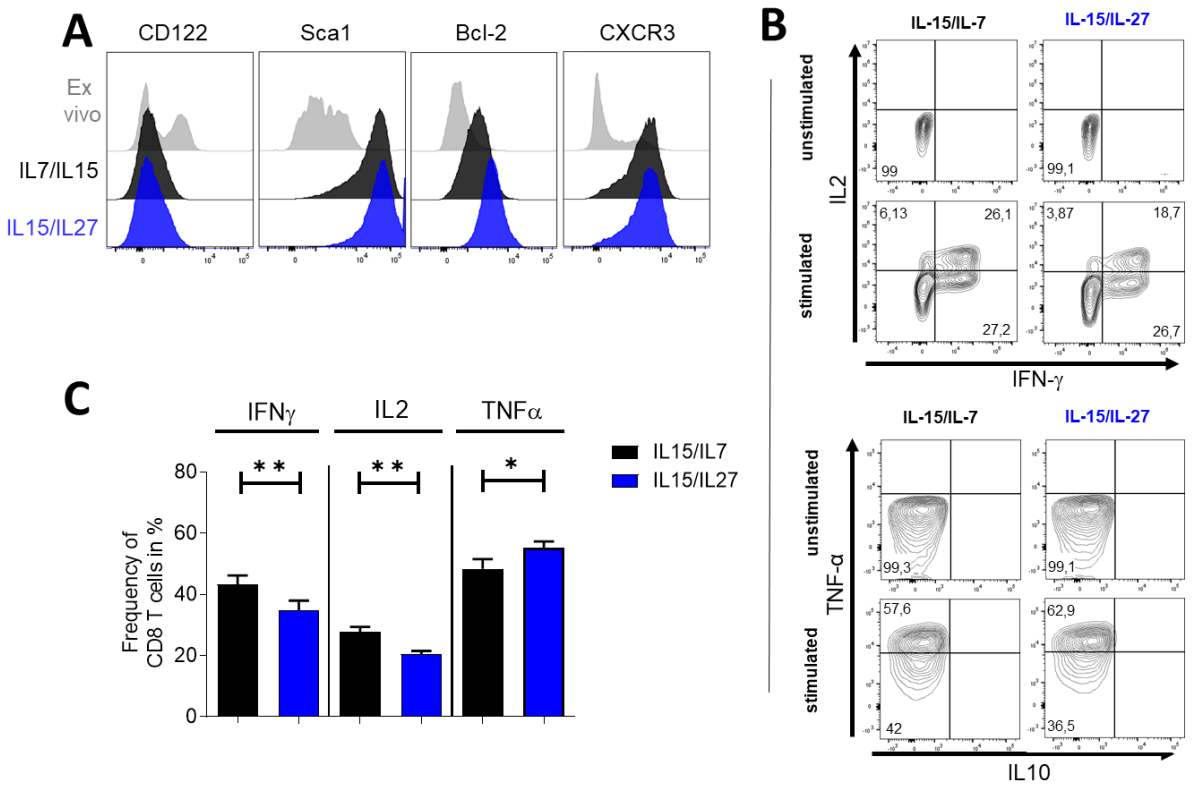

Figure 15. *In vitro* properties of CD8 T cells are comparable between IL7/IL15 and IL15/IL27 culture. Polyclonal CD8 T cells isolated from C5BL/6 mice were activated via antiCD3, antiCD28 and IL2 for 72 hours and further expanded with IL7/IL15 or IL15/IL27 for one week. For analysis of effector function IL7/IL15 or IL15/IL27 expanded CD8 T cells were re-stimulated with antiCD3 and antiCD28 for 4 hours. The phenotypical and measured cytokine expression were gained via flow cytometry. A) The CD8 Tcm subpopulation resulting from the T cell culture was further characterized by CD122, Sca-1, Bcl-2 and CXCR3 and compared to ex vivo CD8 Tcm cells. B) Representative FACS plots of pregated CD3+CD8 cells. C) Quantified expression of IFN-γ, IL-2 or TNF-α from IL7/IL15 versus IL15/IL27 expanded CD8 T cells. Mean data ± SEM from 2 independent experiments with n = 5. $^{**}p < 0.01$, $^{*}p < 0.05$. A two-tailed paired t-test was performed

In addition, the *in vitro* properties of isolated polyclonal CD4 T cells were analyzed and similar results were found as in CD8 T cells. The expression of Tscm markers was similar between IL7/IL15 and IL15/IL27 expanded CD4 T cells, beside CD122, which was less expressed in IL15/IL27 than in IL7/IL15 expanded T cells (Figure 16 A). The re-stimulation of CD4 T cells after one week of expanding did not result in a significant difference between the culture conditions for IFNγ, IL2 or TNFα. IL-10 was not detectable for any cytokine condition (Figure 16 B and C). Taken together, these data suggest that the *in vitro* properties with characteristic features related to Tcm and Tscm were similar between IL7/IL15 and IL15/IL27 expanded T cells.

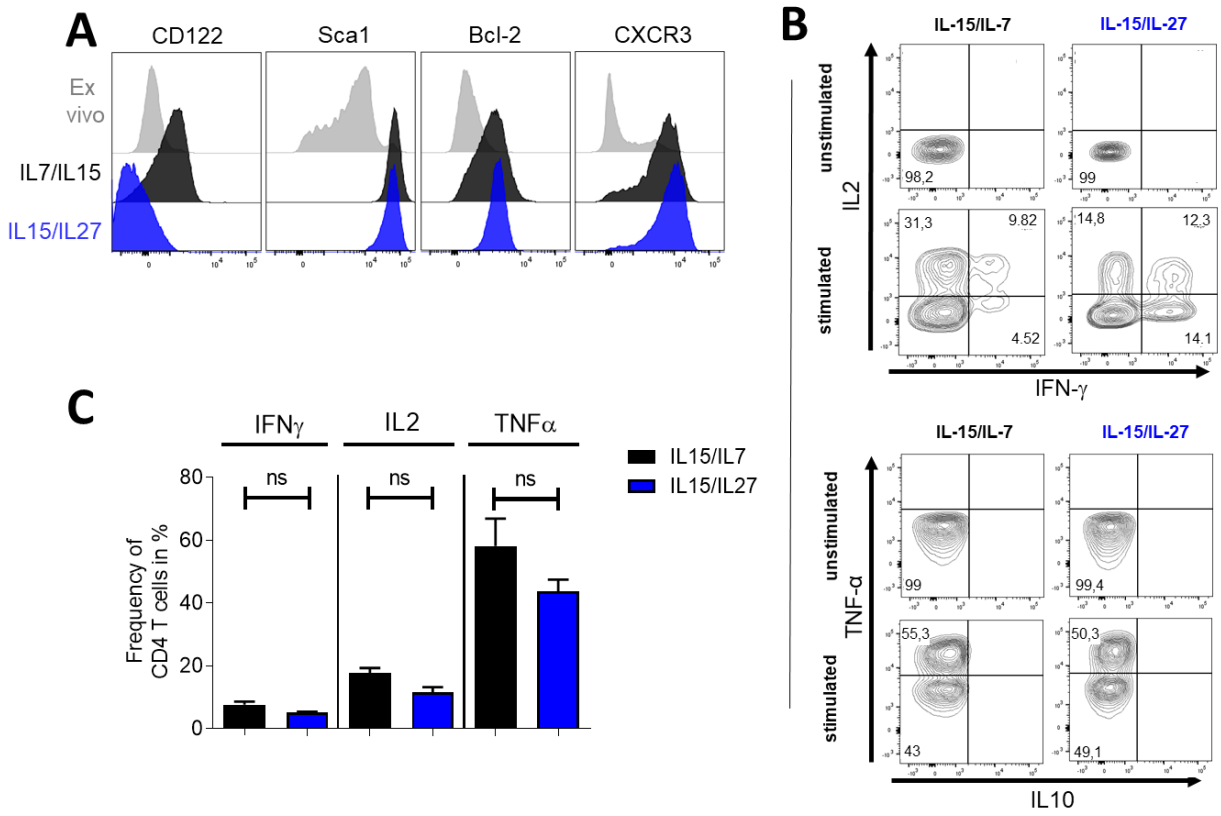

Figure 16. ***In vitro*** **properties of CD4 T cells are comparable between IL7/IL15 and IL15/IL27 culture.** Polyclonal CD4 T cells isolated from C57BL/6 mice were activated via antiCD3, antiCD28 and IL2 for 72 hours and further expanded with IL7/IL15 or IL15/IL27 for one week. For analysis of effector function IL7/IL15 or IL15/IL27 expanded CD4 T cells were re-stimulated with antiCD3 and antiCD28 for 4 hours. The phenotypical and measured cytokine expression were gained via flow cytometry. A) The CD4 Tcm subpopulation resulting from the T cell culture was further characterized by CD122, Sca-1, Bcl-2 and CXCR3 and compared to ex vivo CD4 Tcm cells. B) Representative FACS plots of previously gated CD3+CD4 cells. C) Quantified expression of IFN-γ, IL-2 or TNF-α from IL7/IL15 vs. IL15/IL27 expanded CD4 T cells. Mean data ± SEM from 2 independent experiments with n = 5. A two-tailed paired t-test was performed

5.2.4. IL7/IL15 and IL15/IL27 expanded Tcm cells share similar transciptome signatures

In cooperation with Dr. Benedikt Obermayer

In order to elucidate the mechanisms behind the improved *in vitro* expansion and enhanced granzyme expression of IL15/IL27 expanded CD8 T cells, the comparability of the transcriptome signatures of differently expanded Tcm cells (Figure 17 A top) and the longitudinal changes between the transciptome signatures of differently expanded Tcm cells were examined (Figure 17 A bottom). Tcm cells were generated by isolated murine CD4 or CD8 T cells and FACS sorted (Figure 17 B) on week 1 (short-term expansion, ST) or on week 3 (CD4) respectively week 4 (CD8, long-term expansion, LT) (see section 4.1.1, 4.3.1 and 4.4.2). The FACS sorted T cells were gated as shown in Figure 17 B. After RNA isolation the samples were submitted to the genomic facility

(Dr. Tomasz Zemojtel, *Berlin Institute of Health*, Berlin Germany) (see section 4.1.6). Subsequently, the generated sequencing data were then analyzed in collaboration with the bioinformatics facility (Dr. Dieter Beule, *Berlin Institute of Health*, Berlin Germany). Thereupon, differential expression analysis of 22050 protein-coding genes was performed using DESeq2 [197] (see section 4.1.7).

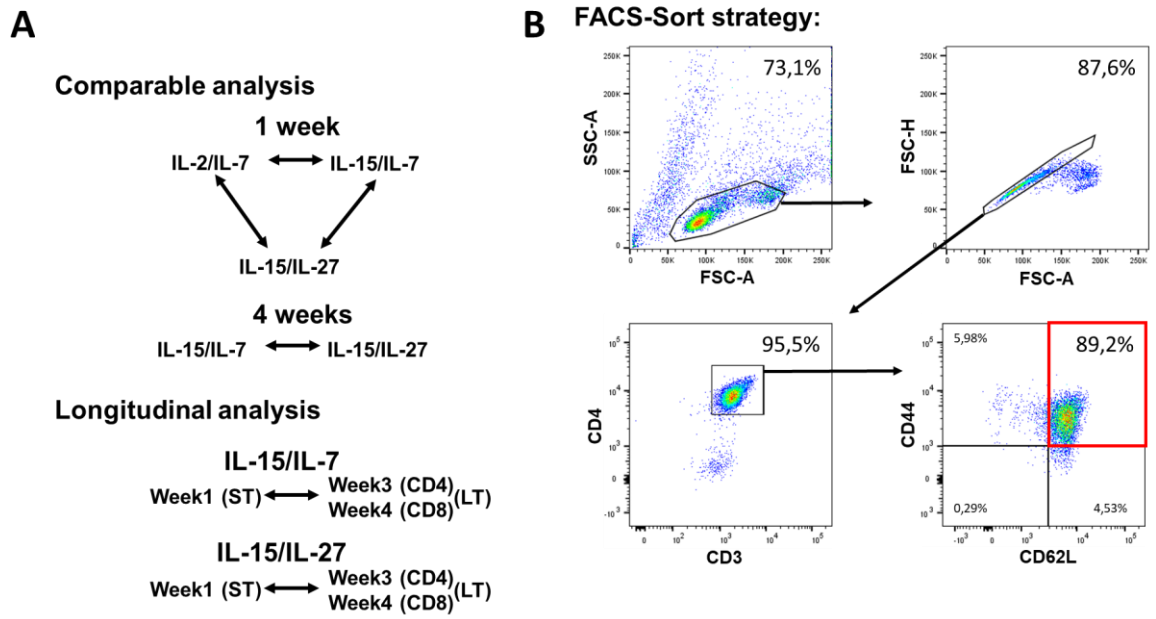

Figure 17. Schematic overview of transcriptomic analysis and Tcm-gating strategy A) Overview schema of performed transcriptome analysis. B) Representative FACS plot of the used FACS sort gaiting strategy.

As expected, the effector driving cytokine combination IL2/IL7, which was used as negative control condition, showed striking differences in gene expression, compared to the other culture conditions. Surprisingly no significant difference in gene expression between IL7/IL15 and IL15/IL27 expended Tcm cells was observed. The transcriptome signatures from both cytokine combinations clustered strongly together, which is clearly represented in the hierarchical clustering (Figure 18 A) and also in the principal compound analysis (PCA – Figure 18 B).

Hierarchical clustering and PCA for CD4 Tcm cells resulted in similar distinct clusters as in CD8 Tcm cells, without significant differences in gene expression between IL7/IL15 and IL15/IL27 expanded CD4 T cells (Figure 18 C and D). These results indicate that there is no transcriptional difference between IL7/IL15 and IL15/IL27 expanded Tcm cells.

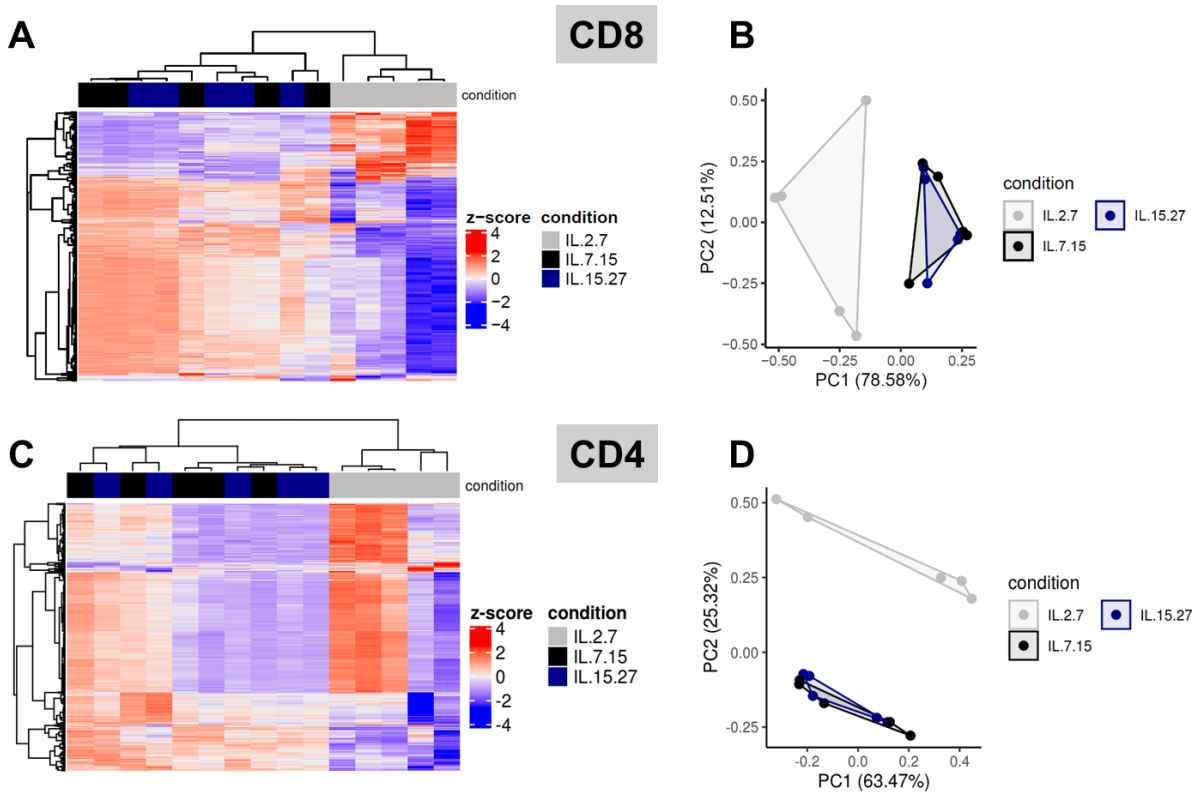

Figure 18. Transcriptome signatures of IL7/IL15 and IL15/IL27 do not show differently expressed genes. RNA sequencing of polyclonal CD8 or CD4 Tcm cells expanded with IL2/IL7, IL7/IL15 or IL15/IL27. The data are presented as a clustering analysis of the gene expression. A) Hierarchical clustering of differently expanded Tcm cells. Red and blue colors indicate increased and decreased expression differential genes (adj. P < 0.05, absolute log2 fold change > 0.5). Each column represents a sample and each row a gene. B) Principal component analysis (PCA) of these genes for CD8 Tcm cells. C) As described for A, but here for CD4 Tcm cells. D) Principal component analysis (PCA) of these genes for CD4 Tcm cells. RNA isolation was performed by AH, sequencing was performed by the BIH Genomic facility and data evaluation was performed by Benedikt Obermayer (OB). The result is representative of 4-5 independent culture experiments using the RNA from FACS sorted Tcm.

5.2.5. Longitudinal transcriptome signatures revealed differences between short-term and long-term expanded Tcm cells

In cooperation with Dr. Benedikt Obermayer

The next step was to compare the transcriptome signatures of ST and LT expanded Tcm cells to identify longitudinal transcriptional alterations, which are suspected of having a functional impact on LT Tcm cells. 2612 differently expressed genes between ST vs. LT CD8 T cells (adjusted P < 0.05 and fold changes > 0.5) were identified and visualized by hierarchical clustering and PCA (Figure 19 A and B). 60.2 % of these genes (1573) were down-regulated and 39.8 % (1039) were up-regulated. The majority of these genes showed moderate expression alterations between 1.5 and 2.0-fold.

The CD4 Tcm cells differed between ST and LT culture in 1511 genes with 38.4 % (580) up-regulated and 61.6 % (931) down-regulated as shown by hierarchical

clustering and PCA (Figure 19 C and D). These findings suggest a transcriptional impact of long-term expansion on Tcm cells.

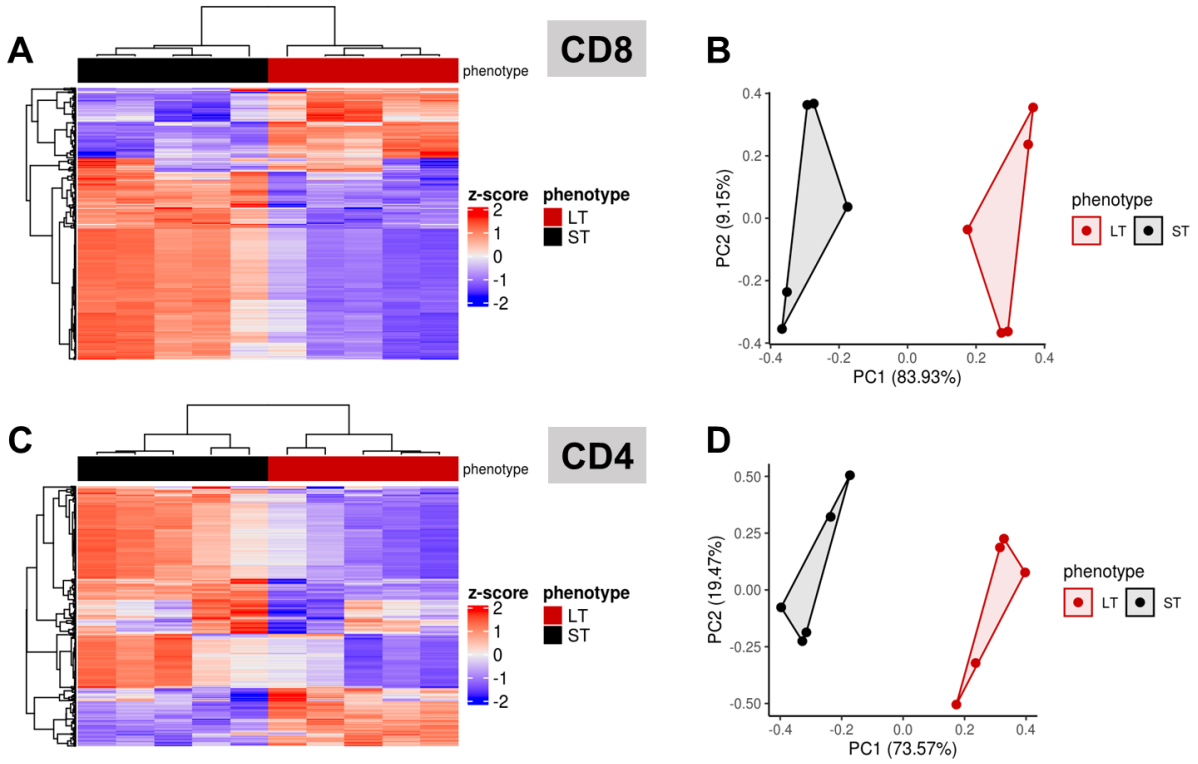

Figure 19. Significant differences in gene expression of short-term compared to long-term expanded Tcm cells. RNA sequencing of polyclonal CD8 or CD4 Tcm cells generated via ST or LT expansion with IL7/IL15. The data are presented as a clustering analysis of the gene expression. A) Hierarchical clustering of differently expanded Tcm cells. Red and blue colors indicate increased and decreased expression of the 2790 differential genes (adj. $P < 0.05$, absolute log2 fold change > 0.5). Each column represents a sample and each row a gene. B) Principal component analysis (PCA) of these genes for CD8 Tcm cells. C) As described for A, but here for CD4 Tcm cells. D) Principal component analysis (PCA) of these genes for CD4 Tcm cells. RNA isolation was performed by AH, sequencing was performed by the BIH Genomic facility and data evaluation was performed by OB. The result is representative of 4-5 independent culture experiments using the RNA from FACS sorted Tcm.

5.2.6. Long-term Tcm cells have a maintained Tcm/Tscm transcriptome signature

In cooperation with Dr. Benedikt Obermayer

To investigate whether longitudinal differences in gene expression have functional effects on LT expanded Tcm cells, the sequencing data were compared to transcriptome signatures from published data sets. For this purpose, the focus was placed on IL7/IL15 expanded T cells, due to the fact that no significant transcriptional differences were found, and the fact that the combination of IL7/IL15 has already been established in some clinical expansion protocols and for reasons of comparability, as some drawn data sets have also been expanded with IL7/IL15 [134, 195]. The transcriptome profile of ST and LT expanded CD4 or CD8 Tcm cells was compared

with published gene sets from naturally occurring CD8 T cell subsets and differently induced Tscm [134, 139-141, 195] Unsupervised hierarchical clustering and PCA using the gene set of Gattinoni et al. revealed that both ST and LT CD8 Tcm cells were closely related to annotated CD8 Tcm as well as naturally occurring and induced CD8 Tscm (Figure 20 A and B). In Pulko's dataset (GSE80306), Tscm were originally labelled as memory T cells with naïve phenotype [TMNP], and in Cieri's dataset (GSE41909) as naïve-derived T cells [TTN]. ST and LT CD4 Tcm cells consistently grouped closely with annotated CD4 Tcm and naturally or Notch-induced CD4 Tscm subsets (Figure 20 C and D). The grouping was independent of murine [140] or human [196] T cell origin. Taken together, these data suggest that even while there are significant differences between ST and LT transcriptome signatures, comparing hierarchical clustering and PCA with published data, they stay closely within annotated Tcm and Tscm cells with a stable functional phenotype.

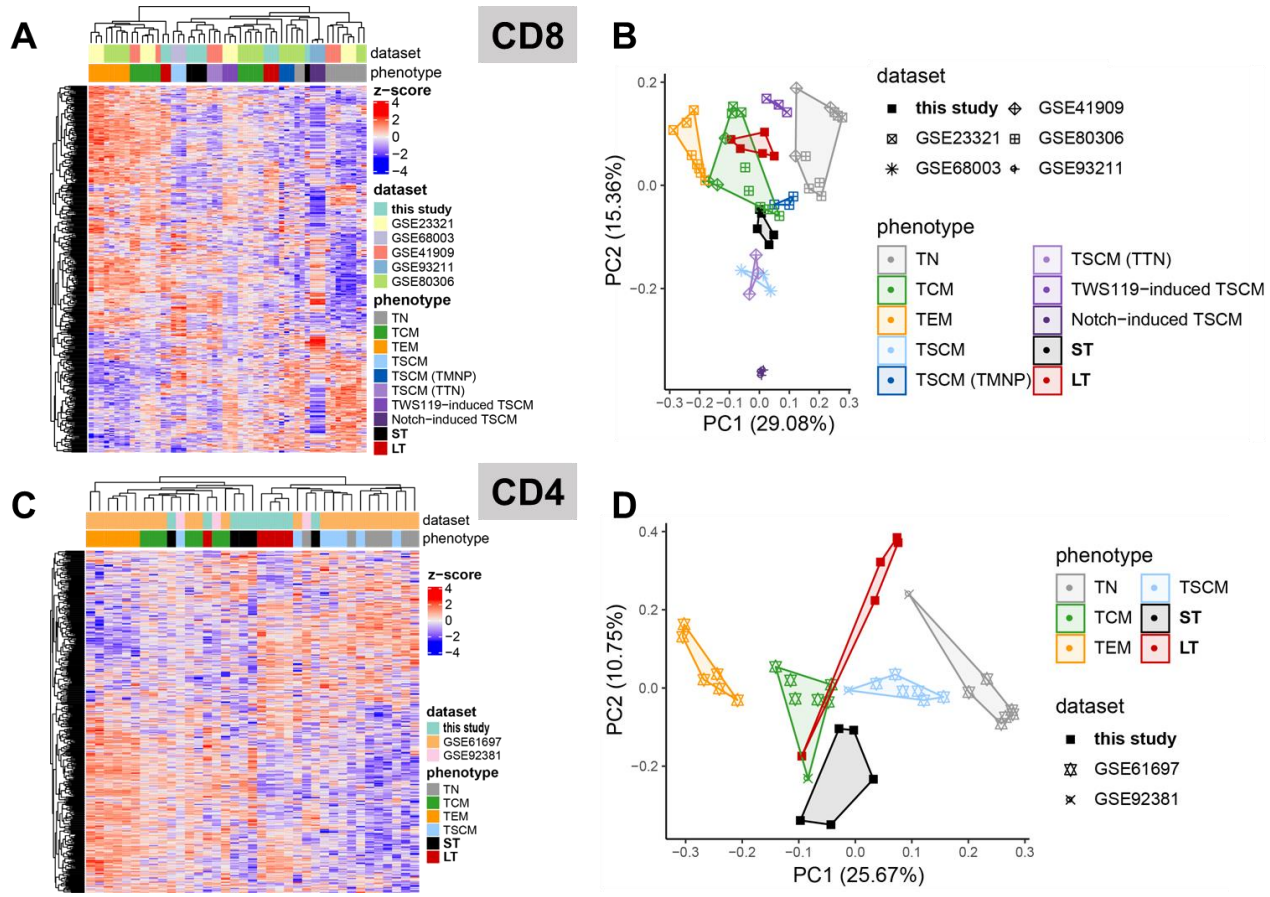

Figure 20. Short-term and long-term expanded Tcm cells show similar transcriptome signatures within annotated Tcm/Tscm spectrum. Comparable analysis of RNA sequencing of polyclonal CD8 and CD4 Tcm cells generated via ST and LT IL7/IL15 culture with published data of Tcm and Tscm cells. RNA isolation was performed by AH, sequencing was performed by the BIH Genomic facility and data evaluation was performed by OB. A) Hierarchical clustering of ST and LT CD8 Tcm, IL7/IL15-generated Tscm cells (Cieri et al., GSE41909), naturally occurring CD8 T cell subsets (Gattinoni et al., GSE23321), TWS119-enriched Tscm (Sabatino et al., GSE68003) and

Notch-induced Tscm (Kondo et al., GSE93211) based on 852 genes described by Gattinoni et al., from which 427 genes were expressed in all data sets (red, up-regulated genes; blue, down-modulated genes). Each column represents a sample and each row represents a gene. B) Principal component analysis (PCA) of all datasets of CD8 T cells. C): Hierarchical clustering of ST and LT expanded CD4 Tcm, naturally occurring CD4 T cell subsets (Takeshita et al., GSE61697) and Notch-induced Tscm (Kondo et al., GSE92381) based on 447 of the Gattinoni et al. genes that are expressed in all data sets. Each column represents a sample and each row a gene. D) Principal component analysis (PCA) of all data sets of CD4 T cells.

5.2.7. *In vitro* functional properties of CD8 and CD4 T cells are retained by long-term expansion

For the purpose of identifying gene expression patterns that elucidate biological functions or pathways affected in LT CD8 and CD4 T cells, GO term enrichment analysis was performed in order to assign the differently expressed genes to selected biologically meaningful gene ontology (GO) categories (Figure 21 A). Genes encoding key regulators of proliferation were down-regulated in both T cell subsets, whereas regulators of cellular responses, cell differentiation and signalling were up-regulated over time. Genes encoding markers for Wnt signalling and apoptotic process were only up-regulated in LT CD8 T cells. Interestingly, regulators of programmed cell death and apoptotic process were down-regulated in LT CD4 T cells (Figure 21 and appendix Table 2). Additionally, the overlap of deregulated genes in CD8 and CD4 Tcm cell signatures was compared. Of 931 down-regulated genes in LT CD4 T cells, 74 % (688) were also down-regulated and only 0.5 % (5) were up-regulated in LT CD8 Tcm cells. 53 % (305 of 580) up-regulated genes in LT CD4 T cells were also up-regulated in LT CD8 T cells and only 14 were down-regulated (Figure 21 B). Furthermore, the altered genes were set against ST and LT CD8 versus ST and LT CD4 Tcm cells, revealing a relatively high correlation illustrated by the Venn diagram (Figure 21 B) and the scatter plot with highlighted selected genes (Figure 21 C). The T cell inhibitory receptors (TIRs) CD200 (*Cd200*), PD-1 (*Pdcd1*) and LAG-3 (*Lag3*) were down-regulated in both CD8 and CD4 LT Tcm cells indicating lower exhaustion potential [203, 204]. *Dusp4, Tox* and *Nr4a1* associated with T cell dysfunction [205-208] were also down-regulated over time, whereas genes for effector molecules Granzyme c-g were highly up-regulated in LT CD8 T cells, supporting the previous *in vitro* findings.

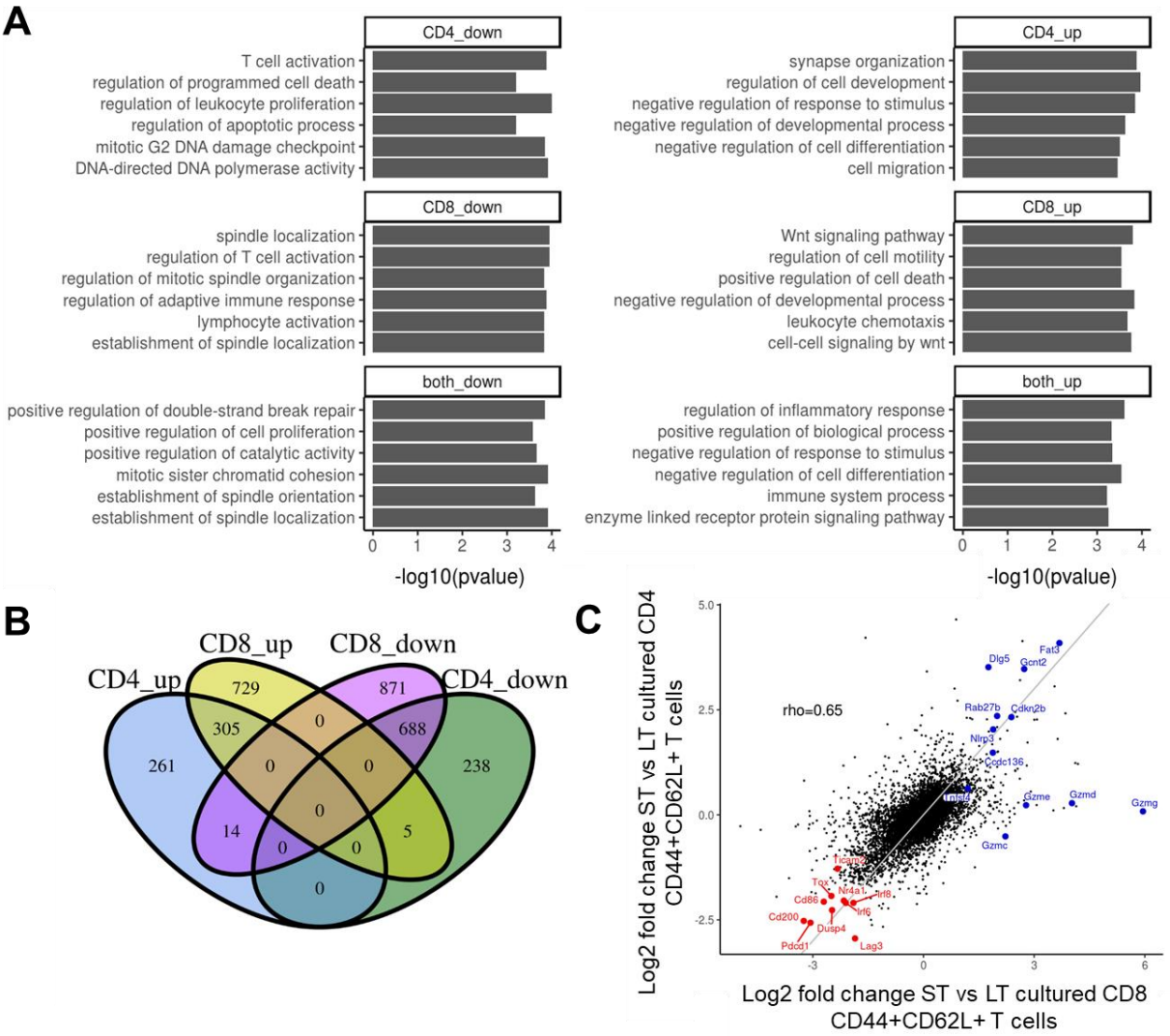

Figure 21. Strong overlap of differentially expressed genes between CD4 and CD8 long-term signatures. RNA sequencing of polyclonal CD8 Tcm cells generated via ST or LT expansion with IL-7/IL-15. RNA isolation was performed by AH, sequencing was performed by the BIH Genomic facility and data evaluation was performed by OB. A) Gene list with GO terms. B) Venn diagram with numbers of differentially regulated genes compared between differently long expanded CD8 Tcm and CD4 Tcm cells. C) Scatter plot with log2 fold changes between ST and LT CD8 Tcm versus CD4 Tcm cells. Selected genes were highlighted.

To test whether some of the up-coming GO terms are verifiable, several *in vitro* experiments were conducted. The functional properties of ST and LT CD8 and CD4 T cells were analyzed by performing dissection of Tscm phenotype markers, cytokine and granzyme B production, proliferation capacity, extent of cell death and up-regulation of exhaustion markers (CTLA-4, PD-1, TIM-3 and LAG-3) upon re-stimulation with antiCD3 and antiCD28 for four hours (cytokine expression, granzyme B production and extent of apoptosis), 10 or 11 days (exhaustion markers and proliferation). The Tscm surface marker analysis revealed comparable expression levels of Sca-1 and CXCR3 or even higher expression levels of CD122 and Bcl-2 in LT

CD8 Tcm cells (Figure 22 A). On CD4 T cells, only CD122 was higher expressed on LT CD4 Tcm cells, whereas the expression of Sca-1, Bcl-2 and CXCR3 was comparable (Figure 22 B). The cytokines IL2, IFNγ and TNFα of LT CD8 T cells was significantly higher expressed compared to ST CD8 T cells (Figure 22 C and E). Similar results were observed for LT CD4 T cells with exception of TNF-α, which remained comparable between ST and LT CD4 T cells (Figure 22 D and F). IL10 was not detectable at any time. In addition to previous *in vitro* analyses, the proliferation capacity, extent of cell death and expression of exhaustion markers was further analyzed (see section 4.3.4, 4.3.5 and 4.3.6). Regarding the proliferation capacity (Figure 22 G and H) or apoptosis (Figure 22 I and J), no differences between both groups for CD8 and CD4 T cells were observed. The up-regulation of exhaustion markers was provoked by a lower permanent re-stimulation with diluted antiCD3 and antiCD28 for 10 days. ST and LT CD8 or CD4 T cells all showed a similar up-regulation of exhaustion markers, beside LAG3 expression (Figure 22 K and L). LAG3 was significantly less expressed in LT CD8 T cells compared to the ST culture, which correlated with lower LAG3 expression in the transcriptome analysis (Figure 21 C – and appendix Table 3). Taken together, these data suggest that murine CD8 and CD4 T cells might be expanded over three (CD4) or four (CD8) weeks, maintaining characteristic features related to Tcm and Tscm and without losing *in vitro* functionality by simple expanding with IL7/IL15.

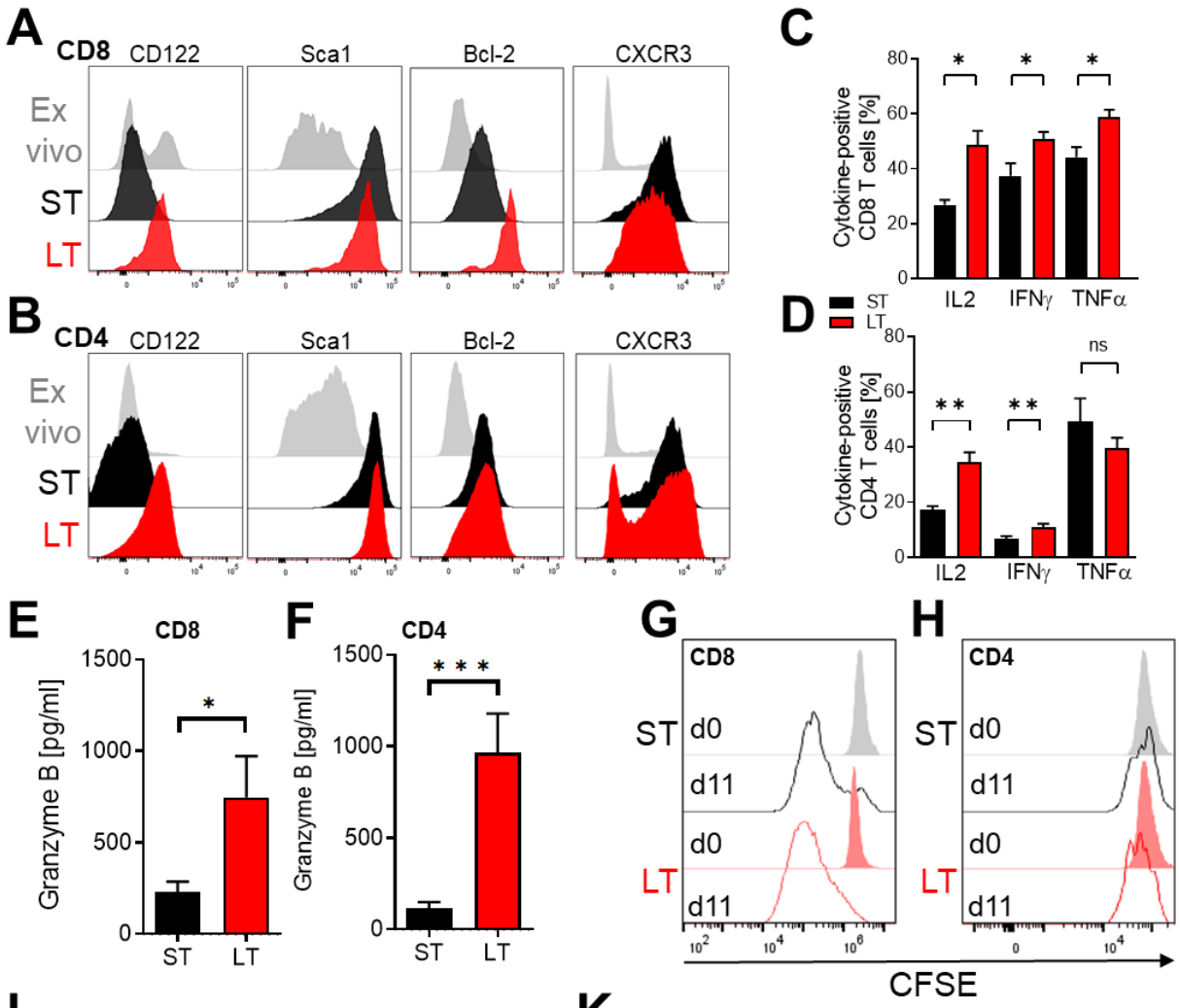
A
CD8
CD122
Sca1
Bcl-2
CXCR3
Ex vivo
ST
LT
B
CD4
CD122
Sca1
Bcl-2
CXCR3
Ex vivo
ST
LT
C
Cytokine-positive CD8 T cells [%]
IL2
IFNγ
TNFα
D
ST
LT
Cytokine-positive CD4 T cells [%]
IL2
IFNγ
TNFα
ns
E
CD8
Granzyme B [pg/ml]
ST
LT
F
CD4
Granzyme B [pg/ml]
ST
LT
G
CD8
ST
d0
d11
LT
d0
d11
CFSE
H
CD4
ST
d0
d11
LT
d0
d11
I
Percentage of CD8 T cells [%]
ST
LT
DAPI+ Annexin+
DAPI- Annexin-
J
Percentage of CD4 T cells [%]
ST
LT
DAPI+ Annexin+
DAPI- Annexin-
K
MFI of CD8 T cells
ST
LT
CTLA-4
PD-1
TIM-3
LAG-3
L
MFI of CD4 T cells
ST
LT
CTLA-4
PD-1
TIM-3
LAG-3

Figure 22. Retained phonotypical and functional properties of long-term expanded T cells in vitro. Polyclonal CD8 or CD4 T cells were isolated from C57BL/6 mice, activated via antiCD3, antiCD28 and IL2 for 72 hours and further expanded with IL7/IL15 for 4 (ST) or 18 (LT CD4) respectively 25 (LT CD8) days. ST and LT CD8 or CD4 T cells were re-stimulated with antiCD3 and antiCD28 for 4 hours (C, D, E, F, I, J), 10 (K and L) or 11 days (G and H). The phenotypical analysis was conducted by flow cytometry. Granzyme B measurement was performed as ELISA. A) The CD8 or B) CD4 Tcm cell subset resulting from the T cell culture was further characterized by CD122, Sca-1, Bcl-2 and CXCR3 and compared to ex vivo Tcm cells. C)+D) The bars show frequencies of cytokine-expressing CD8 (C) or CD4 (D) T cells with mean values ± SEM. **p < 0.01, *p < 0.05, paired t-test. 3/7 of measurements were performed by SH, 4/7 by AH. E)+F) The granzyme B concentration in supernatants of re-stimulated CD8 (E) or CD4 (F) T cells were analyzed in triplicates via ELISA. 3/6 of the data for E) were compiled by SH. The bars show mean values ± SEM. ***p < 0.001, *p < 0.05 paired t-test. G)+H) Representative histograms of re-simulated CFSE-labeled ST and LT CD8 (G) or CD4 (H) T cells. I)+J) The bars show frequencies of apoptotic and dead cells (DAPI+, Annexin+) vs. living cells (DAPI-, Annexin-) from re-stimulated CD8 (I) or CD4 (J) T cells with mean values ± SEM. K)+L) The bars show mean values ± SEM of inhibitory T cell receptor expression on CD8 (K) or CD4 (L) after re-stimulation over 10 days. The data were generated in 2-3 independent experiments with n = 6-9. *p < 0.05, paired t-test.

5.2.8. Long-term CD8 and CD4 T cells don't lose their engraftment and persistence capacity under lymphopenic conditions *in vivo*

Next, *in vivo* experiments were performed to investigate how feasible the *in vitro* findings about persistence were. Hence, our dual-luciferase reporter system was applied, allowing migration, expansion and activation of adoptively transferred T cells to be monitored [92]. Polyclonal ST or LT CD8 (Figure 23 A) or CD4 (Figure 24 A) BLITC cells were expanded and injected iv into sublethally irradiated RagKO mice. First, the engraftment capacity after 30 days was assessed (see section 4.4.1, 4.5.1 and 4.5.7). Renilla luciferase (Rluc) signals in cervical and inguinal lymph nodes (cLN and iLN) were quantified by digitally setting regions of interest (ROI) and by computing total flux values. The signal intensity between ST and LT CD8 (Figure 23 B and F) as well as for CD4 T cells (Figure 24 B and F) was comparable. Additionally, peripheral lymph nodes and the spleen were isolated, in order to quantify absolute numbers of infiltrated CD8 or CD4 T cell numbers using flow cytometry. The absolute numbers of CD8 (Figure 23 C) or CD4 (Figure 24 C) were comparable in both groups supporting the BLI data and thus suggest that there are no differences in regard to the engraftment capability. In the follow-up, Rluc signals were detectable for further two (CD4) or five (CD8) months, suggesting similar persistence of transferred T cells (Figure 23 D; Figure 24 D). ST and LT CD4 T cells showed a potent expansion in RagKO recipients, even though it was a syngeneic ATT (Figure 24 F). Because of the strong expansion and an increasing burden in the mice, the CD4 recipients were sacrificed after three months post ATT. The absolute numbers of peripheral lymph nodes and spleen after three (CD4) or six months (CD8) turned out comparable for ST and LT T cells (Figure

23 E, Figure 24 E). These findings suggest a preserved engraftment and persistence capacity for CD4 and CD8 T cells *in vivo*.

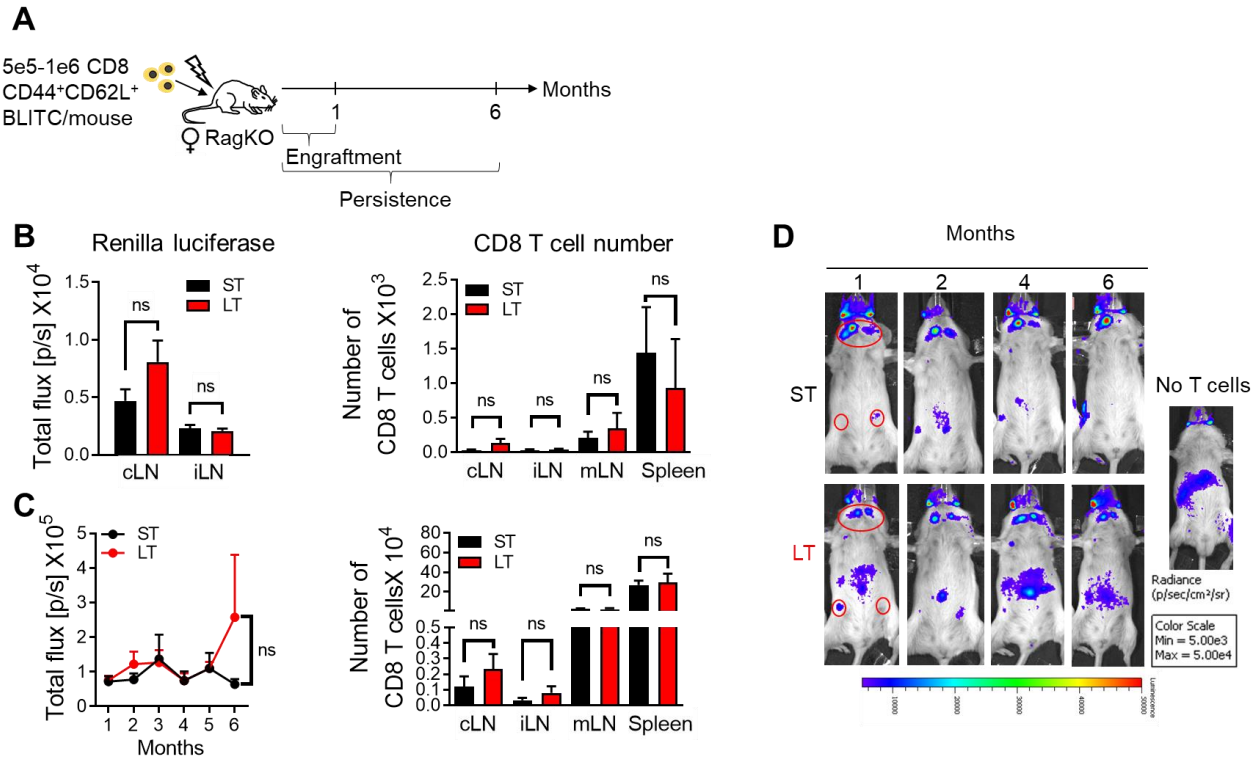

Figure 23. Long-term CD8 T cells show retained engraftment end persistence capacity. A) Scheme for T cell transfer into female RagKO mice in order to analyze in vivo engraftment and persistence. B, C) The diagrams on the left show the mean ± SEM of Renilla luciferase flux values in the cervical (cLN) and inguinal lymph nodes (iLN) one month (B) and six months (C) after transfer. Mice were sacrificed after one or six months and CD8 T cells were quantified in different organs via flow cytometry. The bar diagrams on the right show the mean data ± SEM of total T cell numbers. D) Representative Renilla luciferase signals of ST or LT CD8 Tcm cells one to six months after transfer into female RagKO mice. All data were generated in 2 independent experiments with n = 6-8 mice per group. A two-tailed t-test was performed.

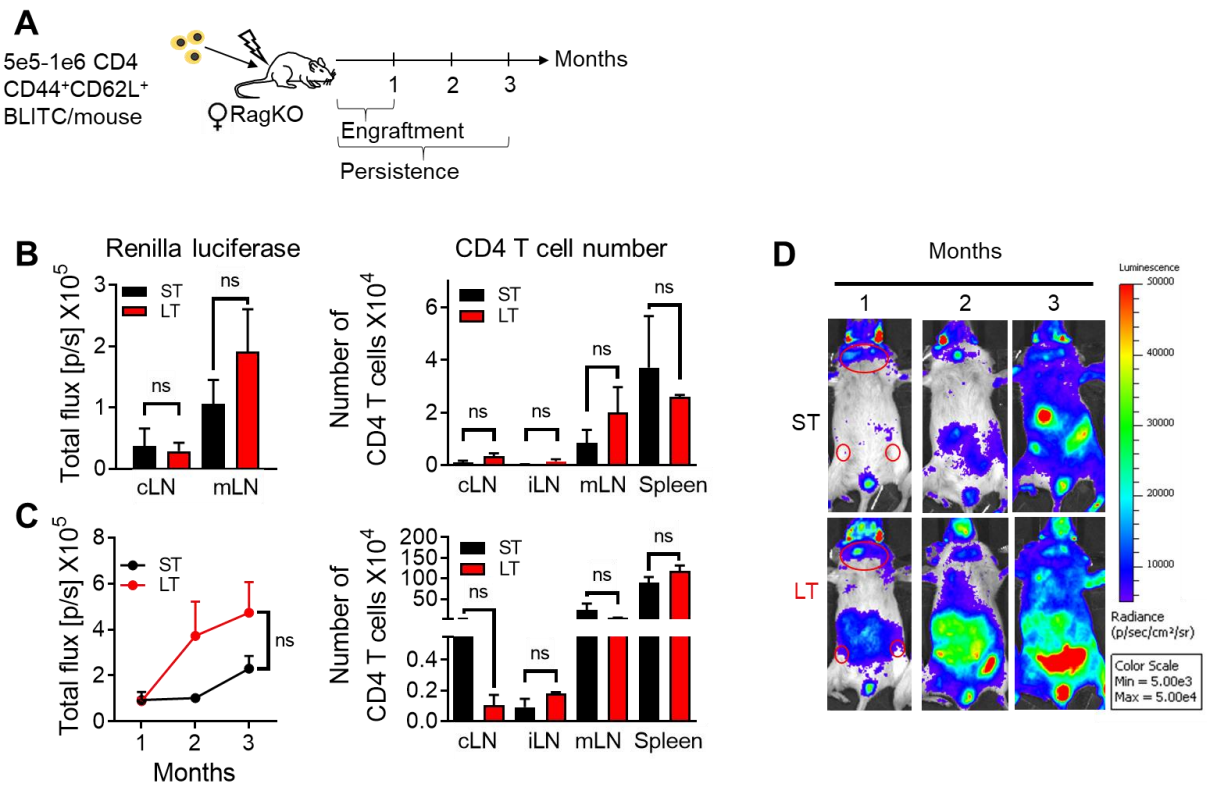

Figure 24. Long-term CD4 T cells show retained engraftment end persistence capacity. A) Scheme for T cell transfer into female RagKO mice in order to analyze in vivo engraftment and persistence. B, C) The diagramson the left show mean ± SEM of Renilla luciferase flux values in the cervical (cLN) and inguinal lymph nodes (iLN) one month (B) and three months (C) after transfer. Mice were sacrificed after 1 or 3 months and CD4 T cells were quantified in different organs via flow cytometry. The bar diagrams on the right show mean data ± SEM of total T cell numbers. D) Representative Renilla luciferase signals of ST or LT CD4 Tcm cells 1 to 3 months after transfer into female RagKO mice. All data were generated in 2 independent experiments with n = 6-8 mice per group. Two-tailed t-test was performed.

5.2.9. Antigen-challenged CD8 T cells have a preserved proliferation ability, persistence capacity and killing efficacy *in vivo*

Maintained or even enhanced functional capabilities of adoptively transferred T cells after (tumor-) antigen encounter is crucial for the efficacy of an ATT. To investigate antigen-dependent proliferation, persistence and killing capacity, the well-known minor histocompatibility antigen H-Y was used, which is ubiquitously expressed in male RagKO mice. In order to provoke an antigen stimulus, CD8 T cells were isolated from female BLITC (Figure 25 A) or H-Y transgenic MataHari-BLITC mice [92] (Figure 25 B) and expanded ST or LT (see section 4.5.1 and 4.5.4). ST and LT T cells were then FACS sorted for CD44+CD62L+ T cells (Tcm phenotype) and transferred into male RagKO recipients. After 11 days, comparable Rluc signals in cLN and iLN for polyclonal and transgenic ST and LT CD8 Tcm cells were detected (Figure 25 A and B), indicating comparable proliferation capacity of ST and LT CD8 H-Y specific T cells

from WT or MataHari (MH) donors upon antigen challenge *in vivo*. In the follow-up of the transgenic ATT, the Rluc intensity increased within the first two weeks. Subsequently, the Rluc intensity declined and stayed stable for more than three months (Figure 25 B – right graph). These kinetics turned out comparable between ST and LT MH T cells, suggesting an analogous persistence capability after antigen encounter of H-Y specific CD8 T cells. Next, the ability of ST and LT MH Tcm to kill H-Y expressing target cells *in vivo* was tested. For this purpose, ST and LT MH Tcm were administered into female RagKO recipients. After four hours, $CFSE^{high}$-labeled male and $CFSE^{low}$-labeled female splenocytes (from RagKO donors) were injected. 20 hours later, the frequencies of CFSE-labeled cells were measured via flow cytometry. The killing capacity was determined by forming ratios between female ($CFSE^{low}$) and male ($CFSE^{high}$) target cells, which were calculated for each sample (see section 4.5.5.). The killing capacity was comparable between ST and LT MH Tcm cells (Figure 25 C). In summary, these data suggest that LT CD8 T cells have a sustained proliferation, persistence and killing potential upon antigen encounter.

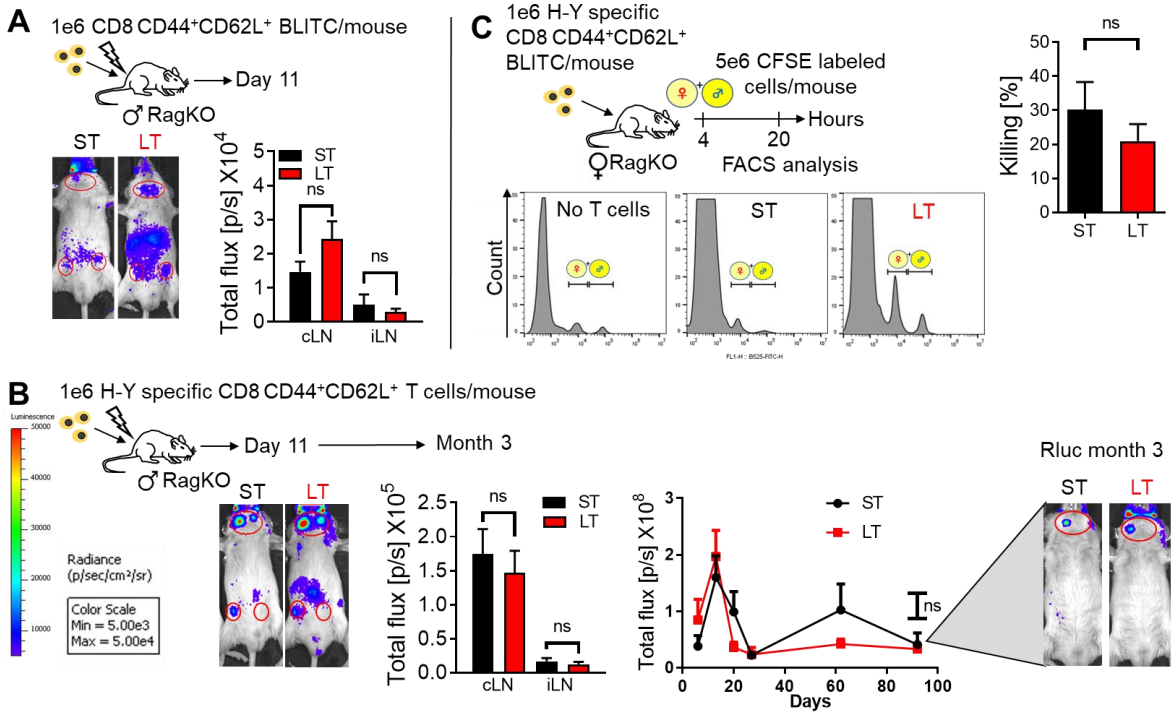

Figure 25. Long-term CD8 T cells demonstrate preserved encounter functionality. A) Scheme for T cell transfer into male RagKO mice in order to analyze in vivo proliferation. Representative Renilla luciferase signals of ST or LT CD8 Tcm cells 11 days after transfer into male RagKO mice. The diagram shows the mean ± SEM of Renilla luciferase (Rluc) flux values in the cervical (cLN) and inguinal lymph nodes (iLN). B) Scheme for MataHari (MH) Tcm cell transfer into male RagKO mice to analyze in vivo proliferation. Representative Rluc signals of ST or LT MH Tcm cells 11 days or over time period of three month after transfer into male RagKO mice. Diagram shows mean ± SEM of Rluc flux values in the cervical (cLN) and inguinal lymph nodes (iLN). The right diagram shows mean ± SEM of Rluc flux values in the cLN over three months. C) Scheme for in vivo kill. Representative CFSE profiles of splenocytes isolated from mice that received no T cells, ST or LT MH Tcm. Numbers indicate the killing

frequency. Killing frequency was calculated by 100-(100/$CFSE^{high}$x$CFSE^{low}$). The bar charts show killing frequencies of ST and LT MH Tcm cells minus control (no T cells) in mean ± SEM. Data for C) were generated together with SH. All data were generated in 2 independent experiments with n = 6-8 mice per group. A two-tailed t-test was performed.

5.2.10. Long-term transduced and transgenic CD8 and transgenic CD4 T cells demonstrate a retained anti-tumor killing efficacy *in vivo*

Beyond endogenous antigen encounter, it is important to investigate the functionality of expanded T cells for tumor challenge. Therefore, experiments with 3 different tumor entities were performed (see section 4.5.6, 4.5.8 and 4.5.9). First, ST and LT MH Tcm cells were expanded and transferred into female RagKO recipients with an established H-Y expressing WR21 tumor [201]. T cell migration was monitored via Rluc and T cell activation was monitored via NFAT-CBR signals *in vivo*. The ST and LT H-Y TCR transgenic CD8 T cells both infiltrated rapidly into the tumor tissue where they showed strong infiltration and activation, resulting in a slightly decelerated tumor growth compared to the control group (Figure 26 A). However, the entire anti-tumor-response by the ATT was weaker than expected, due to rapid antigen-loss (Appendix Fig.1). Secondly, ST and LT TCR-1 specific transduced T cells were tested in the SV40 Tag tumor model [98, 99] (see section 4.4.4). Based on the work of Szyska and colleagues, polyclonal BLITC T cells were transduced with a TCR-I containing retrovirus and expanded for one or four weeks. Meanwhile, the 200ΔLuc tumor [92] was established for about 40 days in albino RagKO mice, which then received ST or LT TCR-1 transduced CD8 BLITC Tcm cells. Bright Rluc on day 8 and distinct NFAT-CBR signals on day 7 demonstrated a strong activation and infiltration into tumor tissue. As a result, one week after ATT, the tumors of both groups started to regress, being completely rejected after two weeks without relapse over 90 days, whereas tumors from the control mice (no T cells) grew out within four weeks (Figure 26 B). As for CD8 T cells, the anti-tumor efficacy of ST and LT H-Y TCR transgenic CD4 T cells was investigated. Thus, they were isolated from Marilyn-BLITC mice [92] and expanded for one or three weeks. RagKO mice bearing DBY-positive MB49 tumors [200] received ST or LT H-Y transgenic CD4 Tcm cells. Tumor infiltration and T cell activation was observed in both groups, leading to a fast tumor regression, but followed by tumor relapses occurring comparably for ST and LT T cell recipients (Figure 26 C). In conclusion, these findings suggest a retained anti-tumor capability of LT CD4 and CD8 T cells.

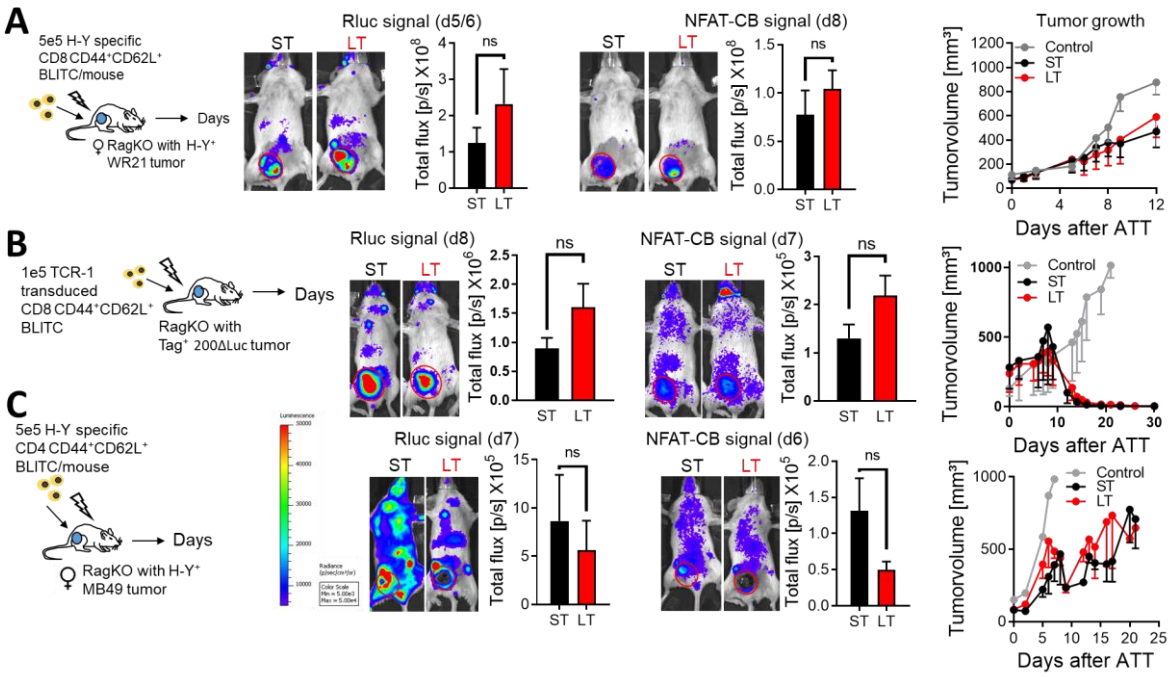

Figure 26. Long-term expanded T cells maintain potent anti-tumor functionality. A) Scheme for T cell transfer into WR21-tumor-bearing female RagKO mice. Tumor growth kinetics are displayed by the line diagrams, mean ± SEM. The diagram shows renilla and NFAT-click beetle luciferase signals of differently expanded CD44$^+$CD62L$^+$ MataHari T cells 5 or 8 days after transfer into WR21-tumor-bearing mice. The line diagrams show mean ± SEM of luciferase flux values in the tumor region. One out of two experiments was performed by SH. B) Scheme for T cell transfer into 200ΔLuc-tumor-bearing female RagKO mice. Tumor growth kinetics are displayed by line diagram, mean ± SEM. The diagram shows renilla and NFAT-click beetle luciferase signals of differently expanded TCR-1 transduced T cells 7 or 8 days after transfer into 200ΔLuc -tumor bearing mice. The line diagram shows mean ± SEM of luciferase flux values in the tumor region. C) Scheme for T cell transfer into MB49-tumor-bearing female RagKO mice. Tumor growth kinetics are displayed by line diagram, mean ± SEM. The diagram shows renilla and NFAT-click beetle luciferase signals of differently expanded transgenic H-Y specific CD4 Tcm cells 7 or 8 days after transfer into MB49-tumor-bearing mice. Line diagram show mean ± SEM of luciferase flux values in the tumor region. Tumor growth kinetics are displayed by line diagram, mean ± SEM. For each setting representative BLI pictures are shown. All data were generated in 2 independent experiments with n = 6-15 mice per group. Two-tailed t-test was performed.

5.2.11. Elongation of human T cell expansion increases total amount of CD8 and CD4 Tcm cells with maintained *in vitro* function

A further aim of this thesis was to transfer the findings from murine to human T cell expansion. For this purpose, the expansion kinetics and phenotype development of T cells from healthy donors were analyzed. Human T cells were enriched by density gradient centrifugation, followed by T cell activation via antiCD3, antiCD28 and IL2 for three days with further expansion using IL7/IL15. The expansion kinetics of CD8 and CD4 T cells were in line with my murine data. Thus, a distinct increased in human CD8 and CD4 T cell numbers became apparent during the first three weeks. The plateau of expansion for CD8 T cells was reached after four weeks. Next, the developed phenotype of expanded CD8 and CD4 T cells was analyzed by detecting CD45RO and

CCR7 expression using flow cytometry (see section 4.3.2 and 4.4.1). The elongated expansion of CD8 T cells resulted in a 10,000-fold increase of human CD8 CD45RO+CCR7+ T cells (Tcm), which is associated with human Tcm (Figure 27 A, right graph). Interestingly, the expansion of human CD4 T cells was accompanied by a stronger and longer increase than murine CD4 T cells, which resulted in 50-fold higher numbers of human CD4 Tcm T cells after three weeks (Figure 27 B).

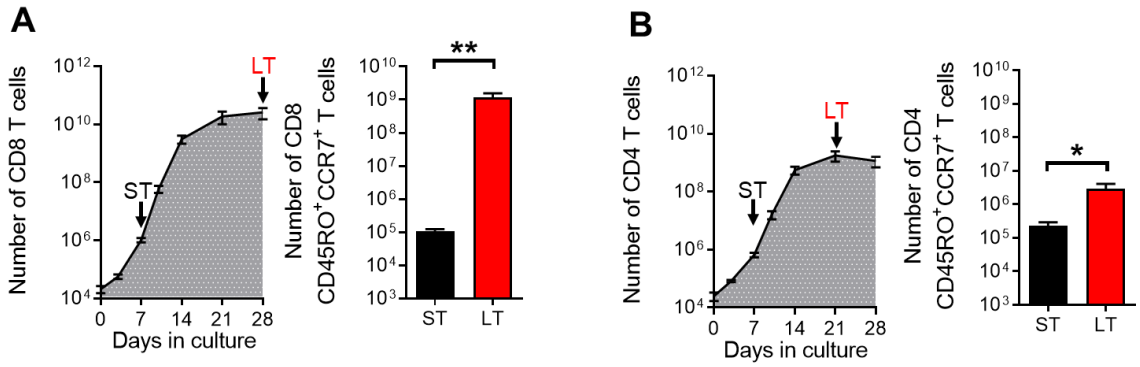

Figure 27. Long-term IL7/IL15 expanded leads to strong increased numbers for human CD8 and CD4 T cells. T cells from healthy donors were enriched using a ficoll density gradient, activated via anti-CD3/CD28 and IL-2 for 72 hours and further expanded with IL7/IL15 for 4 (ST) or 25 (LT) days. The quantification and phenotypical analysis were conducted by flow cytometry. A) Growth kinetic of CD8 T cells is displayed by line diagram as mean values ± SEM. The before-after-diagram shows the mean ± SEM of total CD8 CD45RO$^+$CCR7$^+$ T cell numbers. B) Growth kinetic of CD4 T cells is displayed by line diagram as mean values ± SEM. The before-after-diagram shows mean ± SEM of total CD4 CD45RO$^+$CCR7$^+$ T cell numbers. Data were generated in 2 independent experiments with n = 4 healthy donors with one out of two experiments by SH. **p < 0.01, *p < 0.05, two-tailed paired t-test.

As previously analyzed for murine T cells *in vitro*, the properties of human ST and LT CD8 and CD4 T cells were tested regarding the extent of cell death, exhaustion and cytokine expression after re-stimulation with antiCD3 and antiCD28 for 4 hours (cell death, cytokine expression) or 10 days (TIRs) (see section 4.3.3, 4.3.4 and 4.3.5). The extent of cell death in human CD8 and CD4 T cells was lower than in murine T cells. However, the extent of cell death between ST and LT CD8 and CD4 T cells was comparable (Figure 28 A and D). The level of TIR expression also proved similar between both groups of CD8 and CD4 T cells (Figure 28 B and E). During expansion, human CD8 T cells expressed increasing amounts of IFNγ and TNFα within the first three weeks, followed by a rapid decline of these cytokines after four weeks (Figure 28 C). Expanded CD4 T cells also expressed higher amounts of IFNγ and TNFα during the first three weeks, followed by a down-regulation in week 4 of TNFα and a stable amount of IFNγ. However, the detected cytokine expression for CD4 T cells in week 4 was still higher than in week 1 (Figure 28 F). In summary, these data suggest that the

results regarding prolonged murine T cell expansion are applicable to human T cell culture and thus relevant for clinical ATT approach.

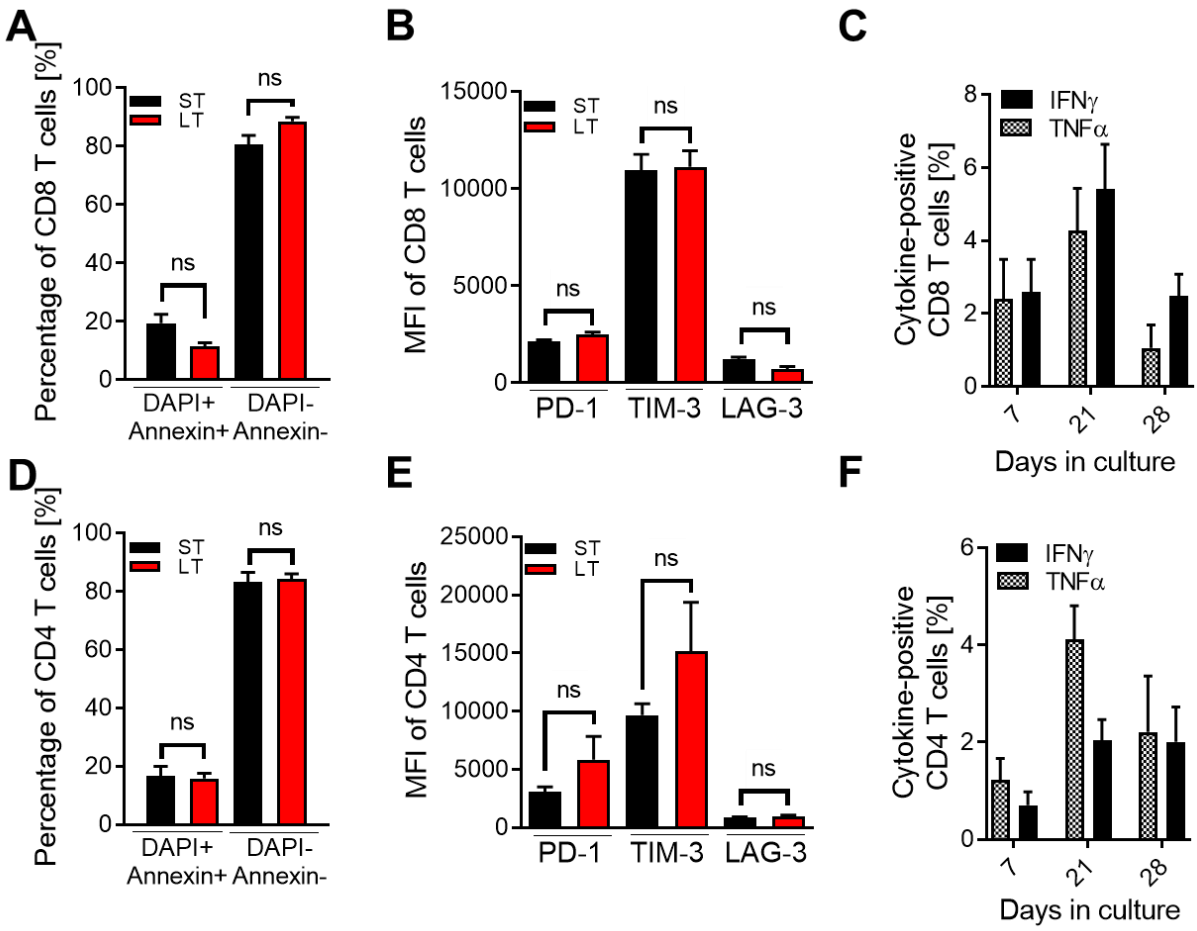

Figure 28. Long-term expanded human T cells show comparable *in vitro* properties to short-term expanded T cells. A) ST and LT CD8 T cells were re-stimulated for 4 hours using anti-CD3/CD28. The bars show mean values ± SEM of frequencies of apoptotic / dead cells (Annexin+, DAPI+) and living cells (Annexin-DAPI-) CD8 T cells. B) The bars show mean values ± SEM of inhibitory T cell receptor expression on CD8 T cells after re-stimulation over 10 days. C) Expanded CD8 T cells were re-stimulated at the indicated time points as described in B. The line diagram shows mean values ± SEM of IFN-γ and TNF-α expressing CD8 T cells over time. D) ST and LT CD4 T cells were re-stimulated for 4 hours using anti-CD3/CD28. The bar charts show mean values ± SEM of frequencies of apoptotic / dead cells (Annexin+, DAPI+) and living cells (Annexin-DAPI-) CD4 T cells. E) The bars show mean values ± SEM of inhibitory T cell receptor expression on CD4 T cells after re-stimulation over 10 days. F) Expanded CD4 T cells were re-stimulated at the indicated points in time as described in B. The line diagram shows mean values ± SEM of IFN-γ and TNF-α expressing CD4 T cells over time. Data were generated in 3 independent experiments with n = 9 healthy donors. A two-tailed paired t-test was performed.

6. Discussion

6.1. Feasibility of treatment with LPAM-1 antibody

The humanized antibody against LPAM-1, Vedolizumab, has already achieved FDA approval, followed by first promising clinical trials with patients suffering from severe GvHD. One aim of this study was to verify this antibody potential of treating “on-target, off-tumor” toxicity in our mouse model. A further goal beyond the mitigation of “on-target, off-tumor” toxicity was to test for the maintenance or even improvement of GVT. An amelioration in “on-target, off-tumor” toxicity was initially endorsed and follow-up experiments with tumor bearing mice were promising, showing diminished toxicity and increased tumor infiltration resulting in slower tumor growth. However, these results were not reproducible. The difference between the first and latest experiments was the source of antibody. Although the antibody-producing hybridoma clone was the same (DATK32 [111]) in both experiments, a self-produced and purified version was used initially, while the follow-up experiment involved a purchased antibody product. Subsequently, failure analysis was performed by comparing peptide constellation via mass spectrometry. These results did not show any difference in functional peptides. As previous quality analysis showed endotoxin contamination in the self-produced antibody, the next step was to test the impact of sole endotoxin in our model. Endotoxin-treated mice showed similar tumor infiltration and growth to the promising experiments with the self-produced antibody, while the purchased antibody did not show any effect on “on-target, off-tumor” toxicity or GVT burden. These studies revealed that the LPAM-1 blocking antibody was not constantly able to reduce “on-target, off-tumor” toxicity. Moreover, the observed improvement in tumor infiltration and growth deceleration might have resulted from endotoxin.

6.1.1. Does LPAM-1 antibody ameliorate “on-target, off-tumor” toxicity?

Specific blocking of LPAM-1 on lymphocytes in order to inhibit migration into the mucosal site of mice [111, 117, 209] or to ameliorate intestinal inflammation in human [123-125] has been shown by a variety of studies. However, a successful blockade of LPAM-1 was not always noticed. With a Crohn’s disease-like ileitis mouse model, there was no amelioration in acute or chronic intestinal infiltration compared to the isotope

control [210]. Similar results were observed for a clinical trial with Vedolizumab, treating Crohn's disease patients with failed tumor necrosis factor antagonist treatment [211]. These contradictory data demonstrate that a successful inhibition of T cell migration into intestinal tissue might be dependent on more than LPAM-1.

Beilhack et al. impressively showed that secondary lymphoid organs (SLOs) are needed for GvHD initiation. It has been previously demonstrated, that the blockade of access to all potential SLOs is required to reduce GvHD since involvement of only one SLO is sufficient to mediate GvHD [212]. Additionally, it has been reported that alternatively to LPAM-1, T cells can migrate into small intestine lamina via the C-C chemokine receptor 9 (CCR9) and chemokine (C-C motif) ligand 25 (CCL25) axis [213-216]. Moreover, Stenstad et al. observed CD4 T cells migrating into small bowl independently of CCR9, suggesting there could be even a third adhesion mechanism [217]. Each of these findings might provide an explanation for sustained toxicity in the experiments applying the purchased antibody.

6.1.2. Endotoxin, but not LPAM-1 antibody, has an impact on anti-tumor response of ATT

This initial experiment demonstrated an enhanced T cell infiltration into tumor tissue in recipients undergoing treatment with the self-produced LPAM-1 antibody. These data were not reproducible with the purchased LPAM antibody, so further studies were performed to clarify the mechanism. Mass spectrometric analysis revealed similar peptide composition and an *in vivo* "on-target, off-tumor" toxicity experiment with endotoxin injection into tumor bearing mice indicated that the observed anti-tumor effect originated by endotoxin contamination.

This finding is in line with the literature, which describes an improved anti-tumor response by low doses of endotoxin infusion one day after ATT [218, 219]. The mechanism behind this could be explained by toll like receptor 4 (TLR4) expression on tumor cells. Especially the used MB49 tumor expresses TLR4 on his surface and shows no or decelerated tumor growth in tumor-bearing C57BL/6 or $TLR4^{lps\text{-}del}$ mice treated with lipopolysaccharides (LPS). A potential signal pathway might be secreted IFNγ and IL6 due to TLR4 stimulation with LPS. This stimulates dendritic cells to express TNFα and IL12, which activates CD4 T cells and promote a Th1 response against the growing tumor [220] (summarized in Figure 29).

These findings were in line with published data and supported them with bioluminescent imaging showing stronger T cell infiltration into tumor tissue triggered by LPS infusion.

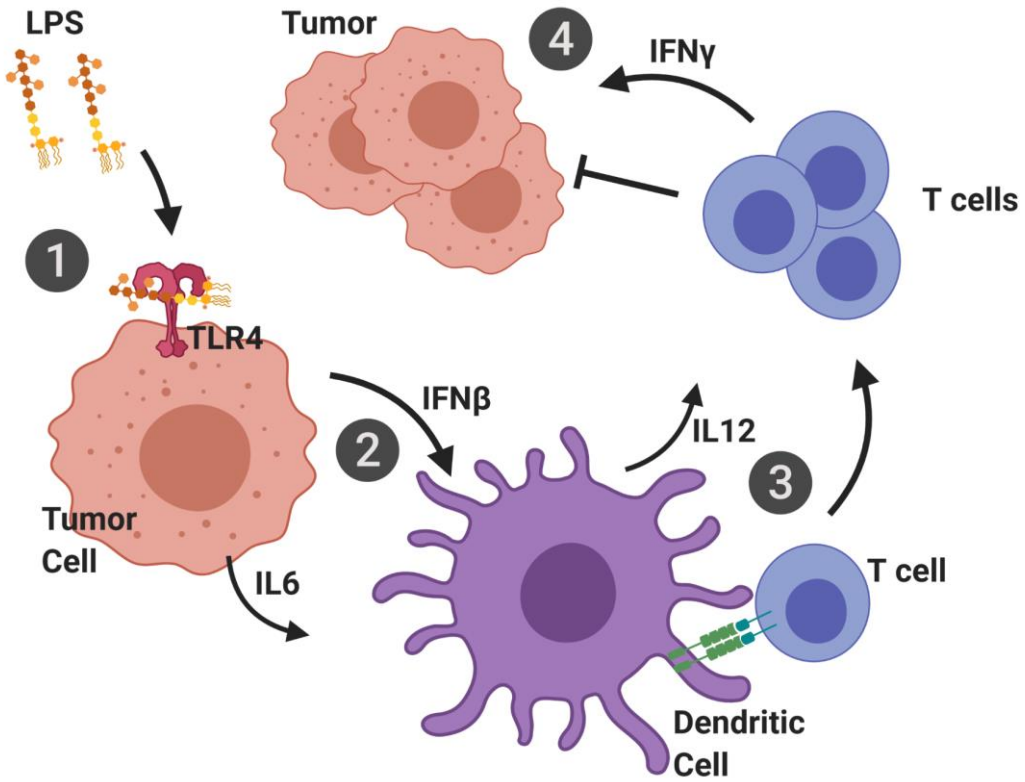

Figure 29. Schema of potential mechanism behind lipopolysaccharide signal cascade. LPS = Lipopolysaccharide, TLR4 = Toll like receptor 4, IL = Interleucin , IFN = Interferon, 1) LPS binds on TLR4 expressing tumor cell. 2) IFNbeta secretion and other modulators of dendritic cell (DC) activity. 3) IFNbeta can restore the IL12-secreting capacity of DCs at the site of inoculation, improving their maturation state. 4) DCs promote a T_H1 response against the growing tumor. Adapted from Nunez et al. 2011.

6.2. Modified T cell expansion for ATT

One aim of this project was to set up a T cell expansion protocol for ATT to up-scale the generation of long-term surviving T cells with high effector potential. This is important for ATT, because dropouts in clinics are due to manufacturing, lacking persistence of adoptively transferred T cells or rapid disease progression. TCR-engineered T cells in particular are compromised by their limited persistence and expansion [221]. It is therefore important to optimize recent expansion methods in order to generate sufficient amounts of transplantable T cells. Furthermore, this will maintain the possibility of performing a later second donor lymphocyte infusion (DLI) with long-term expanded T cells, if the first infusion does not approach the desired clinical outcome. Another promising avenue for ameliorating ATT is the treatment with CD4 T cells. Antitumor immunoreaction has primarily been described for CD8 T cells, while the awareness of cytotoxic CD4 T cells increased in the past few years, due their interactions with Fas- Fas-L, perforin or granzymes [222].

6.2.1. IL15 and IL27 as a novel cytokine cocktail for enhanced T cell expansion

In order to generate potent CD8 T cells by a feasible expansion protocol, a new cytokine combination was tested using IL27. Initial experiments with IL27 showed higher expression of granzyme B, which is in line with published data [177], but the culture did not last long and nearly all T cells became apoptotic. IL27 has also described as enhancing the expression of memory precursor-like effector cell markers like Bcl-6, SOCS3, Sca-1 and IL-10 in CD8 T cells and favoring the early differentiation of CD4 T cells into T_H1 [175, 176, 193], so it remained a promising candidate. Together with IL15, which is known as growth factor for T cells and to promote their survival [223], it was possible to establish a new cytokine combination. By using this novel protocol, T cells with a mainly Tcm phenotype could be generated accompanied by stronger CD4 and CD8 T cell expansions compared to the established protocol with IL7/IL15.

Further in vitro analysis did not show any strong deterioration in expression of stem cell associated surface markers or cytokine expression after re-stimulation, using IL15/IL27. These results were different to previous studies showing that IL27 promoted

IFNγ expression in CD8 T cells and a TH1 differentiation for CD4 T cells [175, 176, 193]. This discrepancy might result from the combination of IL27 with IL15. The homeostatic effect on memory T cells [224, 225] might potentially decelerate cytokine expression, compared to IL27 alone. However, T cells expanded with IL15/IL27 did not show suppressed suppressive functions as IL10 expression as described by Murugaiyan et al. [226].

In-depth analysis via transcriptome sequencing did not feature any significantly different expressed gene between the IL7/IL15 and IL15/IL27 expanded cells. The functional differences we have detected might be due to posttranslational effects, a potential dominant effect of IL15, which drowns transcriptional effects of IL7 or IL27 or the fact, that the receptors of IL7, IL15 and IL27 phosphorylate all JAK1 followed by similar transcriptional pathways [227, 228]. Another explanation could be that at the time of RNA isolation (week 1 vs. week 3/4) there was no difference in the expansion kinetics of the cells when comparing IL7/IL15 with IL15/IL27 (described in 4.2.2). In summary, these findings suggest a novel potent expansion condition regarding enhanced T cell expansion with maintained Tcm/Tscm properties, but further investigations (e.g. in epigenetic differences, further cytotoxic analyses, etc.) are needed.

6.2.2. Long-term expanded T cells are enriched and revealed a stable Tcm/Tscm phenotype profile

For T cell expansion it is well established to use IL2 as growth factor, but in the past decade this routine has been modified by homeostatic cytokines like IL7, IL15 and IL21 [80, 229, 230]. It has emerged that it is possible to shift the T cell phenotype towards Tcm/Tscm by using IL7/IL15 for expansion [134, 137, 138, 231]. It could also be shown that IL7/IL15 promotes better growth and homeostatic properties than IL2 [78, 135], and improved ATT efficacy [232]. However, Gong et al. have recently demonstrated that for NY-ESO-1-specific T cells, IL7/IL15 culture does not unrestrictedly improve T cell properties, compared to IL2 culture, indicating that each genetic modified T cell product needs its own adapted and optimized expansion protocol [233]. With exception of Cieri et al, all expansion protocols have in common that they extend over a maximum period of two weeks. Long-term expansion was studied by Cieris group in order to test the expansion potential of individual T cell subsets, but detailed data about longitudinal changes in T cell transcriptome, phenotype and function are lacking. It was thus the

aim of this PhD project to understand not only the expansion potential of T cells over a period above two weeks, but at the same time to investigate in detail the longitudinal changes of transcriptome and the function of Tcm cells during long-lasting expansion over four weeks. For reasons of comparability with previous studies from Cieri and Pulko [134, 195], the clinical relevance due to already established clinical protocols with IL7/IL15 and the fact that transcriptomic signatures of IL7/IL15 and IL15/IL27 did not show any difference in gene expression, the detailed investigations were performed with IL7/IL15 expanded T cells.

Cieri et al. long-term expanded murine and human CD8 T cells from healthy donors over four weeks. As published, this resulted in significantly an increased Tcm cell count of LT compared to ST CD8 T cells. Expansion of murine CD4 T cells was also practicable for three weeks, but the net yield of ST and LT CD4 T cells was almost the same. Interestingly, human CD4 T cells from healthy donors demonstrated a significant increase over time. Only few studies have shown differences in murine and human T cell differentiation or priming, but differences in the *in vitro* expansion potential of CD4 T cells has not yet been described [234].

Recently, Zhang et al. defined IL2 expansion over 10 days as long-term expansion and reported terminal T cell differentiation and reduced CAR T cell function [235]. This PhD project has demonstrated that a genuine long-term expansion with IL7/IL15 can boost CD8 and CD4 T cell differentiation into desired Tcm and Tscm phenotypes represented by increased expression levels of CD44, CD62L, CD122, Sca1, Bcl-2 and CXCR3 for murine T cells and CD45Ro, CCR7 for human T cells. This study is the first to elucidate the gene expression profile of long-term expanded memory T cells. Thus, RNA sequencing data of ST and LT CD8 and CD4 Tcm cells were compared with published signatures of murine and human T cell subtypes also specified by cell surface markers of CCR7 and CD45RO/CD45RA or CD44 and CD62L [134, 139-141, 195, 196]. These comprehensive comparisons by unsupervised hierarchical clustering and principal component analysis revealed that both ST and LT CD8 Tcm cells were closely related to CD8 Tcm, Tscm and Wnt pathway-induced CD8 Tscm subsets. ST and LT CD4 Tcm cells were most closely associated with CD4 Tcm and naturally or Notch-induced CD4 Tscm subsets emphasizing a stable profile over time. Moreover, the entire transcriptome of ST and LT Tcm cells was compared and 2786 altered genes during CD8 and 912 altered genes during CD4 T cell expansion were found. This revealed,

that over half of the differently expressed genes in CD4 T cells were analogously deregulated in CD8 T cells. The large overlap indicates specific T cell gene alterations induced by expansion with IL7 and IL15. Additional GO term enrichment analysis highlighted down-regulated gene pathways known to be key regulators of proliferation and cell cycle in both LT CD8 and CD4 T cells that might be an explanation for the plateaus of the expansion curves. A corresponding cell cycle arrest has already been described for IL15-induced memory-like CD8 T cells by Carrio et al. [231]. Moreover, LT CD8 and CD4 T cells highly down-regulated genes associated with immune checkpoint inhibition (*Cd200, Pdcd1, Lag3*) [203, 204] and T cell dysfunction (*Dusp4, Tox and Nr4a1*) [205-208], suggesting the absence of culture-induced T cell dysfunction. In summary, the longitudinal phenotypical and molecular analyses indicate that a prolonged expansion using IL7 and IL15 enhances T cell expansion with desired Tcm/Tscm phenotype and largely preserved transcriptional activity.

6.2.3. *In vitro* and *in vivo* analyses of long-term expanded T cells demonstrate feasibility for ATT

Next, the *in vitro* function of ST vs. LT murine and human T cells was tested and similar proliferation capacity, apoptosis susceptibility and up-regulation of TIIRs upon polyclonal stimulation with antiCD3/CD28 were observed. Furthermore, a higher IL2, IFNγ and granzyme B production in re-stimulated LT CD8 and CD4 T cells was found. The TNFα expression was enriched only in murine LT CD8 T cells. Human CD8 and CD4 T cells from healthy donors showed increasing IFNγ and TNFα expression over the first three weeks, with subsequent cytokine decrease, achieving the expression level of ST T cells (except for TNFα in CD8 T cells), which suggests an enhanced *in vitro* T cell function for three weeks and stably expression until week 4.

A clear correlation between the engraftment and persistence of adoptively transferred T cells and the clinical outcome has been shown by several studies [25, 236-238]. It has also been shown that short-term T cell expansion with IL2 exhibits improved T cell survival capacity, expansion and anti-tumor activity in vivo compared to long-term expanded T cells [128, 235, 239, 240]. This study revealed a significant increase of T cell numbers available for ATT by long-term expansion and that this could be attained without loss in T cell functionality via IL7/IL15 expansion. *In vivo* properties for engraftment, persistence and anti-tumor activity of ST and LT T cells were compared under lymphopenic conditions by taking advantage of the bioluminescent

dual-luciferase reporter mouse called BLITC, enabling simultaneous monitoring of migration, expansion and activation of adoptively transferred T cells in situ [92]. Engraftment, persistence and antigen encounter functionality were potent for ST and LT CD8 T cells without loss of strength during long-term expansion. Even with constitutive antigen challenge of ST and LT MH-BLITC T cells into male recipients it was possible to measure their homeostatic presence and demonstrate strong persistence over three months. The engraftment and persistence capacity of CD4 T cells was even stronger compared to CD8 T cells. This might result from the T cell culture, which, among other genes, down-regulates LAG3. Published research has reported that T cells from LAG3$^{-/-}$ showed increased expansion in ATT-recipients (Workman et al. 2004). Anti-tumor activity was tested in different tumor models. The ability of ST and LT H-Y transgenic CD4 and CD8 T cells and TCR-1 transducer CD8 T cells to eradicate target antigen expressing tumor cells in immunosuppressed mice was also comparable between both groups, suggesting stable Tcm/Tscm-like properties and a preserved effector function of adoptively transferred murine LT T cells. Further functional analysis of ST and LT human T cells *in vivo* - for instance transfer experiments in NOD/SCID mice – have not yet been performed. Nevertheless, the revealed findings on cytokine expression are similar to what was observed for the murine T cells, implying strong functionality of LT human T cells to provide effective cytotoxic anti-tumor activity. These findings will have to be tested with material from potential ATT patients, e.g. DLBCL patients with refractory immune checkpoint therapy. As dropouts in clinical trials were due to failure of CAR T cell expansion, the clinical need for ameliorated T cell expansion is obvious [70-72].

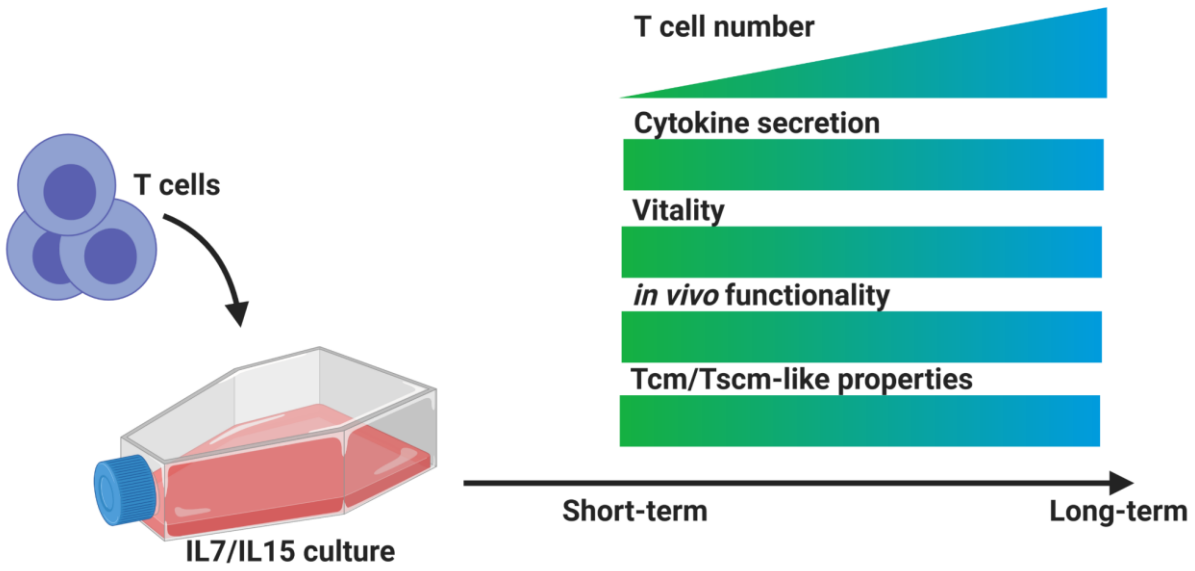

Figure 30. Schema of summerized properties compared between ST and LT. Cytokine secretion, vitality, in vivo functionality as engraftment, persistence and anti-tumor activity and the expression of Tcm/Tscm-like surface markers are retained during long-term T cell expansion, compared to short-term expanded T cells. Consequently, total T cell number increases significally during long-term expansion.

In summary, this work shows the practicability of manufacturing an increased number of desired CD4 and CD8 T cells with Tcm/Tscm-like properties feasible for ATT by means of a prolonged expansion with the cytokines IL7/IL15 (see Figure 30). Although elongation of GMP-compatible expansion is certainly cost-intensive, it could be an option for low-expanding T cells, e.g. those originating from pre-treated DLBCL patients. Another option would be to produce a backup T cell graft for a second infusion in case of failed engraftment or in order to boost anti-tumor activity.

7. Abstract

Adoptive T cell therapy (ATT) is a promising cancer immunotherapy. However, targeting a tumor antigen also expressed in peripheral tissues harbors the risk of „on-target, off-tumor“ toxicity. Furthermore, ATT is highly dependent on the rapid generation of sufficient numbers of tumor-reactive T cells, for which activation and expansion of T cells is indispensable. The properties of the final cell product decisively determine the success of ATT. Central memory T cells (Tcm) and stem cell memory T cells (Tscm) are valuable candidates for ATT because of their ability to self-renew and differentiate into potent effector T cells.

Different questions were addressed using the unique *bioluminescence imaging of T cells* (BLITC) reporter system, which is able to monitor T cell migration and activation patterns *in vivo*.

1) Shifting the balance between “on-target, off-tumor“ toxicity and Graft versus Tumor (GvT) within the HY minor histocompatibility antigen mismatch model by treatment with lymphocyte Peyer’s patch adhesion molecule (LPAM)-1. Reduced T cell infiltration into the mesenteric tissue was not traceable in bioluminescence measurements and treatment with LPAM-1 antibody did not lead to an ameliorated “on-target, off-tumor“ toxicity.

2) Expanding T cell numbers and effector functionality by using the new cytokine combination IL15/IL27. Thus, IL15/IL27 expanded T cells were compared with IL7/IL15 expanded T cells, which is already in use for some clinical trials. The present PhD project demonstrated a doubling of T cell numbers with retained cytokine expression *in vitro* compared to IL7/IL15 expanded T cells. However, comparison of whole transcriptome signatures did not show significant differences in gene expression.

3) Extended T cell expansion with IL7/IL15 revealed enhanced yield of Tcm cells without lacking T cell functionality. Long-term (LT) T cell expansion was compared with commonly used short-term expanded T cells regarding *in vitro* cytokine expression, expression of T cell inhibiting receptors (TIRs), apoptosis and proliferation capacity. Further longitudinal changes of the Tcm transcriptome were characterized by RNA sequencing and revealed a high overlap of CD8 and CD4 up- or down-regulated genes over time. This might occur due to LT expansion, but *in vivo* analysis of LT T cells demonstrated preserved engraftment, persistence, proliferation and anti-tumor capacities. It was possible to confirm *in vitro* findings for human T cells.

This thesis demonstrates a feasible manufacturing protocol by simply using the cytokines IL7/IL15 for extended T cell expansion resulting in significant increased numbers of favorable T cells with central memory or stem cell like properties and widely preserved T cell functionality. This could be of clinical relevance for hampered T cell manufacturing or for providing an optional second donor lymphocyte infusion.

8. Zusammenfassung

Die adoptive T-Zelltherapie (ATT) ist eine vielversprechende Krebsimmuntherapie. Allerdings birgt das spezifische Angreifen von Tumorantigenen oftmals das Risiko, dass diese Antigene auch auf anderem Gewebe exprimiert sind und es somit zu einer "on-target, off-tumor" Toxizität kommen kann. Für den Erfolg der ATT sind Produktionsdauer und die Eigenschaften des T-Zellprodukts mitentscheidend. Zentrale Gedächtnis-T-Zellen (Tcm) und Stammzellen-Gedächtnis-T-Zellen (Tscm) stellen aufgrund ihrer Fähigkeit zur Selbsterneuerung und reaktiven Differenzierung zu potenten Effektor-T-Zellen hierbei wertvolle Kandidaten für die ATT dar. Über das Biolumineszenz-Imaging von T-Zellen (BLITC)-Reportersystem, das die Verlaufsbeobachtung von Migration, Expansion und Aktivierung adoptiv transferierter T-Zellen *in vivo* ermöglicht, wurde Folgendes untersucht:

1) Die Verschiebung der "on-target, off-tumor" Toxizität und Transplantat-gegen-Tumor (GvT)-Aktivität innerhalb des HY-Antigen-Modells mittels spezifischer Antikörperblockierung von Lymphozyten Peyer's Patch Adhäsionsmolekül (LPAM)-1. Eine reduzierte T-Zellinfiltration in intestinales Gewebe war bei den Biolumineszenz-Messungen nicht nachweisbar und die Behandlung mit dem LPAM-1-Antikörper führte nicht zu einer verbesserten "on-target, off-tumor" Toxizität.

2) Erhöhung der T-Zellzahl und der Effektorfunktionalität mittels neuer Zytokinkombination IL15/IL27. Dazu wurden T-Zellen nach Expansion mit IL15/IL27 versus IL7/IL15, einer Standardkombination in klinischen Studien, verglichen. In der vorliegenden Promotionsarbeit zeigte sich eine Verdoppelung der T-Zellzahl nach IL15/IL27 Expansion bei vergleichbarer Zytokinexpression *in vitro* – verglichen mit IL7/IL15 expandierten T-Zellen. Der Vergleich von Transkriptomdaten zeigte allerdings keine signifikanten Unterschiede in der Genexpression.

3) Die Verlängerung der T-Zell-Expansion mit IL7/IL15 ergab eine erhöhte Ausbeute an Tcm-Zellen bei gleichbleibender T-Zell-Funktionalität. Die verlängerte (LT) T-Zellexpansion wurde mit den üblicherweise verwendeten kurzzeitig (ST) expandierten T-Zellen hinsichtlich der *in vitro* Zytokinexpression, der Expression von T-Zell-inhibierenden Rezeptoren (TIRs), der Apoptose und der Proliferationskapazität verglichen. Weitere longitudinale Veränderungen des Tcm-Transkriptoms wurden durch RNA-Sequenzierung charakterisiert und zeigten eine hohe Überlappung der CD8 und CD4 hoch- oder runter-exprimierten Gene. *In vivo* Ergebnisse bzgl. Anwachsen, Persistenz, Proliferation und Anti-Tumor-Kapazität der T-Zellen waren vergleichbar. Die *in vitro* Ergebnisse konnten für humane T-Zellen bestätigt werden.

Die vorliegende Arbeit zeigt ein praktikables Herstellungsprotokoll für eine Langzeit T-Zell Kultur durch die Standardkombination IL7 /IL15, mit dem eine signifikant erhöhte Anzahl bevorzugter T-Zellen mit Gedächtnis- oder Stammzell-ähnlichen Eigenschaften und einer weitgehend erhaltenen T-Zell-Funktionalität erzielt werden kann. Die Ergebnisse sind von klinischer Relevanz für schlecht expandierende T-Zellen oder für die Bereitstellung einer optionalen zweiten T-Zellinfusion.

9. References

1. Murphy, K. and C. Weaver, *Janeway's IMMUNOBIOLOGY 9th edition*, ed. 9th. 2017, New York: Garland Science.
2. Riera Romo, M., D. Perez-Martinez, and C. Castillo Ferrer, *Innate immunity in vertebrates: an overview.* Immunology, 2016. **148**(2): p. 125-39.
3. Kennedy, M.A., *A brief review of the basics of immunology: the innate and adaptive response.* Vet Clin North Am Small Anim Pract, 2010. **40**(3): p. 369-79.
4. Ping, Y., C. Liu, and Y. Zhang, *T-cell receptor-engineered T cells for cancer treatment: current status and future directions.* Protein Cell, 2018. **9**(3): p. 254-266.
5. Couzin-Frankel, J., *Breakthrough of the year 2013. Cancer immunotherapy.* Science, 2013. **342**(6165): p. 1432-3.
6. Kruger, S., et al., *Advances in cancer immunotherapy 2019 - latest trends.* J Exp Clin Cancer Res, 2019. **38**(1): p. 268.
7. Altmann, D.M., *A Nobel Prize-worthy pursuit: cancer immunology and harnessing immunity to tumour neoantigens.* Immunology, 2018. **155**(3): p. 283-284.
8. June, C.H., et al., *CAR T cell immunotherapy for human cancer.* Science, 2018. **359**(6382): p. 1361-1365.
9. Ribas, A. and J.D. Wolchok, *Cancer immunotherapy using checkpoint blockade.* Science, 2018. **359**(6382): p. 1350-1355.
10. Luke, J.J., et al., *Targeted agents and immunotherapies: optimizing outcomes in melanoma.* Nat Rev Clin Oncol, 2017. **14**(8): p. 463-482.
11. Mayor, M., et al., *Immunotherapy for non-small cell lung cancer: current concepts and clinical trials.* Eur J Cardiothorac Surg, 2016. **49**(5): p. 1324-33.
12. Sahin, U. and O. Tureci, *Personalized vaccines for cancer immunotherapy.* Science, 2018. **359**(6382): p. 1355-1360.
13. Thomas, S. and G.C. Prendergast, *Cancer Vaccines: A Brief Overview.* Methods Mol Biol, 2016. **1403**: p. 755-61.
14. Spiess, P.J., J.C. Yang, and S.A. Rosenberg, *In vivo antitumor activity of tumor-infiltrating lymphocytes expanded in recombinant interleukin-2.* J Natl Cancer Inst, 1987. **79**(5): p. 1067-75.
15. Rosenberg, S.A., et al., *Use of tumor-infiltrating lymphocytes and interleukin-2 in the immunotherapy of patients with metastatic melanoma. A preliminary report.* N Engl J Med, 1988. **319**(25): p. 1676-80.
16. Rosenberg, S.A., P. Spiess, and R. Lafreniere, *A new approach to the adoptive immunotherapy of cancer with tumor-infiltrating lymphocytes.* Science, 1986. **233**(4770): p. 1318-21.
17. Gross, G., T. Waks, and Z. Eshhar, *Expression of immunoglobulin-T-cell receptor chimeric molecules as functional receptors with antibody-type specificity.* Proc Natl Acad Sci U S A, 1989. **86**(24): p. 10024-8.
18. Dudley, M.E., et al., *Cancer regression and autoimmunity in patients after clonal repopulation with antitumor lymphocytes.* Science, 2002. **298**(5594): p. 850-4.
19. Maher, J., et al., *Human T-lymphocyte cytotoxicity and proliferation directed by a single chimeric TCRzeta /CD28 receptor.* Nat Biotechnol, 2002. **20**(1): p. 70-5.
20. Brentjens, R.J., et al., *Eradication of systemic B-cell tumors by genetically targeted human T lymphocytes co-stimulated by CD80 and interleukin-15.* Nat Med, 2003. **9**(3): p. 279-86.
21. Morgan, R.A., et al., *Cancer Regression in Patients After Transfer of Genetically Engineered Lymphocytes.* Science, 2006. **314**(5796): p. 126-129.
22. Kochenderfer, J.N., et al., *Eradication of B-lineage cells and regression of lymphoma in a patient treated with autologous T cells genetically engineered to recognize CD19.* Blood, 2010. **116**(20): p. 4099-102.
23. Porter, D.L., et al., *Chimeric antigen receptor-modified T cells in chronic lymphoid leukemia.* N Engl J Med, 2011. **365**(8): p. 725-33.
24. Brentjens, R.J., et al., *CD19-targeted T cells rapidly induce molecular remissions in adults with chemotherapy-refractory acute lymphoblastic leukemia.* Sci Transl Med, 2013. **5**(177): p. 177ra38.
25. Grupp, S.A., et al., *Chimeric antigen receptor-modified T cells for acute lymphoid leukemia.* N Engl J Med, 2013. **368**(16): p. 1509-1518.
26. Kalos, M., et al., *T cells with chimeric antigen receptors have potent antitumor effects and can establish memory in patients with advanced leukemia.* Sci Transl Med, 2011. **3**(95): p. 95ra73.

27. Robbins, P.F., et al., *Tumor regression in patients with metastatic synovial cell sarcoma and melanoma using genetically engineered lymphocytes reactive with NY-ESO-1.* J Clin Oncol, 2011. **29**(7): p. 917-24.
28. Vairy, S., et al., *CTL019 (tisagenlecleucel): CAR-T therapy for relapsed and refractory B-cell acute lymphoblastic leukemia.* Drug Des Devel Ther, 2018. **12**: p. 3885-3898.
29. Seimetz, D., K. Heller, and J. Richter, *Approval of First CAR-Ts: Have we Solved all Hurdles for ATMPs?* Cell Medicine, 2019. **11**.
30. Rohaan, M.W., S. Wilgenhof, and J. Haanen, *Adoptive cellular therapies: the current landscape.* Virchows Arch, 2019. **474**(4): p. 449-461.
31. Rapoport, A.P., et al., *NY-ESO-1-specific TCR-engineered T cells mediate sustained antigen-specific antitumor effects in myeloma.* Nat Med, 2015. **21**(8): p. 914-921.
32. Klebanoff, C.A., S.A. Rosenberg, and N.P. Restifo, *Prospects for gene-engineered T cell immunotherapy for solid cancers.* Nat Med, 2016. **22**(1): p. 26-36.
33. Zhu, W., et al., *Identification of alpha-fetoprotein-specific T-cell receptors for hepatocellular carcinoma immunotherapy.* Hepatology, 2018. **68**(2): p. 574-589.
34. Jiang, X., et al., *Adoptive CD8(+) T cell therapy against cancer:Challenges and opportunities.* Cancer Lett, 2019. **462**: p. 23-32.
35. Quezada, S.A., et al., *Tumor-reactive CD4(+) T cells develop cytotoxic activity and eradicate large established melanoma after transfer into lymphopenic hosts.* J Exp Med, 2010. **207**(3): p. 637-50.
36. Lu, Y., et al., *Th9 Cells Represent a Unique Subset of CD4(+) T Cells Endowed with the Ability to Eradicate Advanced Tumors.* Cancer Cell, 2018. **33**(6): p. 1048-1060 e7.
37. Hunder, N.N., et al., *Treatment of metastatic melanoma with autologous CD4+ T cells against NY-ESO-1.* N Engl J Med, 2008. **358**(25): p. 2698-703.
38. Tran, E., et al., *Cancer immunotherapy based on mutation-specific CD4+ T cells in a patient with epithelial cancer.* Science, 2014. **344**(6184): p. 641-5.
39. Lu, Y.C., et al., *Treatment of Patients With Metastatic Cancer Using a Major Histocompatibility Complex Class II-Restricted T-Cell Receptor Targeting the Cancer Germline Antigen MAGE-A3.* J Clin Oncol, 2017. **35**(29): p. 3322-3329.
40. Dudley, M.E., et al., *Adoptive cell transfer therapy following non-myeloablative but lymphodepleting chemotherapy for the treatment of patients with refractory metastatic melanoma.* J Clin Oncol, 2005. **23**(10): p. 2346-57.
41. Ellebaek, E., et al., *Adoptive cell therapy with autologous tumor infiltrating lymphocytes and low-dose Interleukin-2 in metastatic melanoma patients.* J Transl Med, 2012. **10**: p. 169.
42. Andersen, R., et al., *Long-Lasting Complete Responses in Patients with Metastatic Melanoma after Adoptive Cell Therapy with Tumor-Infiltrating Lymphocytes and an Attenuated IL2 Regimen.* Clin Cancer Res, 2016. **22**(15): p. 3734-45.
43. Neelapu, S.S., et al., *Axicabtagene Ciloleucel CAR T-Cell Therapy in Refractory Large B-Cell Lymphoma.* N Engl J Med, 2017. **377**(26): p. 2531-2544.
44. Marabondo, S. and H.L. Kaufman, *High-dose interleukin-2 (IL-2) for the treatment of melanoma: safety considerations and future directions.* Expert Opin Drug Saf, 2017. **16**(12): p. 1347-1357.
45. Dudley, M.E., et al., *Generation of tumor-infiltrating lymphocyte cultures for use in adoptive transfer therapy for melanoma patients.* J Immunother, 2003. **26**(4): p. 332-42.
46. Besser, M.J., et al., *Minimally cultured or selected autologous tumor-infiltrating lymphocytes after a lympho-depleting chemotherapy regimen in metastatic melanoma patients.* J Immunother, 2009. **32**(4): p. 415-23.
47. Aranda, F., et al., *Trial Watch: Adoptive cell transfer for anticancer immunotherapy.* Oncoimmunology, 2014. **3**: p. e28344.
48. Hilders, C.G., et al., *Isolation and characterization of tumor-infiltrating lymphocytes from cervical carcinoma.* Int J Cancer, 1994. **57**(6): p. 805-13.
49. Yannelli, J.R., et al., *Growth of tumor-infiltrating lymphocytes from human solid cancers: summary of a 5-year experience.* Int J Cancer, 1996. **65**(4): p. 413-21.
50. Turcotte, S., et al., *Phenotype and function of T cells infiltrating visceral metastases from gastrointestinal cancers and melanoma: implications for adoptive cell transfer therapy.* J Immunol, 2013. **191**(5): p. 2217-25.
51. Webb, J.R., et al., *Tumor-infiltrating lymphocytes expressing the tissue resident memory marker CD103 are associated with increased survival in high-grade serous ovarian cancer.* Clin Cancer Res, 2014. **20**(2): p. 434-44.

52. Andersen, R., et al., *T-cell Responses in the Microenvironment of Primary Renal Cell Carcinoma-Implications for Adoptive Cell Therapy.* Cancer Immunol Res, 2018. **6**(2): p. 222-235.
53. Mayor, P., K. Starbuck, and E. Zsiros, *Adoptive cell transfer using autologous tumor infiltrating lymphocytes in gynecologic malignancies.* Gynecol Oncol, 2018. **150**(2): p. 361-369.
54. Liu, D. and J. Zhao, *Cytokine release syndrome: grading, modeling, and new therapy.* J Hematol Oncol, 2018. **11**(1): p. 121.
55. van den Berg, J.H., et al., *Case Report of a Fatal Serious Adverse Event Upon Administration of T Cells Transduced With a MART-1-specific T-cell Receptor.* Mol Ther, 2015. **23**(9): p. 1541-50.
56. Borbulevych, O.Y., et al., *TCRs used in cancer gene therapy cross-react with MART-1/Melan-A tumor antigens via distinct mechanisms.* J Immunol, 2011. **187**(5): p. 2453-63.
57. Morgan, R.A., et al., *Cancer regression and neurological toxicity following anti-MAGE-A3 TCR gene therapy.* J Immunother, 2013. **36**(2): p. 133-51.
58. Garrido, F., F. Ruiz-Cabello, and N. Aptsiauri, *Rejection versus escape: the tumor MHC dilemma.* Cancer Immunol Immunother, 2017. **66**(2): p. 259-271.
59. Gardner, R., et al., *Acquisition of a CD19-negative myeloid phenotype allows immune escape of MLL-rearranged B-ALL from CD19 CAR-T-cell therapy.* Blood, 2016. **127**(20): p. 2406-10.
60. Turtle, C.J., et al., *Immunotherapy of non-Hodgkin's lymphoma with a defined ratio of CD8+ and CD4+ CD19-specific chimeric antigen receptor-modified T cells.* Sci Transl Med, 2016. **8**(355): p. 355ra116.
61. Sotillo, E., et al., *Convergence of Acquired Mutations and Alternative Splicing of CD19 Enables Resistance to CART-19 Immunotherapy.* Cancer Discov, 2015. **5**(12): p. 1282-95.
62. Srivastava, S. and S.R. Riddell, *Chimeric Antigen Receptor T Cell Therapy: Challenges to Bench-to-Bedside Efficacy.* J Immunol, 2018. **200**(2): p. 459-468.
63. Rohaan, M.W., et al., *Adoptive transfer of tumor-infiltrating lymphocytes in melanoma: a viable treatment option.* J Immunother Cancer, 2018. **6**(1): p. 102.
64. Johnson, L.A., et al., *Gene therapy with human and mouse T-cell receptors mediates cancer regression and targets normal tissues expressing cognate antigen.* Blood, 2009. **114**(3): p. 535-46.
65. Morgan, D.A., F.W. Ruscetti, and R. Gallo, *Selective in vitro growth of T lymphocytes from normal human bone marrows.* Science, 1976. **193**(4257): p. 1007-8.
66. Cantrell, D.A. and K.A. Smith, *The interleukin-2 T-cell system: a new cell growth model.* Science, 1984. **224**(4655): p. 1312-6.
67. Joseph, R.W., et al., *Impact of clinical and pathologic features on tumor-infiltrating lymphocyte expansion from surgically excised melanoma metastases for adoptive T-cell therapy.* Clin Cancer Res, 2011. **17**(14): p. 4882-91.
68. Rosenberg, S.A., et al., *Durable complete responses in heavily pretreated patients with metastatic melanoma using T-cell transfer immunotherapy.* Clin Cancer Res, 2011. **17**(13): p. 4550-7.
69. Svane, I.M. and E.M. Verdegaal, *Achievements and challenges of adoptive T cell therapy with tumor-infiltrating or blood-derived lymphocytes for metastatic melanoma: what is needed to achieve standard of care?* Cancer Immunol Immunother, 2014. **63**(10): p. 1081-91.
70. Petersen, C.T., et al., *Improving T-cell expansion and function for adoptive T-cell therapy using ex vivo treatment with PI3Kδ inhibitors and VIP antagonists.* Blood Advances, 2018. **2**(3): p. 210-223.
71. Schuster, S., et al., *Global Pivotal Phase 2 Trial of the CD19-Targeted Therapy CTL019 In Adult Patients with Relapsed or Refractory (R/R) Diffuse Large B-Cell Lymphoma (DLBCL)—An Interim Analysis.* Clinical Lymphoma Myeloma and Leukemia, 2017. **17**: p. S373-S374.
72. Singh, N., et al., *Early memory phenotypes drive T cell proliferation in patients with pediatric malignancies.* Sci Transl Med, 2016. **8**(320): p. 320ra3.
73. Jin, J., et al., *Enhanced clinical-scale manufacturing of TCR transduced T-cells using closed culture system modules.* Journal of Translational Medicine, 2018. **16**(1).
74. Yao, X., et al., *Isolation and Characterization of an HLA-DPB1*04: 01-restricted MAGE-A3 T-Cell Receptor for Cancer Immunotherapy.* J Immunother, 2016. **39**(5): p. 191-201.
75. Nguyen, L.T., et al., *Expansion and characterization of human melanoma tumor-infiltrating lymphocytes (TILs).* PLoS One, 2010. **5**(11): p. e13940.
76. Kalia, V., et al., *Prolonged interleukin-2Ralpha expression on virus-specific CD8+ T cells favors terminal-effector differentiation in vivo.* Immunity, 2010. **32**(1): p. 91-103.
77. Pipkin, M.E., et al., *Interleukin-2 and inflammation induce distinct transcriptional programs that promote the differentiation of effector cytolytic T cells.* Immunity, 2010. **32**(1): p. 79-90.

78. Cha, E., et al., *IL-7 + IL-15 are superior to IL-2 for the ex vivo expansion of 4T1 mammary carcinoma-specific T cells with greater efficacy against tumors in vivo.* Breast Cancer Res Treat, 2010. **122**(2): p. 359-69.
79. Hinrichs, C.S., et al., *Adoptively transferred effector cells derived from naive rather than central memory CD8+ T cells mediate superior antitumor immunity.* Proc Natl Acad Sci U S A, 2009. **106**(41): p. 17469-74.
80. Yang, S., et al., *Modulating the differentiation status of ex vivo-cultured anti-tumor T cells using cytokine cocktails.* Cancer Immunol Immunother, 2013. **62**(4): p. 727-36.
81. Lim, W.A. and C.H. June, *The Principles of Engineering Immune Cells to Treat Cancer.* Cell, 2017. **168**(4): p. 724-740.
82. Collins, R.H., Jr., et al., *Donor leukocyte infusions in 140 patients with relapsed malignancy after allogeneic bone marrow transplantation.* J Clin Oncol, 1997. **15**(2): p. 433-44.
83. Ferrara, J.L.M., et al., *Graft-versus-host disease.* The Lancet, 2009. **373**(9674): p. 1550-1561.
84. Welniak, L.A., B.R. Blazar, and W.J. Murphy, *Immunobiology of allogeneic hematopoietic stem cell transplantation.* Annu Rev Immunol, 2007. **25**: p. 139-70.
85. Bleakley, M. and S.R. Riddell, *Molecules and mechanisms of the graft-versus-leukaemia effect.* Nat Rev Cancer, 2004. **4**(5): p. 371-80.
86. Riddell, S.R., et al., *Restoration of viral immunity in immunodeficient humans by the adoptive transfer of T cell clones.* Science, 1992. **257**(5067): p. 238-41.
87. Walter, E.A., et al., *Reconstitution of cellular immunity against cytomegalovirus in recipients of allogeneic bone marrow by transfer of T-cell clones from the donor.* N Engl J Med, 1995. **333**(16): p. 1038-44.
88. Heslop, H.E., et al., *Long-term restoration of immunity against Epstein-Barr virus infection by adoptive transfer of gene-modified virus-specific T lymphocytes.* Nat Med, 1996. **2**(5): p. 551-5.
89. Yee, C., et al., *Adoptive T cell therapy using antigen-specific CD8+ T cell clones for the treatment of patients with metastatic melanoma: in vivo persistence, migration, and antitumor effect of transferred T cells.* Proc Natl Acad Sci U S A, 2002. **99**(25): p. 16168-73.
90. Morgan, R.A., et al., *Case report of a serious adverse event following the administration of T cells transduced with a chimeric antigen receptor recognizing ERBB2.* Mol Ther, 2010. **18**(4): p. 843-51.
91. Beatty, G.L., et al., *Correction: Mesothelin-Specific Chimeric Antigen Receptor mRNA-Engineered T Cells Induce Antitumor Activity in Solid Malignancies.* Cancer Immunol Res, 2015. **3**(2): p. 217.
92. Szyska, M., et al., *A Transgenic Dual-Luciferase Reporter Mouse for Longitudinal and Functional Monitoring of T Cells In Vivo.* Cancer Immunol Res, 2018. **6**(1): p. 110-120.
93. Toubai, T., et al., *Induction of acute GVHD by sex-mismatched H-Y antigens in the absence of functional radiosensitive host hematopoietic-derived antigen-presenting cells.* Blood, 2012. **119**(16): p. 3844-53.
94. Randolph, S.S., et al., *Female donors contribute to a selective graft-versus-leukemia effect in male recipients of HLA-matched, related hematopoietic stem cell transplants.* Blood, 2004. **103**(1): p. 347-52.
95. Kim, Y.H., et al., *In situ detection of HY-specific T cells in acute graft-versus-host disease-affected male skin after sex-mismatched stem cell transplantation.* Biol Blood Marrow Transplant, 2012. **18**(3): p. 381-7.
96. Lantz, O., et al., *Gamma chain required for naive CD4+ T cell survival but not for antigen proliferation.* Nat Immunol, 2000. **1**(1): p. 54-8.
97. Valujskikh, A., et al., *Cross-primed CD8(+) T cells mediate graft rejection via a distinct effector pathway.* Nat Immunol, 2002. **3**(9): p. 844-51.
98. Staveley-O'Carroll, K., et al., *In vivo ligation of CD40 enhances priming against the endogenous tumor antigen and promotes CD8+ T cell effector function in SV40 T antigen transgenic mice.* J Immunol, 2003. **171**(2): p. 697-707.
99. Anders, K., et al., *Oncogene-targeting T cells reject large tumors while oncogene inactivation selects escape variants in mouse models of cancer.* Cancer Cell, 2011. **20**(6): p. 755-67.
100. Hynes, R.O., *Integrins: bidirectional, allosteric signaling machines.* Cell, 2002. **110**(6): p. 673-87.
101. Ley, K., et al., *Integrin-based therapeutics: biological basis, clinical use and new drugs.* Nat Rev Drug Discov, 2016. **15**(3): p. 173-83.
102. Yang, J.T., H. Rayburn, and R.O. Hynes, *Cell adhesion events mediated by alpha 4 integrins are essential in placental and cardiac development.* Development, 1995. **121**(2): p. 549-60.

103. Georges-Labouesse, E., et al., *Absence of integrin alpha 6 leads to epidermolysis bullosa and neonatal death in mice.* Nat Genet, 1996. **13**(3): p. 370-3.
104. Luo, B.H., C.V. Carman, and T.A. Springer, *Structural basis of integrin regulation and signaling.* Annu Rev Immunol, 2007. **25**: p. 619-47.
105. Frampton, J.E. and G.L. Plosker, *Efalizumab: a review of its use in the management of chronic moderate-to-severe plaque psoriasis.* Am J Clin Dermatol, 2009. **10**(1): p. 51-72.
106. Tauber, J., et al., *Lifitegrast Ophthalmic Solution 5.0% versus Placebo for Treatment of Dry Eye Disease: Results of the Randomized Phase III OPUS-2 Study.* Ophthalmology, 2015. **122**(12): p. 2423-31.
107. Raab-Westphal, S., J.F. Marshall, and S.L. Goodman, *Integrins as Therapeutic Targets: Successes and Cancers.* Cancers (Basel), 2017. **9**(9).
108. Holzmann, B., B.W. McIntyre, and I.L. Weissman, *Identification of a murine Peyer's patch--specific lymphocyte homing receptor as an integrin molecule with an alpha chain homologous to human VLA-4 alpha.* Cell, 1989. **56**(1): p. 37-46.
109. Holzmann, B. and I.L. Weissman, *Peyer's patch-specific lymphocyte homing receptors consist of a VLA-4-like alpha chain associated with either of two integrin beta chains, one of which is novel.* EMBO J, 1989. **8**(6): p. 1735-41.
110. Berlin, C., et al., *Alpha 4 beta 7 integrin mediates lymphocyte binding to the mucosal vascular addressin MAdCAM-1.* Cell, 1993. **74**(1): p. 185-95.
111. Hamann, A., et al., *Role of alpha 4-integrins in lymphocyte homing to mucosal tissues in vivo.* J Immunol, 1994. **152**(7): p. 3282-93.
112. Erle, D.J., et al., *Expression and function of the MAdCAM-1 receptor, integrin alpha 4 beta 7, on human leukocytes.* J Immunol, 1994. **153**(2): p. 517-28.
113. Petrovic, A., et al., *LPAM (α4β7 integrin) is an important homing integrin on alloreactive T cells in the development of intestinal graft-versus-host disease.* Blood, 2004. **103**(4): p. 1542-1547.
114. Waldman, E., et al., *Absence of beta7 integrin results in less graft-versus-host disease because of decreased homing of alloreactive T cells to intestine.* Blood, 2006. **107**(4): p. 1703-11.
115. Ferrara, J.L., et al., *Altered homeostatic regulation of innate and adaptive immunity in lower gastrointestinal tract GVHD pathogenesis.* J Clin Invest, 2017. **127**(7): p. 2441-2451.
116. Andrew, D.P., et al., *Distinct but overlapping epitopes are involved in alpha 4 beta 7-mediated adhesion to vascular cell adhesion molecule-1, mucosal addressin-1, fibronectin, and lymphocyte aggregation.* J Immunol, 1994. **153**(9): p. 3847-61.
117. Katayama, Y., et al., *Integrin alpha4beta7 and its counterreceptor MAdCAM-1 contribute to hematopoietic progenitor recruitment into bone marrow following transplantation.* Blood, 2004. **104**(7): p. 2020-6.
118. Hesterberg, P.E., et al., *Rapid resolution of chronic colitis in the cotton-top tamarin with an antibody to a gut-homing integrin alpha 4 beta 7.* Gastroenterology, 1996. **111**(5): p. 1373-80.
119. Kent, S.J., et al., *A monoclonal antibody to alpha 4 integrin suppresses and reverses active experimental allergic encephalomyelitis.* J Neuroimmunol, 1995. **58**(1): p. 1-10.
120. Leger, O.J., et al., *Humanization of a mouse antibody against human alpha-4 integrin: a potential therapeutic for the treatment of multiple sclerosis.* Hum Antibodies, 1997. **8**(1): p. 3-16.
121. Miller, D.H., et al., *A controlled trial of natalizumab for relapsing multiple sclerosis.* N Engl J Med, 2003. **348**(1): p. 15-23.
122. Gonzalez-Suarez, I., et al., *Catastrophic outcome of patients with a rebound after Natalizumab treatment discontinuation.* Brain Behav, 2017. **7**(4): p. e00671.
123. Feagan, B.G., et al., *Treatment of active Crohn's disease with MLN0002, a humanized antibody to the alpha4beta7 integrin.* Clin Gastroenterol Hepatol, 2008. **6**(12): p. 1370-7.
124. McLean, L.P., T. Shea-Donohue, and R.K. Cross, *Vedolizumab for the treatment of ulcerative colitis and Crohn's disease.* Immunotherapy, 2012. **4**(9): p. 883-98.
125. Lightner, A.L., et al., *Postoperative Outcomes in Vedolizumab-Treated Patients Undergoing Abdominal Operations for Inflammatory Bowel Disease.* J Crohns Colitis, 2017. **11**(2): p. 185-190.
126. Floisand, Y., et al., *Targeting Integrin alpha4beta7 in Steroid-Refractory Intestinal Graft-versus-Host Disease.* Biol Blood Marrow Transplant, 2017. **23**(1): p. 172-175.
127. Somerville, R.P., et al., *Clinical scale rapid expansion of lymphocytes for adoptive cell transfer therapy in the WAVE(R) bioreactor.* J Transl Med, 2012. **10**: p. 69.
128. Gattinoni, L., et al., *Acquisition of full effector function in vitro paradoxically impairs the in vivo antitumor efficacy of adoptively transferred CD8+ T cells.* J Clin Invest, 2005. **115**(6): p. 1616-26.

129. Rosenberg, S.A., et al., *Treatment of patients with metastatic melanoma with autologous tumor-infiltrating lymphocytes and interleukin 2.* J Natl Cancer Inst, 1994. **86**(15): p. 1159-66.
130. Yee, C., et al., *Melanocyte destruction after antigen-specific immunotherapy of melanoma: direct evidence of t cell-mediated vitiligo.* J Exp Med, 2000. **192**(11): p. 1637-44.
131. Restifo, N.P. and L. Gattinoni, *Lineage relationship of effector and memory T cells.* Curr Opin Immunol, 2013. **25**(5): p. 556-63.
132. Gattinoni, L., et al., *Removal of homeostatic cytokine sinks by lymphodepletion enhances the efficacy of adoptively transferred tumor-specific CD8+ T cells.* J Exp Med, 2005. **202**(7): p. 907-12.
133. Klebanoff, C.A., et al., *Central memory self/tumor-reactive CD8+ T cells confer superior antitumor immunity compared with effector memory T cells.* Proc Natl Acad Sci U S A, 2005. **102**(27): p. 9571-6.
134. Cieri, N., et al., *IL-7 and IL-15 instruct the generation of human memory stem T cells from naive precursors.* Blood, 2013. **121**(4): p. 573-84.
135. Zoon, C.K., et al., *Expansion of melanoma-specific lymphocytes in alternate gamma chain cytokines: gene expression variances between T cells and T-cell subsets exposed to IL-2 versus IL-7/15.* Cancer Gene Ther, 2014. **21**(10): p. 441-7.
136. Klebanoff, C.A., et al., *Determinants of successful CD8+ T-cell adoptive immunotherapy for large established tumors in mice.* Clin Cancer Res, 2011. **17**(16): p. 5343-52.
137. Gomez-Eerland, R., et al., *Manufacture of gene-modified human T-cells with a memory stem/central memory phenotype.* Hum Gene Ther Methods, 2014. **25**(5): p. 277-87.
138. Gargett, T. and M.P. Brown, *Different cytokine and stimulation conditions influence the expansion and immune phenotype of third-generation chimeric antigen receptor T cells specific for tumor antigen GD2.* Cytotherapy, 2015. **17**(4): p. 487-95.
139. Gattinoni, L., et al., *A human memory T cell subset with stem cell–like properties.* Nature Medicine, 2011. **17**(10): p. 1290-1297.
140. Kondo, T., et al., *Notch-mediated conversion of activated T cells into stem cell memory-like T cells for adoptive immunotherapy.* Nat Commun, 2017. **8**: p. 15338.
141. Sabatino, M., et al., *Generation of clinical-grade CD19-specific CAR-modified CD8+ memory stem cells for the treatment of human B-cell malignancies.* Blood, 2016. **128**(4): p. 519-28.
142. Kondo, T., et al., *Generation and application of human induced-stem cell memory T cells for adoptive immunotherapy.* Cancer Sci, 2018. **109**(7): p. 2130-2140.
143. Fiorentino, D.F., M.W. Bond, and T.R. Mosmann, *Two types of mouse T helper cell. IV. Th2 clones secrete a factor that inhibits cytokine production by Th1 clones.* J Exp Med, 1989. **170**(6): p. 2081-95.
144. Welch, P.A., et al., *Human IL-7: a novel T cell growth factor.* J Immunol, 1989. **143**(11): p. 3562-7.
145. Leonard, W.J., E.W. Shores, and P.E. Love, *Role of the common cytokine receptor gamma chain in cytokine signaling and lymphoid development.* Immunol Rev, 1995. **148**: p. 97-114.
146. Asao, H., et al., *Cutting edge: the common gamma-chain is an indispensable subunit of the IL-21 receptor complex.* J Immunol, 2001. **167**(1): p. 1-5.
147. Tan, J.T., et al., *IL-7 is critical for homeostatic proliferation and survival of naive T cells.* Proc Natl Acad Sci U S A, 2001. **98**(15): p. 8732-7.
148. Puel, A., et al., *Defective IL7R expression in T(-)B(+)NK(+) severe combined immunodeficiency.* Nat Genet, 1998. **20**(4): p. 394-7.
149. Peschon, J.J., et al., *Early lymphocyte expansion is severely impaired in interleukin 7 receptor-deficient mice.* J Exp Med, 1994. **180**(5): p. 1955-60.
150. Johnson, S.E., et al., *Murine and human IL-7 activate STAT5 and induce proliferation of normal human pro-B cells.* J Immunol, 2005. **175**(11): p. 7325-31.
151. Barata, J.T., et al., *Molecular and functional evidence for activity of murine IL-7 on human lymphocytes.* Exp Hematol, 2006. **34**(9): p. 1133-42.
152. Palmer, M.J., et al., *Interleukin-7 receptor signaling network: an integrated systems perspective.* Cell Mol Immunol, 2008. **5**(2): p. 79-89.
153. Krawczenko, A., C. Kieda, and D. Dus, *The biological role and potential therapeutic application of interleukin 7.* Arch Immunol Ther Exp (Warsz), 2005. **53**(6): p. 518-25.
154. Cantley, L.C., *The phosphoinositide 3-kinase pathway.* Science, 2002. **296**(5573): p. 1655-7.
155. Khaled, A.R. and S.K. Durum, *Lymphocide: cytokines and the control of lymphoid homeostasis.* Nat Rev Immunol, 2002. **2**(11): p. 817-30.
156. Soares, M.V., et al., *IL-7-dependent extrathymic expansion of CD45RA+ T cells enables preservation of a naive repertoire.* J Immunol, 1998. **161**(11): p. 5909-17.

157. Raeber, M.E., et al., *The role of cytokines in T-cell memory in health and disease.* Immunol Rev, 2018. **283**(1): p. 176-193.
158. Burton, J.D., et al., *A lymphokine, provisionally designated interleukin T and produced by a human adult T-cell leukemia line, stimulates T-cell proliferation and the induction of lymphokine-activated killer cells.* Proc Natl Acad Sci U S A, 1994. **91**(11): p. 4935-9.
159. Grabstein, K.H., et al., *Cloning of a T cell growth factor that interacts with the beta chain of the interleukin-2 receptor.* Science, 1994. **264**(5161): p. 965-8.
160. Rochman, Y., R. Spolski, and W.J. Leonard, *New insights into the regulation of T cells by gamma(c) family cytokines.* Nat Rev Immunol, 2009. **9**(7): p. 480-90.
161. Waldmann, T.A., *The biology of interleukin-2 and interleukin-15: implications for cancer therapy and vaccine design.* Nat Rev Immunol, 2006. **6**(8): p. 595-601.
162. Giri, J.G., et al., *Identification and cloning of a novel IL-15 binding protein that is structurally related to the alpha chain of the IL-2 receptor.* EMBO J, 1995. **14**(15): p. 3654-63.
163. Dubois, S., et al., *IL-15Ralpha recycles and presents IL-15 In trans to neighboring cells.* Immunity, 2002. **17**(5): p. 537-47.
164. Steel, J.C., T.A. Waldmann, and J.C. Morris, *Interleukin-15 biology and its therapeutic implications in cancer.* Trends Pharmacol Sci, 2012. **33**(1): p. 35-41.
165. Bergamaschi, C., et al., *Circulating IL-15 exists as heterodimeric complex with soluble IL-15Ralpha in human and mouse serum.* Blood, 2012. **120**(1): p. e1-8.
166. Ma, A., R. Koka, and P. Burkett, *Diverse functions of IL-2, IL-15, and IL-7 in lymphoid homeostasis.* Annu Rev Immunol, 2006. **24**: p. 657-79.
167. Kennedy, M.K., et al., *Reversible defects in natural killer and memory CD8 T cell lineages in interleukin 15-deficient mice.* J Exp Med, 2000. **191**(5): p. 771-80.
168. Fehniger, T.A., et al., *Fatal leukemia in interleukin 15 transgenic mice follows early expansions in natural killer and memory phenotype CD8+ T cells.* J Exp Med, 2001. **193**(2): p. 219-31.
169. Stoklasek, T.A., K.S. Schluns, and L. Lefrancois, *Combined IL-15/IL-15Ralpha immunotherapy maximizes IL-15 activity in vivo.* J Immunol, 2006. **177**(9): p. 6072-80.
170. Purton, J.F., et al., *Antiviral CD4+ memory T cells are IL-15 dependent.* J Exp Med, 2007. **204**(4): p. 951-61.
171. Kastelein, R.A., C.A. Hunter, and D.J. Cua, *Discovery and biology of IL-23 and IL-27: related but functionally distinct regulators of inflammation.* Annu Rev Immunol, 2007. **25**: p. 221-42.
172. Yoshida, H. and C.A. Hunter, *The immunobiology of interleukin-27.* Annu Rev Immunol, 2015. **33**: p. 417-43.
173. Hirahara, K., et al., *Asymmetric Action of STAT Transcription Factors Drives Transcriptional Outputs and Cytokine Specificity.* Immunity, 2015. **42**(5): p. 877-89.
174. Pflanz, S., et al., *IL-27, a heterodimeric cytokine composed of EBI3 and p28 protein, induces proliferation of naive CD4+ T cells.* Immunity, 2002. **16**(6): p. 779-90.
175. Harker, J.A., A. Dolgoter, and E.I. Zuniga, *Cell-intrinsic IL-27 and gp130 cytokine receptor signaling regulates virus-specific CD4(+) T cell responses and viral control during chronic infection.* Immunity, 2013. **39**(3): p. 548-59.
176. Harker, J.A., et al., *Interleukin-27R Signaling Mediates Early Viral Containment and Impacts Innate and Adaptive Immunity after Chronic Lymphocytic Choriomeningitis Virus Infection.* J Virol, 2018. **92**(12).
177. Morishima, N., et al., *Augmentation of effector CD8+ T cell generation with enhanced granzyme B expression by IL-27.* J Immunol, 2005. **175**(3): p. 1686-93.
178. Schneider, R., et al., *IL-27 increases the proliferation and effector functions of human naive CD8+ T lymphocytes and promotes their development into Tc1 cells.* Eur J Immunol, 2011. **41**(1): p. 47-59.
179. de Aquino, M.T., et al., *IL-27 limits central nervous system viral clearance by promoting IL-10 and enhances demyelination.* J Immunol, 2014. **193**(1): p. 285-94.
180. Liu, F.D., et al., *Timed action of IL-27 protects from immunopathology while preserving defense in influenza.* PLoS Pathog, 2014. **10**(5): p. e1004110.
181. Perona-Wright, G., et al., *Persistent loss of IL-27 responsiveness in CD8+ memory T cells abrogates IL-10 expression in a recall response.* Proc Natl Acad Sci U S A, 2012. **109**(45): p. 18535-40.
182. Salcedo, R., et al., *IL-27 mediates complete regression of orthotopic primary and metastatic murine neuroblastoma tumors: role for CD8+ T cells.* J Immunol, 2004. **173**(12): p. 7170-82.
183. Liu, Z., et al., *IL-27 enhances the survival of tumor antigen-specific CD8+ T cells and programs them into IL-10-producing, memory precursor-like effector cells.* Eur J Immunol, 2013. **43**(2): p. 468-79.

184. Chihara, N., et al., *Induction and transcriptional regulation of the co-inhibitory gene module in T cells.* Nature, 2018. **558**(7710): p. 454-459.
185. Porter, D.L., et al., *Induction of graft-versus-host disease as immunotherapy for relapsed chronic myeloid leukemia.* N Engl J Med, 1994. **330**(2): p. 100-6.
186. Blott, E.J. and G.M. Griffiths, *Secretory lysosomes.* Nat Rev Mol Cell Biol, 2002. **3**(2): p. 122-31.
187. Huse, M., et al., *T cells use two directionally distinct pathways for cytokine secretion.* Nat Immunol, 2006. **7**(3): p. 247-55.
188. Ramirez-Montagut, T., et al., *IFN-gamma and Fas ligand are required for graft-versus-tumor activity against renal cell carcinoma in the absence of lethal graft-versus-host disease.* J Immunol, 2007. **179**(3): p. 1669-80.
189. Borsotti, C., et al., *Absence of donor T-cell-derived soluble TNF decreases graft-versus-host disease without impairing graft-versus-tumor activity.* Blood, 2007. **110**(2): p. 783-6.
190. Ferrara, J.L., R. Levy, and N.J. Chao, *Pathophysiologic mechanisms of acute graft-vs.-host disease.* Biol Blood Marrow Transplant, 1999. **5**(6): p. 347-56.
191. Anderson, B.E., et al., *Memory CD4+ T cells do not induce graft-versus-host disease.* J Clin Invest, 2003. **112**(1): p. 101-8.
192. Zheng, H., et al., *Central memory CD8+ T cells induce graft-versus-host disease and mediate graft-versus-leukemia.* J Immunol, 2009. **182**(10): p. 5938-48.
193. Kim, G., et al., *A novel role for IL-27 in mediating the survival of activated mouse CD4 T lymphocytes.* J Immunol, 2013. **190**(4): p. 1510-8.
194. Perica, K., et al., *Adoptive T cell immunotherapy for cancer.* Rambam Maimonides Med J, 2015. **6**(1): p. e0004.
195. Pulko, V., et al., *Human memory T cells with a naive phenotype accumulate with aging and respond to persistent viruses.* Nat Immunol, 2016. **17**(8): p. 966-75.
196. Takeshita, M., et al., *Polarization diversity of human CD4+ stem cell memory T cells.* Clin Immunol, 2015. **159**(1): p. 107-17.
197. Love, M.I., W. Huber, and S. Anders, *Moderated estimation of fold change and dispersion for RNA-seq data with DESeq2.* Genome Biol, 2014. **15**(12): p. 550.
198. Rappsilber, J., Y. Ishihama, and M. Mann, *Stop and go extraction tips for matrix-assisted laser desorption/ionization, nanoelectrospray, and LC/MS sample pretreatment in proteomics.* Anal Chem, 2003. **75**(3): p. 663-70.
199. Tyanova, S., T. Temu, and J. Cox, *The MaxQuant computational platform for mass spectrometry-based shotgun proteomics.* Nat Protoc, 2016. **11**(12): p. 2301-2319.
200. Lattime, E.C., L.G. Gomella, and P.A. McCue, *Murine bladder carcinoma cells present antigen to BCG-specific CD4+ T-cells.* Cancer Res, 1992. **52**(15): p. 4286-90.
201. Nielsen, L.L., et al., *Development of a nude mouse model of ras-mediated neoplasia using WR21 cells from a transgenic mouse salivary tumor.* In Vivo, 1994. **8**(3): p. 295-302.
202. Gattinoni, L., et al., *Wnt signaling arrests effector T cell differentiation and generates CD8+ memory stem cells.* Nat Med, 2009. **15**(7): p. 808-13.
203. Thommen, D.S. and T.N. Schumacher, *T Cell Dysfunction in Cancer.* Cancer Cell, 2018. **33**(4): p. 547-562.
204. Wherry, E.J. and M. Kurachi, *Molecular and cellular insights into T cell exhaustion.* Nat Rev Immunol, 2015. **15**(8): p. 486-99.
205. Bignon, A., et al., *DUSP4-mediated accelerated T-cell senescence in idiopathic CD4 lymphopenia.* Blood, 2015. **125**(16): p. 2507-18.
206. Liu, X., et al., *Genome-wide analysis identifies NR4A1 as a key mediator of T cell dysfunction.* Nature, 2019. **567**(7749): p. 525-529.
207. Nowyhed, H.N., et al., *Cutting Edge: The Orphan Nuclear Receptor Nr4a1 Regulates CD8+ T Cell Expansion and Effector Function through Direct Repression of Irf4.* J Immunol, 2015. **195**(8): p. 3515-9.
208. Khan, O., et al., *TOX transcriptionally and epigenetically programs CD8(+) T cell exhaustion.* Nature, 2019. **571**(7764): p. 211-218.
209. Ludviksson, B.R., et al., *Administration of mAb against alpha E beta 7 prevents and ameliorates immunization-induced colitis in IL-2-/- mice.* J Immunol, 1999. **162**(8): p. 4975-82.
210. Rivera-Nieves, J., et al., *L-selectin, alpha 4 beta 1, and alpha 4 beta 7 integrins participate in CD4+ T cell recruitment to chronically inflamed small intestine.* J Immunol, 2005. **174**(4): p. 2343-52.
211. Sands, B.E., et al., *Effects of vedolizumab induction therapy for patients with Crohn's disease in whom tumor necrosis factor antagonist treatment failed.* Gastroenterology, 2014. **147**(3): p. 618-627 e3.

212. Beilhack, A., et al., *Prevention of acute graft-versus-host disease by blocking T-cell entry to secondary lymphoid organs.* Blood, 2008. **111**(5): p. 2919-28.
213. Zabel, B.A., et al., *Human G protein-coupled receptor GPR-9-6/CC chemokine receptor 9 is selectively expressed on intestinal homing T lymphocytes, mucosal lymphocytes, and thymocytes and is required for thymus-expressed chemokine-mediated chemotaxis.* J Exp Med, 1999. **190**(9): p. 1241-56.
214. Kunkel, E.J., et al., *Lymphocyte CC chemokine receptor 9 and epithelial thymus-expressed chemokine (TECK) expression distinguish the small intestinal immune compartment: Epithelial expression of tissue-specific chemokines as an organizing principle in regional immunity.* J Exp Med, 2000. **192**(5): p. 761-8.
215. Johansson-Lindbom, B., et al., *Selective generation of gut tropic T cells in gut-associated lymphoid tissue (GALT): requirement for GALT dendritic cells and adjuvant.* J Exp Med, 2003. **198**(6): p. 963-9.
216. Svensson, M., et al., *CCL25 mediates the localization of recently activated CD8αβ+ lymphocytes to the small-intestinal mucosa.* Journal of Clinical Investigation, 2002. **110**(8): p. 1113-1121.
217. Stenstad, H., et al., *Gut-associated lymphoid tissue-primed CD4+ T cells display CCR9-dependent and -independent homing to the small intestine.* Blood, 2006. **107**(9): p. 3447-54.
218. Paulos, C.M., et al., *Microbial translocation augments the function of adoptively transferred self/tumor-specific CD8+ T cells via TLR4 signaling.* J Clin Invest, 2007. **117**(8): p. 2197-204.
219. Nelson, M.H., et al., *Toll-like receptor agonist therapy can profoundly augment the antitumor activity of adoptively transferred CD8(+) T cells without host preconditioning.* J Immunother Cancer, 2016. **4**: p. 6.
220. Nunez, N.G., et al., *IFNbeta produced by TLR4-activated tumor cells is involved in improving the antitumoral immune response.* Cancer Res, 2012. **72**(3): p. 592-603.
221. Vallet, S., M. Pecherstorfer, and K. Podar, *Adoptive cell therapy in multiple Myeloma.* Expert Opin Biol Ther, 2017. **17**(12): p. 1511-1522.
222. Brown, D.M., A.T. Lampe, and A.M. Workman, *The Differentiation and Protective Function of Cytolytic CD4 T Cells in Influenza Infection.* Front Immunol, 2016. **7**: p. 93.
223. Fehniger, T.A. and M.A. Caligiuri, *Interleukin 15: biology and relevance to human disease.* Blood, 2001. **97**(1): p. 14-32.
224. Pilipow, K., et al., *IL15 and T-cell Stemness in T-cell-Based Cancer Immunotherapy.* Cancer Res, 2015. **75**(24): p. 5187-5193.
225. Lugli, E., et al., *Transient and persistent effects of IL-15 on lymphocyte homeostasis in nonhuman primates.* Blood, 2010. **116**(17): p. 3238-48.
226. Murugaiyan, G., et al., *IL-27 is a key regulator of IL-10 and IL-17 production by human CD4+ T cells.* J Immunol, 2009. **183**(4): p. 2435-43.
227. González-García, S., et al., *Notch1 and IL-7 Receptor Signalling in Early T-cell Development and Leukaemia*, in *Notch Regulation of the Immune System*. 2012. p. 47-73.
228. Iwasaki, Y., et al., *Interleukin-27 in T cell immunity.* Int J Mol Sci, 2015. **16**(2): p. 2851-63.
229. Yang, S., et al., *A cytokine cocktail directly modulates the phenotype of DC-enriched anti-tumor T cells to convey potent anti-tumor activities in a murine model.* Cancer Immunol Immunother, 2013. **62**(11): p. 1649-62.
230. Xu, X.J., et al., *Multiparameter comparative analysis reveals differential impacts of various cytokines on CART cell phenotype and function ex vivo and in vivo.* Oncotarget, 2016. **7**(50): p. 82354-82368.
231. Carrio, R., O.F. Bathe, and T.R. Malek, *Initial antigen encounter programs CD8+ T cells competent to develop into memory cells that are activated in an antigen-free, IL-7- and IL-15-rich environment.* J Immunol, 2004. **172**(12): p. 7315-23.
232. Xu, Y., et al., *Closely related T-memory stem cells correlate with in vivo expansion of CAR.CD19-T cells and are preserved by IL-7 and IL-15.* Blood, 2014. **123**(24): p. 3750-9.
233. Gong, W., et al., *Comparison of IL-2 vs IL-7/IL-15 for the generation of NY-ESO-1-specific T cells.* Cancer Immunol Immunother, 2019. **68**(7): p. 1195-1209.
234. Mestas, J. and C.C. Hughes, *Of mice and not men: differences between mouse and human immunology.* J Immunol, 2004. **172**(5): p. 2731-8.
235. Zhang, X., X. Lv, and Y. Song, *Short-term culture with IL-2 is beneficial for potent memory chimeric antigen receptor T cell production.* Biochem Biophys Res Commun, 2018. **495**(2): p. 1833-1838.
236. Huang, J., et al., *Survival, persistence, and progressive differentiation of adoptively transferred tumor-reactive T cells associated with tumor regression.* J Immunother, 2005. **28**(3): p. 258-67.

237. Robbins, P.F., et al., *Cutting edge: persistence of transferred lymphocyte clonotypes correlates with cancer regression in patients receiving cell transfer therapy.* J Immunol, 2004. **173**(12): p. 7125-30.
238. Louis, C.U., et al., *Antitumor activity and long-term fate of chimeric antigen receptor-positive T cells in patients with neuroblastoma.* Blood, 2011. **118**(23): p. 6050-6.
239. Tran, K.Q., et al., *Minimally cultured tumor-infiltrating lymphocytes display optimal characteristics for adoptive cell therapy.* J Immunother, 2008. **31**(8): p. 742-51.
240. Ghassemi, S., et al., *Reducing Ex Vivo Culture Improves the Antileukemic Activity of Chimeric Antigen Receptor (CAR) T Cells.* Cancer Immunol Res, 2018. **6**(9): p. 1100-1109.

10. INDEX of publications

- Martin Szyska, Stefanie Herda, Stefanie Althoff, Andreas Heimann, Josefine Russ, Daniele D'Abundo, Tra My Dang, Isabell Durieux, Bernd Dörken, Thomas Blankenstein and Il-Kang Na, *A Transgenic Dual-Luciferase Reporter Mouse for Longitudinal and Functional Monitoring of T Cells In Vivo,* Cancer Immunology Research 2017
- Stefanie Herda, Andreas Heimann, Benedikt Obermayer, Stefanie Althoff, Josefine Ruß, Lars Bullinger, Antonio Pezzutto, Thomas Blankenstein, Dieter Beule, Il-Kang Na, *Long-Term T Cell Expansion Results in Increased Numbers of Central Memory T Cells with Sustained Functional Properties for Adoptive T Cell Therapy*, Poster for 61nd ASH Annual Meeting & Exposition 2019
- Stefanie Herda, Andreas Heimann, Benedikt Obermayer, Stefanie Althoff, Josefine Ruß, Lars Bullinger, Antonio Pezzutto, Thomas Blankenstein, Dieter Beule, Il-Kang Na, *Extended expansion with IL-7/IL-15 increases T cell yield with preserved Tcm/Tscm properties for adoptive T cell therapy,* in submission

11. Curiculum Vitae

Aus datenschutzrechtlichen Gründen ist in der digitalen Version dieser Dissertation der CV nicht enthalten.

http://dx.doi.org/10.17169/refubium-29204

12. Appendix

Appendix Table 1 List of abbreviations

Abbreviation	Full name
ALL	Acute lymphoblastic leukemia
allo-HSCT	Allogeneic-Hematopoietic stem cell transplantation
APC	Antigen presenting cell
ATT	Adoptive T cell therapy
BLI	Bioluminescence imaging
BLITC	Bioluminescence imaging of T cells
CAR	Chimeric antigen receptor
cLN	Cervical lymph nodes
CRS	Cytokine release syndrome
CTLA-4	Cytotoxic T-lymphocyte-associated protein-4
DC	Dendritic cells
DLBCL	Diffuse large B-cell lymphoma
DLI	Donor lymphocyte infusion
dLN	Draining lymph nodes
DMEM	Dulbecco's Modified Eagle's Medium
EBI3	Epstein-Barr virus induced gene-3
ELISA	Enzyme-linked immunosorbent assay
FACS	Fluorescence-activated cell scanning
FasL	Fas-Ligand
FDA	Food and drug administration
FITC	Fluorescein isothiocyanate
GSK3β	Glycogen synthase kinase 3 beta
GvHD	Graft-versus-Host disease
GvT	Graft-versus-Tumor
HLA	Human leukocyte antigen
HPLC	High performance liquid chromatography
ICI	Immune checkpoint inhibitor
IEL	Intraepithelial lymphocytes
IFNγ	Interferon gamma
IL15Rα	Interleukin 15 receptor alpha
IL2/7/15/27	Interleukin 2/7/15/27
iLN	Inguinal lymph nodes
iv	Intravenously
LCMS	Liquid chromatography-mass spectrometry
LPAM-1	Lymphocyte Peyer's patch adhesion molecule
LPS	Lipopolysaccharides
MAdCAM-1	Mucosal addressin cell adhesion molecule-1
MAGE-A3	Melanoma-associated antigen-3

MART-1	Melanoma-associated antigen recognized by T cells
MH	Matahari
MHC (I&II)	Major histocompatibility complex
ML	Marilyn
mLN	Mesenteric lymph nodes
MS	Multiple sclerosis
NFAT-CBR	Nuclear factor of activated T cells-Click beetle luciferase
NK	Natural killer cells
NKT	Natural killer T cells
NY-ESO-1	New York esophageal squamous cell carcinoma-1
PBA	Phosphate buffered saline with BSA
PBS	Phosphate buffered saline
PCA	Principal component analysis
PCR	Polymerase chain reaction
PD-1	Programmed cell death protein-1
PDL-1	Programmed cell death ligand-1
PML	Progressive multifocal leukoencephalopathy
PSMA	Prostate-specific membrane antigen
REP	Rapid expansion protocol
Rluc	Renilla luciferase
ROI	Region of interest
RT-PCR	Reverse transcription PCR
STAT1/3	Signal transducer and activator of transcription-1/3
SV40	Simian virus 40
svFv	Single-chain variable fragment
TAA	Tumor associated antigen
TAg	Large tumor antigen
Tcm	Central memory T cells
TCM	T cell media
TCR	T cell receptor
TCR-I	TAg-specific T cell receptor
Tem	Effector memory T cells
TIL	Tumor infiltrating lymphocyte
TIR	T cell inhibiting receptor
TNFα	Tumor necrosis factor alpha
TPM	Transcripts per million
Tscm	Stem memory T cells
WT	Wildtype

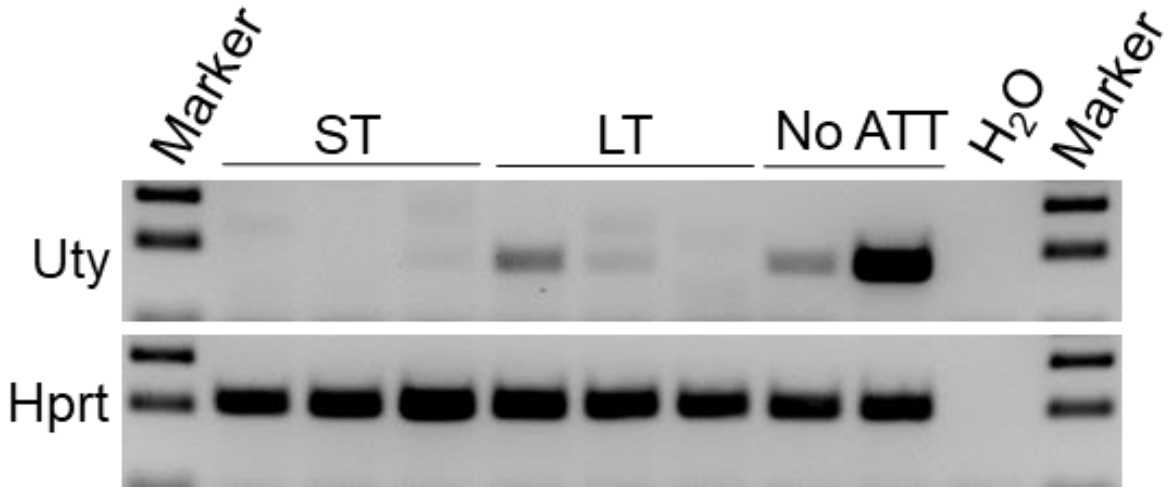

Appendix Figure 1 Antigen loss in outgrowing tumor. WR21 tumors in albino RagKO mice were treated with 1e6 ST or LT H-Y specific CD8 Tcm cells per mouse. *Uty* expression was determined via RT-PCR. *Hprt* was used as internal control.

Appendix Table 2 List of detected peptides via LCSM. K1-3 = purchased antibody; M1-3 = self-produced antibody

Protein IDs	Majority protein IDs	Protein names	Gene names	Fasta headers	Peptides	Peptides K1	Peptides K2	Peptides K3	Peptides M1	Peptides M2	Peptides M3	Sequence coverage [%]	Mol. weight [kDa]	Sequence length	Intensity	Intensity K1	Intensity K2	Intensity K3	Intensity M1	Intensity M2	Intensity M3
P20760;Q5M	P20760;Q5M	Ig gamma-2A	Igg-2a;IgG-2a	>sp|P20760|IGG2A	19	15	18	16	6	6	3	66,5	35,185	322	5,1748E+11	1,4551E+11	1,6397E+11	1,2441E+11	46473000000	30810000000	6316200000
P01836;P018	P01836	Ig kappa chain C region, A		>sp|P01836|KACA	8	5	7	4	1	1	0	55,7	11,732	106	1,2809E+11	28294000000	30251000000	69309000000	123780000	114170000	0
P46462	P46462	Transitional e	Vcp	>sp|P46462|TERA	17	4	5	3	13	11	11	31,6	89,348	806	18192000000	1781900000	493570000	980600000	7282800000	4705600000	2947100000
D3ZJW6	D3ZJW6		rCG_21066	>tr|D3ZJW6|D3ZJV	1	1	0	1	0	0	0	9,4	13,063	117	14743000000	7806700000	0	6936700000	0	0	0
P01805	P01805	Ig heavy chain V region IR2		>sp|P01805|HVR0	1	0	1	1	0	0	0	4,9	16,024	142	7729900000	0	4090100000	3639900000	0	0	0
CON__Q05B5	*CON__Q05B55*			*>Q05B55 TREMBL.*	*2*	*1*	*1*	*2*	*1*	*1*	*1*	*14,6*	*26,59*	*240*	*5366500000*	*49508000*	*203170000*	*389420000*	*1880500000*	*2120400000*	*723460000*
CON__P0426	*CON__P0426*	*Keratin, type*	*Krt1*	*>P04264 SWISS-PR*	*12*	*5*	*10*	*5*	*1*	*4*	*2*	*16,9*	*66,017*	*644*	*4433600000*	*316580000*	*1344300000*	*380630000*	*519790000*	*1057500000*	*814800000*
CON__P0076	*CON__P00761*			*>P00761 SWISS-PR*	*3*	*2*	*0*	*0*	*2*	*1*	*2*	*19,5*	*24,409*	*231*	*3004000000*	*2553500000*	*0*	*0*	*131420000*	*46864000*	*272210000*
CON__ENSEA	*CON__ENSEMBL:ENSBTAP00000024466;*			*>ENSEMBL:ENSBTA*	*5*	*1*	*3*	*1*	*1*	*0*	*0*	*25,9*	*43,9*	*401*	*2617600000*	*534990000*	*1763400000*	*281070000*	*38159000*	*0*	*0*
D4A659;A0A(	D4A659;A0A0G2JZQ5		Zfp532	>tr|D4A659|D4A6	1	1	0	0	0	0	0	1,3	144,87	1332	2525700000	2525700000	0	0	0	0	0
A0A0G2JYT9	A0A0G2JYT9			>tr|A0A0G2JYT9|A	1	0	0	0	0	0	1	2,1	87,352	780	1915200000	0	0	0	0	0	1915200000
CON__Q1RM	*CON__Q1RMN8*			*>Q1RMN8 TREMB*	*2*	*1*	*2*	*1*	*0*	*0*	*0*	*15*	*24,536*	*234*	*1642500000*	*263220000*	*1134400000*	*244890000*	*0*	*0*	*0*
CON__P3552	*CON__P35527*			*>P35527 SWISS-PR*	*5*	*0*	*3*	*2*	*2*	*1*	*1*	*14,4*	*62,129*	*623*	*576870000*	*0*	*164130000*	*40721000*	*118800000*	*203340000*	*49876000*
P20759;F1LN	P20759;F1LN	Ig gamma-1 c	Ighg	>sp|P20759|IGHG	4	4	4	4	2	1	0	16,9	35,945	326	503670000	157680000	200090000	125930000	19962000	0	0
CON__P3590	*CON__P35908*			*>P35908 SWISS-PR*	*6*	*2*	*4*	*3*	*1*	*2*	*1*	*9,5*	*65,865*	*645*	*490980000*	*5609400*	*57126000*	*27407000*	*154630000*	*207870000*	*38337000*
CON__ENSEA	*CON__ENSEMBL:ENSBTAP00000011227*			*>ENSEMBL:ENSBTA*	*1*	*0*	*0*	*0*	*1*	*1*	*1*	*15,3*	*14,629*	*137*	*485360000*	*0*	*0*	*0*	*215970000*	*166290000*	*103100000*
CON__P0276	*CON__P02769*			*>P02769 SWISS-PR*	*6*	*3*	*2*	*1*	*2*	*2*	*2*	*15,5*	*69,293*	*607*	*443190000*	*101790000*	*66792000*	*30116000*	*117980000*	*109450000*	*17069000*
M0RDZ5;M0I	M0RDZ5;M0RC	23;D3ZIL8;A0A0G2K3S3;M		>tr|M0RDZ5|M0RI	2	1	1	1	0	0	0	25,3	10,439	95	351060000	201880000	140900000	8284400	0	0	0
CON__Q95M	*CON__Q95M17*			*>Q95M17 SWISS-P*	*1*	*0*	*0*	*0*	*1*	*1*	*1*	*3,2*	*52,129*	*472*	*301220000*	*0*	*0*	*0*	*132150000*	*57618000*	*111450000*
CON__Q1RM	*CON__Q1RMK2*			*>Q1RMK2 TREMB*	*3*	*0*	*1*	*2*	*1*	*1*	*0*	*9,7*	*65,056*	*597*	*185350000*	*0*	*84248000*	*69036000*	*14863000*	*17207000*	*0*
P20761	P20761	Ig gamma-2B	Igh-1a	>sp|P20761|IGG2	1	0	0	0	1	1	1	6	36,497	333	156710000	0	0	0	31554000	74354000	50799000
D4A529	D4A529		She	>tr|D4A529|D4A5	1	1	0	0	0	0	0	3,4	50,95	469	139750000	139750000	0	0	0	0	0
F1M611	F1M611		RGD1560925	>tr|F1M611|F1M6	1	1	1	1	0	0	0	1,1	136,77	1230	130550000	25212000	29365000	75971000	0	0	0
CON__P0097	*CON__P00978*			*>P00978 SWISS-PR*	*1*	*0*	*0*	*0*	*1*	*1*	*1*	*3,4*	*39,234*	*352*	*120000000*	*0*	*0*	*0*	*49683000*	*46864000*	*23451000*
D3ZYD7	D3ZYD7		Ccdc88a	>tr|D3ZYD7|D3ZY	1	0	1	0	0	0	0	0,7	173,9	1512	114830000	0	114830000	0	0	0	0
CON__ENSEA	*CON__ENSEMBL:ENSBTAP00000014147*			*>ENSEMBL:ENSBTA*	*1*	*0*	*1*	*0*	*0*	*0*	*0*	*13,3*	*11,756*	*113*	*71276000*	*0*	*71276000*	*0*	*0*	*0*	*0*
A0A0G2K7R1	A0A0G2K7R1	Histone H2B	Hist3h2bb;Hi	>tr|A0A0G2K7R1|A	1	1	0	0	1	0	1	12,7	13,134	118	67441000	20144000	0	0	26275000	0	21022000
Q6UA27;F1M	Q6UA27;F1M	Receptor tyro	Erbb4	>tr|Q6UA27|Q6UA	1	1	0	0	0	0	0	2	81,285	732	66471000	66471000	0	0	0	0	0
P04642;B5DE	P04642;B5DE	L-lactate deh	Ldha	>sp|P04642|LDHA	1	1	1	0	0	1	1	4,5	36,45	332	60103000	34198000	11397000	0	0	3642000	10866000
A0A0H2UHM	A0A0H2UHM	Tubulin alpha	Tuba1c;Tuba	>tr|A0A0H2UHM7	2	2	0	0	0	0	0	7,8	49,806	448	54626000	54626000	0	0	0	0	0
CON__ENSEA	*CON__ENSEMBL:ENSBTAP00000032840*			*>ENSEMBL:ENSBTA*	*1*	*0*	*1*	*0*	*0*	*0*	*0*	*2,1*	*92,273*	*825*	*41770000*	*0*	*41770000*	*0*	*0*	*0*	*0*
CON__P0103	*CON__P01030;CON__ENSEMBL:ENSBTAI*			*>P01030 SWISS-PR*	*1*	*0*	*0*	*0*	*1*	*1*	*1*	*1*	*192,79*	*1741*	*39989000*	*0*	*0*	*0*	*21493000*	*11464000*	*7032800*
Q9JI24	Q9JI24	Interleukin-24	Il24	>sp|Q9JI24|IL24_R	1	0	0	0	1	0	0	10,4	21,096	183	38848000	0	0	0	38848000	0	0
P69897;Q6P9	P69897;Q6P9	Tubulin beta-	Tubb5;Tubb4	>sp|P69897|TBB5	1	1	0	0	0	0	0	4,1	49,67	444	29215000	29215000	0	0	0	0	0
CON__P1364	*CON__P13647;CON__P48668;CON__P04*			*>P13647 SWISS-PR*	*3*	*0*	*2*	*0*	*1*	*1*	*1*	*6,6*	*62,378*	*590*	*24981000*	*0*	*24981000*	*0*	*0*	*0*	*0*
F1LUS1;A0A0	F1LUS1;A0A0G2JZV7			>tr|F1LUS1|F1LUS	1	0	0	0	0	1	1	15,5	11,939	110	19248000	0	0	0	0	8553100	10695000
CON__H-INV.	*CON__H-INV: Keratin, type*		*Krt8*	*>H-INV:HIT000292*	*1*	*1*	*0*	*0*	*0*	*0*	*0*	*2,7*	*49,448*	*443*	*15993000*	*15993000*	*0*	*0*	*0*	*0*	*0*
CON__P1549	*CON__P15497*			*>P15497 SWISS-PR*	*1*	*0*	*1*	*0*	*0*	*0*	*0*	*5,3*	*30,276*	*265*	*14977000*	*0*	*14977000*	*0*	*0*	*0*	*0*
A0A0H2UHY(	A0A0H2UHY(	Valine--tRNA	Vars2	>tr|A0A0H2UHY0|	1	0	0	1	0	0	0	1,3	118,37	1060	8658600	0	0	8658600	0	0	0
Q05140-2;A0	Q05140-2;A0	Clathrin coat	Snap91	>sp|Q05140-2|AP	1	1	0	0	0	0	0	1,1	91,43	896	0	0	0	0	0	0	0
A0A0G2K578	A0A0G2K578			>tr|A0A0G2K578|A	1	1	0	0	0	0	0	1,4	54,661	493	0	0	0	0	0	0	0
G3V8T1;Q7TI	G3V8T1;Q7TI	M-phase pho	Mphosph8	>sp|G3V8T1|MPP8	1	1	0	0	0	0	0	0,8	96,782	851	0	0	0	0	0	0	0
CON__Q3MH	*CON__Q3MHN5*			*>Q3MHN5 SWISS-I*	*1*	*0*	*1*	*0*	*0*	*0*	*0*	*1,7*	*53,341*	*474*	*0*	*0*	*0*	*0*	*0*	*0*	*0*
D4A3X7	D4A3X7		Snx33	>tr|D4A3X7|D4A3	1	1	1	0	0	0	0	1,2	65,249	574	0	0	0	0	0	0	0
Q9R230;Q63	Q9R230;Q63	Tumor necros	Fas	>tr|Q9R230|Q9R2	1	0	1	0	0	0	0	4,7	16,645	150	0	0	0	0	0	0	0
Q6P9X2;P42(	Q6P9X2;P426	Signal peptid	Sec11a	>tr|Q6P9X2|Q6P9	1	1	1	1	0	0	0	3,9	20,626	179	0	0	0	0	0	0	0
Q9R0K8	Q9R0K8	Stanniocalcin	Stc2	>sp|Q9R0K8|STC2	1	1	1	0	0	0	0	2,7	32,621	296	0	0	0	0	0	0	0

Appendix Table 3 List of significantly up- or down-regulated genes between ST and LT Tcm transcriptomes (detailed analysis setup in section 4.1.7)

CD4_up	CD8_up	CD4_down	CD8_down	both_up	both_down
1190002N15Rik	1110034G24Rik	1700067K01Rik	1500009L16Rik	1700029J07Rik	2410004P03Rik
1700029J07Rik	1700001C19Rik	2410004P03Rik	1700012D01Rik	1810010D01Rik	2610524H06Rik
1810010D01Rik	1700025G04Rik	2610524H06Rik	1700066B19Rik	1810024B03Rik	2700081O15Rik
1810011H11Rik	1700029J07Rik	2700081O15Rik	1810010H24Rik	5730409E04Rik	4932438H23Rik
1810024B03Rik	1810010D01Rik	2900026A02Rik	1810037I17Rik	9330151L19Rik	A930011G23Rik
3830408C21Rik	1810024B03Rik	4932438H23Rik	1810055G02Rik	Abhd14b	Aacs
5730409E04Rik	2010005H15Rik	A930011G23Rik	2410004P03Rik	Acad10	Aars
9330151L19Rik	2010300C02Rik	Aacs	2610318N02Rik	Acad12	Abhd17c
Abca5	2210416O15Rik	Aars	2610524H06Rik	Acp5	Acat2
Abhd12b	2300009A05Rik	Abhd17c	2700049A03Rik	Acpp	Acsl3
Abhd14a	2510009E07Rik	Acat2	2700081O15Rik	Acvr2a	Adk
Abhd14b	2810021J22Rik	Acsl3	4930404N11Rik	Adat1	Aida
Abhd15	2810474O19Rik	Adamts3	4930503L19Rik	Adgre5	Ajuba
Ablim2	4430402I18Rik	Adk	4930579G24Rik	Adgrg3	Akap12
Acad10	4930548H24Rik	Adora2b	4932438H23Rik	Ago3	Aldh2
Acad12	4932438A13Rik	Agpat4	6430531B16Rik	AI429214	Ankrd9
Acp5	4932443I19Rik	Aida	6720489N17Rik	AI661453	Anp32b
Acpp	5730409E04Rik	Aif1	9530077C05Rik	Alox5	Apobec2
Acsf2	6430550D23Rik	Ajuba	A730008H23Rik	Amigo1	Armcx6
Acss2	9130008F23Rik	Ak6	A830010M20Rik	Ank	Atad5
Acvr2a	9330151L19Rik	Akap12	A930011G23Rik	Ank1	Atcay
Adat1	A430078G23Rik	Akr1c18	Aacs	Arap2	Atrnl1
Adgre5	A630001G21Rik	Alcam	Aars	Arl4c	Bard1
Adgrg3	AA467197	Aldh2	Abca3	AW554918	Bcat1
Agbl3	Abcb1a	Ankrd9	Abcg2	Axin2	Bcl3
Ago3	Abcb4	Anp32b	Abhd10	Bach1	Bcl9
Agpat2	Abcc10	Apcdd1	Abhd17c	BC049715	Bclaf3
AI429214	Abcc5	Apobec2	Abi2	Bend6	Bhlhb9
AI661453	Abcg1	Arhgef10	Ablim2	Btbd11	Blm
Aldh6a1	Abhd14b	Armcx1	Acadl	C030006K11Rik	Cand2
Alox5	Abi3	Armcx3	Acat2	C87436	Capn3
Amigo1	Abi3bp	Armcx6	Ace	Camk2n1	Casp3
Amz1	Ablim3	Atad5	Acsl3	Car12	Cbx2
Ank	Abr	Atcay	Actn2	Car7	Ccdc141
Ank1	Acad10	Atp9a	Ada	Ccdc136	Ccdc50
Aoc2	Acad12	Atrnl1	Adamtsl5	Ccdc38	Ccne1
Appl2	Acp5	B4galt5	Adap1	Cd200r4	Ccne2
Arap2	Acpp	Bambi	Adarb1	Cdh1	Ccrl2
Arhgap23	Acrbp	Bard1	Adcy6	Cdk14	Cd200
Arl4c	Acvr2a	Basp1	Adgrl1	Cdkn2b	Cd5
Asph	Adam1a	Batf	Adk	Chrnb2	Cd6
Atrn	Adam4	Bcas1	Afap1	Cipc	Cd81
AW554918	Adat1	Bcat1	Agbl2	Cnbd2	Cd86
Axin2	Adcy7	Bcl2a1b	Agfg2	Cnpy1	Cdc25a
B3galnt1	Adgre5	Bcl3	Ahcy	Cntnap1	Cdc42ep4
B4galnt4	Adgrg3	Bcl9	Aida	Col20a1	Cdc7
Bach1	Adgrg5	Bclaf3	Aig1	Coq8a	Cdca4
Bbof1	Adrb1	Bhlhb9	Aipl1	Crebl2	Cdh24
BC005561	AF529169	Bicdl1	Ajuba	Ctnnd2	Cdk2
BC048403	Agap1	Blm	Ak1	Cux1	Cdt1
BC049715	Ago3	Cand2	Ak2	Cxcr6	Cenpa
Bend6	Ago4	Capn3	Akap12	Cyb5d2	Cep72
Bpifb4	Ahnak	Car5b	Akip1	Cyb5rl	Cfap77
Btbd11	Ahrr	Card9	Alad	Cyp4f13	Chchd10
C030006K11Rik	AI429214	Casp3	Aldh1l2	CYTB	Chrm4
C2	AI661453	Casp8	Aldh2	Diaph2	Clic4
C530008M17Rik	Aifm2	Cbarp	Aldh5a1	Disc1	Cnn3
C87436	Akap8l	Cblb	Aldh7a1	Dlg5	Coro2a
Camk2n1	Akt1s1	Cbx2	Alg6	Dmrta1	Cox6b2
Car12	Alkbh4	Cbx6	Alg8	Dnah11	Csrp1
Car7	Alox5	Ccdc141	Alms1	Dnajc28	Ctla4

Ccdc136	Alox8	Ccdc28b	Alpk1	Dnhd1	Ctnnbip1
Ccdc38	Amigo1	Ccdc50	Alpk2	Doc2g	Cul7
Ccr2	Ank	Ccne1	Alyref	Dok7	Dbf4
Cd200r1	Ank1	Ccne2	Anapc15	Dse	Dbi
Cd200r4	Ankrd23	Ccrl2	Anapc5	Dtx4	Dclk2
Cd7	Anks3	Cd200	Angptl2	Dusp23	Dek
Cd93	Anks6	Cd248	Angptl6	Dusp3	Dhcr7
Cdh1	Antxr2	Cd24a	Ankle1	Dyrk4	Dhfr
Cdk14	Anxa1	Cd5	Ankrd13b	Echdc2	Dlg3
Cdk18	Ap3m2	Cd6	Ankrd29	Eml6	Dna2
Cdkn2b	Ap5z1	Cd81	Ankrd9	Enpp2	Dnajc9
Celf4	Aplp2	Cd86	Anln	Enpp4	Dnmt1
Chil5	Apobr	Cdc14a	Anp32b	Enpp5	Dnmt3a
Chrnb2	Apol10b	Cdc25a	Anp32e	Evi5	Dpysl2
Cipc	Apol7b	Cdc42ep4	Anxa2	Fam120c	Drp2
Cldn12	Apol7e	Cdc7	Ap1s3	Fam83h	Dsn1
Clec11a	Aqp9	Cdca4	Ap3s1	Fat3	Dusp4
Clstn1	Ar	Cdcp1	Apip	Fbxl2	E2f2
Cnbd2	Araf	Cdh24	Aplf	Fndc10	Eme1
Cnpy1	Arap2	Cdh5	Apln	Frg2f1	Enkd1
Cntnap1	Arhgap25	Cdk2	Apobec2	Frmd4a	Eno2
Col20a1	Arhgap4	Cdkn2d	Apold1	Fut8	Epb41l2
Comp	Arhgap45	Cdt1	Apon	Fv1	Ephx1
Coq8a	Arhgap6	Cenpa	Apoo	Gab3	Ercc6l
Crebl2	Arhgef18	Cep72	App	Gcm2	Ets2
Creg1	Arhgef4	Cfap77	Arf2	Gcnt2	Extl3
Ctnnd2	Arl4a	Chchd10	Arfgef3	Ggnbp1	Fabp5
Cux1	Arl4c	Chpt1	Arhgap11a	Gm1043	Fah
Cxcr6	Armc2	Chrm4	Arhgap19	Gm20219	Fanca
Cyb5d2	Armc7	Chst15	Arhgap29	Golm1	Fancb
Cyb5rl	Art2b	Chst2	Arhgap33	Gpr137b	Fancm
Cyp27b1	Asap2	Clec2i	Arhgef25	Gsto1	Fas
Cyp4f13	Asb13	Clic4	Arhgef39	Guca1b	Fbxo5
CYTB	Asb2	Cnn3	Arhgef40	Hcn3	Fdft1
Daglb	Ash1l	Coro2a	Arhgef9	Hcst	Fdps
Dapk2	Atf7	Cox6b2	Arl11	Herc1	Fen1
Dbndd2	Atg2a	Cradd	Arl6	Hist3h2a	Fkbp11
Dennd5a	Atn1	Csrp1	Arl6ip1	Hoxb4	Fut4
Dgkh	Atp6v0a1	Ctdspl	Arl6ip6	Hpgds	Fxn
Diaph2	Atp6v0c	Ctla4	Armcx6	Hsd17b11	Gamt
Disc1	Atp8a2	Ctnnbip1	Arntl2	Icam5	Gins1
Dlg5	AW146154	Cttn	Arrdc3	Ifitm10	Gins2
Dmrta1	AW549877	Cul7	Arsb	Impact	Gmnn
Dnah11	AW554918	Cxcl10	Arsg	Itga1	Gnb4
Dnajb4	Axin2	Dbf4	Art4	Kctd15	Gpld1
Dnajc28	B3galt2	Dbi	As3mt	Kirrel	Gstt1
Dnhd1	B3galt5	Dcakd	Asap3	Klra2	Gtf2ird1
Doc2g	B4galnt2	Dclk2	Asb16	Kmt2d	H2afv
Dok7	B4galt4	Ddx43	Asf1b	L1cam	Haus4
Dopey1	B4galt7	Dek	Asns	Large1	Hectd2
Dph1	B630019K06Rik	Dhcr7	Aspm	Lcn12	Hells
Dqx1	Bace2	Dhfr	Atad2	Ldlrad4	Helq
Dse	Bach1	Dlg3	Atad5	Leng8	Hif1a
Dtx4	Baiap3	Dna2	Atcay	Lilrb4a	Hist1h1a
Dusp23	Bbc3	Dnajc9	Atf3	Lpar6	Hist1h1d
Dusp3	Bbs9	Dnmt1	Atf4	Lpcat2	Hist1h2ab
Dyrk4	BC024978	Dnmt3a	Atf5	Lrrc24	Hist1h2ag
E2f5	BC025920	Dpysl2	Atl2	Man2a2	Hist1h2ak
Echdc2	BC029722	Drp2	Atp13a3	Maneal	Hist1h2bb
Eda2r	BC030336	Dsn1	Atp1b1	Mcoln2	Hist1h3e
Eml6	BC037034	Dtymk	Atp1b2	Mdn1	Hist1h3g
En2	BC049715	Dusp14	Atpif1	Meis3	Hist1h3i
Enpp2	Bckdhb	Dusp4	Atrnl1	Metap1d	Hist1h4b
Enpp4	Bcl2l11	E2f2	Aunip	Mettl27	Hist1h4f
Enpp5	Bcl6	Ebi3	Aurka	Mettl7a1	Hmgb2

Ermap	Bend6	Ecm1	Aurkb	Mthfsd	Hmgb3
Esrrb	Birc6	Efna4	Azin1	Myl10	Hmgcr
Evi5	Blcap	Egr3	Azin2	Myo18b	Hmgcs1
Exd1	Bmpr1a	Ehhadh	B230217C12Rik	Myo3b	Hmgn3
Fam120c	Borcs8	Eme1	B4galnt4	Naip2	Hmgn5
Fam129a	Brpf3	Enkd1	B4galt2	Naip5	Hnrnpd
Fam222a	Brwd1	Eno2	B9d1	Nbeal1	Hspa12a
Fam83h	Btbd11	Epb41l2	Baiap2	ND4	Hspa4l
Fat3	Btbd16	Epcam	Banf1	ND5	Idh2
Fbxl2	Btc	Ephb6	Bard1	Nedd4	Igf2bp3
Fgfbp3	Btg1	Ephx1	Batf3	Nedd4l	Igsf23
Fgfr1	Btg2	Ephx4	Baz2b	Nhsl2	Ildr1
Fndc10	C030006K11Rik	Ercc6l	Bbip1	Nipa1	Incenp
Frg2f1	C87436	Ets2	BC030867	Nlrp3	Insig1
Frmd4a	Cacng8	Extl3	BC035044	Nmnat3	Iqcb1
Fut8	Calcoco1	Fabp5	BC055324	Nov	Irf4
Fv1	Camk2b	Fah	Bcam	Nr1d1	Irf6
Gaa	Camk2n1	Fam111a	Bcar1	Nr1d2	Irf8
Gab3	Camkk1	Fam84a	Bcat1	Nr6a1	Itga5
Gadd45a	Camta2	Fanca	Bcl2l14	Nt5e	Itpka
Ganc	Car12	Fancb	Bcl3	Olfm1	Izumo1r
Gcm2	Car2	Fancm	Bcl6b	Olig3	Kdm8
Gcnt2	Car7	Fas	Bcl7c	Osgin1	Kifc1
Ggnbp1	Card6	Fbxo44	Bcl9	Ovgp1	Kifc5b
Glipr1	Cbx7	Fbxo5	Bclaf3	Padi2	Klc3
Gm1043	Ccdc136	Fdft1	Begain	Pard3	Klhl23
Gm14085	Ccdc17	Fdps	Bend4	Pclo	Kpna2
Gm20219	Ccdc171	Fen1	Bex1	Pctp	Lacc1
Gm29719	Ccdc38	Fgf2	Bex3	Pde1b	Lad1
Gm29721	Ccdc88c	Fgr	Bex6	Pdlim4	Lag3
Gm35315	Ccdc92	Fkbp11	Bhlhb9	Pfkfb2	Ldhb
Gm5481	Ccl5	Fut4	Birc5	Pgr	Lig1
Gm6109	Ccnd2	Fxn	Blm	Phf21b	Lin9
Gm6570	Ccpg1	Gamt	Blvrb	Pid1	Litaf
Gm7429	Ccr5	Gemin8	Bmp2k	Pigz	Lpcat1
Gm973	Cd200r4	Ggt7	Bmp7	Pkd1l3	Lrmp
Gm9958	Cd300lf	Ggta1	Bora	Plp1	Maged2
Golm1	Cd46	Gins1	Borcs7	Plxdc2	Magi3
Gpr137b	Cdc42bpb	Gins2	Brca1	Prkcz	Mansc1
Grasp	Cdc42ep3	Gm19463	Brca2	Prkd3	Map3k9
Gsto1	Cdh1	Gm20939	Bricd5	Prkx	Map7
Guca1b	Cdh13	Gm5148	Brip1	Prr5	Marcksl1
H2-Q10	Cdhr4	Gmnn	Brsk1	Prss16	Mast2
Hcn3	Cdk14	Gnb4	Bst1	Psd2	Mboat7
Hcst	Cdkl2	Gpc1	Btbd10	Ptger3	Mcm2
Heatr5a	Cdkn1b	Gpld1	Btbd8	Pvrig	Mcm3
Herc1	Cdkn2a	Gpr18	Bub1	Pyroxd2	Mcm4
Hist3h2a	Cdkn2b	Gpr83	Bub1b	Qtrt2	Mcm5
Hlcs	Cdnf	Gsn	Bub3	Rab20	Mcm6
Hoxb4	Cdo1	Gstt1	C1qtnf12	Rab27b	Mcm7
Hpgds	Cebpd	Gtf2ird1	C3	Rab6b	Mcu
Hsd17b11	Chd3	H2afv	C330027C09Rik	Reck	Mms22l
Icam5	Chic1	Haus4	Cacna1b	Rps19	Mnd1
Ids	Chpf2	Hectd2	Cacna1s	Rps21	Msh6
Ifitm1	Chrnb1	Hells	Cacnb3	Rps28	Msmo1
Ifitm10	Chrnb2	Helq	Calm2	Rrp12	Mtbp
Ifitm2	Chrne	Hemk1	Calm3	Rsad1	Mthfd2
Ifitm5	Cipc	Hif1a	Camk4	Rwdd3	Mvd
Igdcc4	Cited4	Hist1h1a	Cand2	Sarm1	Mxra8
Il1rl1	Clcf1	Hist1h1d	Capn3	Sbsn	Mybl2
Impact	Cldnd2	Hist1h2ab	Capn5	Sec31b	Mylpf
Ipo4	Clhc1	Hist1h2ag	Caprin2	Sept8	Nab2
Irgc1	Clic5	Hist1h2ai	Capsl	Setbp1	Nasp
Isca1	Cln3	Hist1h2ak	Car13	Sez6l2	Ncf1
Itga1	Clnk	Hist1h2bb	Carmil1	Sgsh	Ncs1

Itga2	Clock	Hist1h3e	Cars	Shpk	Ndc80
Jag2	Cmklr1	Hist1h3g	Casc1	Six3	Ndufa4
Kazald1	Cnbd2	Hist1h3i	Casp3	Slc25a27	Neu3
Kcna6	Cnpy1	Hist1h4b	Casp4	Slc25a53	Nmral1
Kcnh5	Cnr2	Hist1h4f	Casp7	Slc26a11	Noxred1
Kctd15	Cnrip1	Hivep3	Casp8ap2	Slc26a8	Nr4a1
Kif13a	Cntn1	Hmgb2	Cass4	Slc7a4	Nr4a3
Kif3a	Cntnap1	Hmgb3	Cbwd1	Sorbs3	Nrbp2
Kirrel	Col11a2	Hmgcr	Cbx2	Sorl1	Nrgn
Kit	Col20a1	Hmgcs1	Cbx3	Specc1	Nsd2
Klf12	Col6a2	Hmgn3	Cbx5	Speg	Nsdhl
Klra2	Col9a3	Hmgn5	Cby1	Stc2	Nsmce1
Klrb1c	Coq8a	Hnrnpd	Ccdc106	Ston2	Ntf5
Klrc1	Cpeb3	Hsf4	Ccdc114	Suco	Nup37
Kmt2d	Cpq	Hspa12a	Ccdc138	Sulf2	Nup62
L1cam	Crebl2	Hspa4l	Ccdc14	Sult4a1	Nyap1
Large1	Crebrf	Hspa5	Ccdc141	Susd4	Orc6
Lars2	Crisp1	Idh2	Ccdc18	Syt6	Pabpc1l
Lcn12	Csf2ra	Igf2bp3	Ccdc184	Taz	Pcgf5
Ldlrad4	Csnk1g1	Igsf23	Ccdc25	Tdrp	Pdcd1
Leng8	Ctnnd2	Ildr1	Ccdc34	Tfap2a	Pdgfb
Lilrb4a	Ctsf	Incenp	Ccdc40	Thbs1	Pdk3
Lpar6	Ctxn1	Insig1	Ccdc50	Tmem176a	Phactr2
Lpcat2	Cuedc1	Iqcb1	Ccdc77	Tmem176b	Phf19
Lrrc24	Cul9	Irf4	Ccdc85c	Tmem80	Pkib
Lrrc51	Cux1	Irf6	Ccdc88a	Tnfrsf22	Plcl1
Lrtm2	Cxcr3	Irf8	Ccdc90b	Tnfrsf23	Plek
Lyn	Cxcr6	Isg15	Ccna2	Tnfrsf26	Plekho1
Lyrm9	Cyb5d2	Itga5	Ccnb1	Tob1	Plk4
Man2a2	Cyb5rl	Itpka	Ccnb2	Tom1l1	Plpp1
Maneal	Cyp4f13	Izumo1r	Ccne1	Tpbgl	Plxnb1
Map4k5	Cyp4f16	Jaml	Ccne2	Tpgs2	Plxnd1
Matn1	CYTB	Kcnh2	Ccnf	Trim65	Pml
Mcoln2	D130040H23Rik	Kcnmb4	Ccnyl1	Trio	Pmvk
Mctp1	D3Ertd751e	Kdm2b	Ccp110	Trpc6	Pold3
Mdn1	D930048N14Rik	Kdm8	Ccr1	Ttll3	Pole2
Meis3	Dalrd3	Kifc1	Ccr4	Txnip	Ppp1r16b
Metap1d	Dand5	Kifc5b	Ccr8	Unc5a	Prim1
Mettl27	Dcdc2b	Klc3	Ccr9	Wdr95	Ptgfrn
Mettl7a1	Dcun1d4	Klhl23	Ccrl2	Yes1	Ptms
Mex3a	Ddx60	Kpna2	Ccsap	Zfp420	Ptpn6
Mfsd13b	Dennd1c	Lacc1	Cd101	Zfp493	Pxmp2
Mical2	Dennd2d	Lad1	Cd200	Zfp652	Rasgef1b
Mipol1	Dennd4c	Lag3	Cd22	Zfp661	Rbl1
Mocos	Dglucy	Lancl3	Cd4	Zfp950	Rcan3
Mrm1	Dhrs3	Lcat	Cd5	Zfp970	Rdh11
Mthfsd	Diaph2	Ldhb	Cd6	Zfp992	Recql4
Mturn	Dirc2	Lig1	Cd74	Zrsr1	Rfc2
Mtus1	Disc1	Lin9	Cd79b		Rfc3
Myl10	Dixdc1	Litaf	Cd80		Rfc5
Myo18b	Dlec1	Lmln	Cd81		Ripply3
Myo3b	Dlg5	Lpcat1	Cd83		Rnaseh2b
Myo6	Dlgap4	Lrmp	Cd86		Rnf168
N6amt1	Dmrta1	Lyl1	Cd9		Rnf208
Naip2	Dnah11	Maged2	Cdc20		Rpa2
Naip5	Dnajb14	Magi3	Cdc20b		Sass6
Nbeal1	Dnajb9	Mansc1	Cdc25a		Serinc5
Nckap1	Dnajc28	Map3k12	Cdc25b		Sfmbt2
ND2	Dnhd1	Map3k9	Cdc25c		Sh3rf1
ND4	Doc2g	Map7	Cdc27		Sik1
ND5	Dock4	Marcks	Cdc42ep4		Slamf1
Nedd4	Dok7	Marcksl1	Cdc45		Slc15a3
Nedd4l	Dpp7	Mast2	Cdc6		Slc1a4
Nhsl2	Dsc2	Mboat7	Cdc7		Slc25a13
Nid2	Dscam	Mcm2	Cdca2		Slc31a1

Nipa1	Dse	Mcm3	Cdca3		Slc43a1
Nipal1	Dsg2	Mcm4	Cdca4		Slc43a3
Nlrp3	Dsp	Mcm5	Cdca5		Slc4a11
Nmnat3	Dst	Mcm6	Cdca7		Slc9b2
Nmrk1	Dtx1	Mcm7	Cdca8		Slfn3
Nov	Dtx4	Mcu	Cdh17		Smc5
Npc1l1	Dus3l	Mcub	Cdh24		Spock2
Nr1d1	Dusp23	Mical1	Cdk1		Spred1
Nr1d2	Dusp28	Mmd	Cdk2		Sqle
Nr2c1	Dusp3	Mms22l	Cdk2ap1		St6galnac6
Nr6a1	Dyrk1b	Mnd1	Cdkn2c		Stag3
Nt5e	Dyrk2	Mov10	Cdkn3		Stk39
Nudt8	Dyrk4	Mrpl27	Cdr2		Ston1
Olfm1	Dzank1	Mrpl51	Cdt1		Susd1
Olfm2	Dzip1	Msh6	Ceacam1		Syce2
Olig3	Echdc2	Msl3l2	Cebpg		Syngr1
Osgin1	Eef2kmt	Msmo1	Celf5		Syngr3
Ovgp1	Efcab6	Mtbp	Celsr2		Tbc1d7
P4ha2	Egf	Mthfd2	Cenpa		Tesc
Padi2	Egfl8	Mvd	Cenpc1		Tet1
Pafah2	Eif2ak3	Mxd1	Cenpe		Tex15
Pard3	Elmsan1	Mxra8	Cenpf		Tg
Parvb	Elovl7	Myb	Cenph		Thoc6
Pcdh19	Eme2	Mybl2	Cenpi		Ticam2
Pcdhgb6	Eml5	Mylpf	Cenpk		Timeless
Pclo	Eml6	Nab2	Cenpl		Tlcd1
Pctp	Enpp2	Nasp	Cenpm		Tlcd2
Pde1b	Enpp4	Natd1	Cenpn		Tmcc2
Pde9a	Enpp5	Ncf1	Cenpo		Tmem108
Pdlim4	Entpd1	Ncs1	Cenpp		Tmem120b
Pfkfb2	Entpd6	Ndc80	Cenps		Tmem263
Pgr	Epx	Ndufa4	Cenpt		Tmem9
Phf21b	Ern1	Neu3	Cenpu		Tmie
Pid1	Erp27	Nfix	Cenpv		Tnfrsf4
Pigz	Errfi1	Nmnat1	Cenpw		Tox
Pkd1l3	Espnl	Nmral1	Cep128		Tpmt
Pla2g6	Etfbkmt	Noxred1	Cep55		Tpst1
Plaur	Evi2	Nr4a1	Cep57		Trib1
Plcb3	Evi5	Nr4a3	Cep57l1		Trp53inp2
Plcg2	Eya2	Nrbp2	Cep70		Tspan6
Plekha6	Ezh1	Nrgn	Cep72		Tuft1
Plp1	F2r	Nsd2	Cep76		Twsg1
Plxdc2	F2rl2	Nsdhl	Cep78		Tyms
Plxna4	F830016B08Rik	Nsmce1	Cep83		Ube2l6
Prkcz	Fam109a	Ntf5	Cep89		Utp14b
Prkd3	Fam117a	Nudt22	Cers6		Vav2
Prkx	Fam120b	Nup210l	Cetn4		Vps37d
Prpf40b	Fam120c	Nup37	Cfap77		Wdhd1
Prr5	Fam13b	Nup62	Chac1		Wdr76
Prss16	Fam160a2	Nyap1	Chaf1a		Wdr90
Psd2	Fam174b	Orc6	Chaf1b		Zfp101
Ptger3	Fam189b	Pabpc1l	Chchd10		Zfp365
Pts	Fam19a3	Panx1	Chd3os		Zfp367
Pvrig	Fam214a	Pcgf5	Chd5		Zfp870
Pyroxd2	Fam214b	Pdcd1	Chek1		Zgrf1
Qrfp	Fam217b	Pdgfb	Chml		
Qtrt2	Fam241b	Pdk3	Chrm4		
Rab20	Fam71b	Phactr2	Chtf18		
Rab25	Fam78b	Phf19	Cisd1		
Rab27b	Fam81a	Phlda1	Cit		
Rab6b	Fam83b	Phlpp2	Ckap2		
Raver2	Fam83h	Pik3c2b	Ckap2l		
Reck	Fasl	Pkib	Ckap5		
Rflnb	Fastkd1	Plagl1	Ckm		
Ric3	Fat3	Plcl1	Cks1b		

Riiad1	Fbxl12	Pld4	Cks1brt		
Rnf130	Fbxl2	Plek	Cks2		
Rnf217	Fbxl20	Plekho1	Clec12a		
Rpl12	Fbxl21	Plk4	Clic4		
Rpl22l1	Fbxo32	Plpp1	Clip2		
Rpl30	Fcrl6	Plxnb1	Clip3		
Rpl37a	Fgd3	Plxnd1	Clspn		
Rps19	Fgf13	Pml	Cmc2		
Rps21	Fgl2	Pmvk	Cmtm7		
Rps28	Flad1	Pold3	Cnksr3		
Rrm2b	Flcn	Pole2	Cnn3		
Rrp12	Flt3l	Pop1	Cnnm4		
Rsad1	Fn3k	Pou2f2	Cnot9		
Rubcnl	Fndc10	Ppp1r16b	Cntd1		
Runx2	Fndc4	Ppp1r26	Cntrob		
Rwdd3	Foxo1	Prim1	Col18a1		
Sarm1	Foxo3	Pros1	Commd1		
Sbsn	Foxq1	Prss2	Cops4		
Scn8a	Fpgt	Psd3	Copz2		
Sec31b	Frat1	Ptgfrn	Coq3		
Sept8	Frat2	Ptms	Coq7		
Setbp1	Frg2f1	Ptpn3	Coro2a		
Sez6l2	Frmd4a	Ptpn6	Cox6a2		
Sgms1	Fryl	Ptprf	Cox6b2		
Sgsh	Fsd1l	Pxmp2	Cox7a1		
Sh2d4b	Fut8	Pycard	Cpm		
Sh2d5	Fv1	Rasgef1a	Cpt1c		
Sh3bgrl2	Fxyd4	Rasgef1b	Crip1		
Shb	Gab3	Rbl1	Crip2		
Shpk	Gabbr1	Rcan3	Crocc		
Six3	Gabrb3	Rdh11	Crybg2		
Slc22a4	Galnt10	Recql4	Crybg3		
Slc25a27	Galnt11	Rest	Cryl1		
Slc25a37	Galnt14	Rfc2	Cryz		
Slc25a53	Gas7	Rfc3	Cse1l		
Slc26a11	Gbp8	Rfc5	Csrp1		
Slc26a8	Gcm2	Rgs10	Csrp2		
Slc39a11	Gcnt2	Ripply3	Cst6		
Slc7a4	Gda	Rnaseh2b	Ctc1		
Snx13	Gfra2	Rnf168	Cth		
Snx14	Ggnbp1	Rnf208	Ctla4		
Sorbs3	Gigyf1	Rpa2	Ctnnal1		
Sorl1	Gimap3	Rtl8a	Ctnnbip1		
Sp6	Gimap8	Sall2	Ctps		
Specc1	Gjd3	Sass6	Cul7		
Speg	Gldc	Serinc5	Cxcl16		
Spryd7	Gm1043	Sfmbt2	Cxcr5		
Srgap3	Gm10767	Sh3bp2	Cxxc5		
Sspo	Gm12216	Sh3gl3	Cyb561		
St6galnac5	Gm14305	Sh3rf1	Cyp11a1		
Stard9	Gm14325	Sik1	Cyp20a1		
Stc1	Gm14432	Six5	Cyp2u1		
Stc2	Gm20219	Slamf1	Cyp51		
Ston2	Gm35339	Slc12a4	Cystm1		
Suco	Gm4070	Slc15a3	D630045J12Rik		
Sulf2	Gm42372	Slc1a4	Dao		
Sult4a1	Gm45929	Slc25a13	Dapk1		
Suox	Gm527	Slc31a1	Dars2		
Susd4	Gm6904	Slc43a1	Dbf4		
Syt6	Gnao1	Slc43a3	Dbi		
Sytl3	Gngt2	Slc4a11	Dcbld1		
Taf4b	Gnptg	Slc9b2	Dck		
Tagap1	Gns	Slfn3	Dclk2		
Tarm1	Golga1	Smc5	Dclre1a		
Taz	Golm1	Smim3	Dctpp1		

Tdrd12	Gpc1	Smo	Dcxr		
Tdrd3	Gpn1	Snn	Ddah2		
Tdrp	Gpr132	Snx25	Ddias		
Tfap2a	Gpr137b	Spin4	Ddn		
Tgm7	Gpr15	Spock2	Ddr1		
Thbs1	Gpr45	Spred1	Ddx1		
Tiparp	Gpr87	Sqle	Ddx25		
Tle1	Gramd3	St3gal2	Ddx39		
Tle2	Gramd4	St6galnac6	Dek		
Tma16	Grcc10	Stag3	Depdc1a		
Tmcc1	Grid1	Stk39	Depdc1b		
Tmem116	Grina	Ston1	Dera		
Tmem121b	Grk3	Stx11	Dgat2		
Tmem176a	Grk4	Susd1	Dgkd		
Tmem176b	Grtp1	Sv2a	Dgkg		
Tmem55a	Gsap	Syce2	Dgkh		
Tmem80	Gsto1	Syngr1	Dhcr7		
Tmem86a	Gtf2ird2	Syngr3	Dhdh		
Tnfrsf22	Guca1b	Synj2	Dhfr		
Tnfrsf23	Gvin1	Syp	Dhrs13		
Tnfrsf26	Gzmc	Syt11	Diaph3		
Tob1	Gzmd	Tbc1d7	Dio2		
Tom1l1	Gzme	Tbc1d9	Dlc1		
Top1mt	Gzmf	Tert	Dlg3		
Tpbgl	Gzmg	Tesc	Dlgap5		
Tpgs2	Gzmm	Tet1	Dmc1		
Trim47	H2afj	Tex15	Dmpk		
Trim65	H2-Ke6	Tg	Dmwd		
Trio	Hal	Tgif2	Dna2		
Trpc6	Hbp1	Thoc6	Dnajb3		
Trpm1	Hcn3	Thoc7	Dnajb5		
Trpm2	Hcst	Ticam2	Dnajc10		
Trub1	Hdac11	Timeless	Dnajc6		
Tshz3	Hdhd5	Timp2	Dnajc9		
Tspan13	Heatr9	Tlcd1	Dnase2a		
Tspan4	Hectd4	Tlcd2	Dnm1		
Ttbk1	Herc1	Tmcc2	Dnmt1		
Ttc28	Herc2	Tmem108	Dnmt3a		
Ttc41	Hgfac	Tmem120b	Dnph1		
Ttll3	Hic1	Tmem173	Dntt		
Txnip	Hid1	Tmem263	Dpf1		
Ube2cbp	Hist3h2a	Tmem9	Dpy30		
Uggt2	Hivep2	Tmie	Dpysl2		
Ulk2	Hmbox1	Tmprss13	Dpysl5		
Unc5a	Hopx	Tnfrsf4	Drc3		
Usp3	Hoxa4	Tnks1bp1	Drp2		
Vps13b	Hoxb4	Tns1	Dscc1		
Wdr95	Hpgds	Tns4	Dsn1		
Xpc	Hsd17b11	Tox	Dtl		
Yes1	Icam5	Tpmt	Dusp10		
Zbtb10	Ice2	Tpst1	Dusp22		
Zfp202	Idnk	Tram2	Dusp4		
Zfp420	Ier5	Trib1	Dut		
Zfp493	Iffo1	Trp53inp2	Dynlt1a		
Zfp652	Ifitm10	Tspan6	Dynlt1f		
Zfp661	Ifngr2	Tssc4	Dyrk3		
Zfp950	Igf2bp2	Tuft1	E130308A19Rik		
Zfp970	Igfbp4	Twsg1	E2f1		
Zfp991	Igip	Txndc16	E2f2		
Zfp992	Ikbkb	Tyms	E2f7		
Zfr2	Ikbke	Ube2l6	E2f8		
Zrsr1	Ikzf3	Utp14b	Eaf2		
	Il10rb	Vav2	Ect2		
	Il11ra1	Vps37d	Efcab11		
	Il15	Wdhd1	Efcab12		

	Il18	Wdr76	Efemp2		
	Il18bp	Wdr90	Egfl7		
	Il18r1	Wsb2	Egr2		
	Il27ra	Zbtb3	Ehd1		
	Il4ra	Zbtb32	Ehd2		
	Il7	Zfp101	Ehd4		
	Impact	Zfp286	Eif2s2		
	Impg2	Zfp365	Eif4e		
	Ing4	Zfp367	Eif4ebp1		
	Inha	Zfp467	Elfn2		
	Iqcd	Zfp827	Eme1		
	Irak2	Zfp870	Emilin1		
	Irgq	Zgrf1	Enah		
	Irs1		Endou		
	Itga1		Eng		
	Itga10		Enkd1		
	Itga2b		Eno2		
	Itga9		Enpp1		
	Itgb1		Enthd1		
	Itgb3		Epb41l2		
	Itgb7		Epb41l5		
	Itpr2		Ephx1		
	Itpripl2		Epn2		
	Izumo4		Epor		
	Jade2		Erc1		
	Jak1		Ercc6l		
	Jmjd8		Erfe		
	Jmy		Eri1		
	Jun		Ermn		
	K230010J24Rik		Esco2		
	Kat2b		Esm1		
	Kat6b		Espl1		
	Kbtbd11		Espn		
	Kcnip3		Ets2		
	Kcnj8		Etv4		
	Kctd12		Etv5		
	Kctd15		Evc		
	Kctd21		Exo1		
	Kdm4d		Exosc8		
	Khdc1a		Ext1		
	Kifc2		Extl1		
	Kifc3		Extl3		
	Kirrel		Ezh2		
	Klf3		Faap24		
	Klf4		Fabp5		
	Klhl17		Fads2		
	Klhl21		Fah		
	Klhl24		Fam109b		
	Klhl30		Fam110a		
	Klhl4		Fam124b		
	Klra2		Fam129b		
	Klrc2		Fam162a		
	Klrg1		Fam171a1		
	Kmt2a		Fam171b		
	Kmt2c		Fam183b		
	Kmt2d		Fam212a		
	Kmt5b		Fam213a		
	Krt83		Fam216a		
	Krtcap3		Fam221a		
	Kyat1		Fam60a		
	L1cam		Fam72a		
	Lactbl1		Fam83d		
	Large1		Fam83g		
	Lats2		Fam92a		
	Lax1		Fanca		

	Lbp		Fancb		
	Lcn12		Fancd2		
	Lcn4		Fanci		
	Lcor		Fancl		
	Ldlrad1		Fancm		
	Ldlrad4		Farp1		
	Lef1		Fas		
	Leng8		Fbln1		
	Leng9		Fbxo2		
	Lgals3		Fbxo36		
	Lhfpl1		Fbxo48		
	Lhx6		Fbxo5		
	Lilrb4a		Fcmr		
	Limd1		Fdft1		
	Lime1		Fdps		
	Lmbr1		Fen1		
	Lmo7		Fes		
	LOC108167848		Fgd1		
	LOC108168164		Fgd6		
	Lpar5		Fgf11		
	Lpar6		Fgfr1op		
	Lpcat2		Fibcd1		
	Lpp		Fignl1		
	Lrch4		Fkbp11		
	Lrp11		Fkbp1a		
	Lrp6		Fkbp1b		
	Lrrc24		Fkbp2		
	Lrrc75b		Fkbp3		
	Lrrc8e		Fkbp5		
	Lrrk1		Flywch2		
	Lrrn4		Fmnl3		
	Lysmd1		Fnbp1l		
	Lyst		Fndc3b		
	Macf1		Foxk2		
	Maf		Foxm1		
	Mageh1		Foxp3		
	Maml3		Frem2		
	Man2a2		Frrs1l		
	Maneal		Fsbp		
	Map3k13		Fscn1		
	Map3k15		Fut10		
	Map3k2		Fut4		
	Map4k3		Fxn		
	Mapk1ip1		Fxyd7		
	Mapk8ip1		Fzr1		
	Mapkapk5		G2e3		
	Mapre3		Gab2		
	March3		Gabrr2		
	Masp2		Gadd45b		
	Mbnl1		Gale		
	Mbp		Galk1		
	Mccc1		Gamt		
	Mcl1		Gapdh		
	Mcoln2		Gapdh-ps15		
	Mcpt8		Gars		
	Mdm4		Gas2		
	Mdn1		Gas2l3		
	Mef2b		Gatad1		
	Megf11		Gatm		
	Mei1		Gbe1		
	Meis3		Gca		
	Metap1d		Gcat		
	Metrnl		Gclm		
	Mettl27		Gcnt4		
	Mettl7a1		Gem		

	Mfng		Gemin6		
	Mgat4a		Gen1		
	Mib2		Gins1		
	Mink1		Gins2		
	Mmaa		Gins3		
	Mn1		Gipc1		
	Mospd1		Gipc3		
	Mppe1		Gipr		
	Ms4a6c		Gk		
	Mthfsd		Gk5		
	Mtmr3		Glrp1		
	Mxd4		Gls2		
	Mycbp2		Gltp		
	Myl10		Gm12260		
	Mylip		Gm128		
	Myo18b		Gm1673		
	Myo1e		Gm2036		
	Myo3b		Gm20604		
	Myof		Gm21596		
	Myrip		Gm21948		
	N4bp1		Gm29719		
	N4bp2l1		Gm29721		
	Nabp1		Gm38426		
	Nacc2		Gm4969		
	Nagpa		Gm5134		
	Naip2		Gm996		
	Naip5		Gmds		
	Naip6		Gmnn		
	Naip7		Gnaz		
	Nat10		Gnb4		
	Nav2		Gng3		
	Nbeal1		Gnptab		
	Nbeal2		Golt1b		
	Ncald		Gorasp1		
	Ncam2		Gpat3		
	Nckap5l		Gpld1		
	Ncr1		Gpm6b		
	ND4		Gpr162		
	ND5		Gpr183		
	Ndnf		Gpr19		
	Ndor1		Gprc5b		
	Nedd4		Gprin3		
	Nedd4l		Gpsm2		
	Neu1		Gpt2		
	Nfe2l2		Gpx7		
	Nfkbiz		Grhl1		
	Nhsl2		Grin1		
	Nin		Gstp2		
	Nipa1		Gstt1		
	Nipal3		Gstt2		
	Nlrp1b		Gstt3		
	Nlrp3		Gtdc1		
	Nlrp6		Gtf2e2		
	Nmnat3		Gtf2ird1		
	Nod1		Gtf3c5		
	Notch2		Gtse1		
	Nov		Guca1a		
	Npff		Gucy1a3		
	Nptn		Gucy1b3		
	Nr1d1		Gzmk		
	Nr1d2		H1f0		
	Nr1h3		H2afv		
	Nr6a1		H2afx		
	Nt5e		H2afz		
	Ntng2		H2-Q2		

	Nudt6		Hacd1		
	Nupr1l		Hacl1		
	Obscn		Haspin		
	Obsl1		Hat1		
	Odaph		Haus1		
	Ogt		Haus4		
	Olfm1		Haus5		
	Olfml3		Haus6		
	Olig3		Haus7		
	Oplah		Hccs		
	Orai2		Hck		
	Ormdl3		Hdac6		
	Osbpl5		Hdgf		
	Osgin1		Hebp1		
	Otof		Hectd2		
	Otud3		Helb		
	Ovgp1		Hells		
	Padi2		Helq		
	Pak6		Hemgn		
	Pard3		Hesx1		
	Parm1		Hexim2		
	Parp12		Hhat		
	Parp8		Hic2		
	Pcdhga12		Hif1a		
	Pcdhgb4		Hint1		
	Pced1b		Hipk4		
	Pclo		Hirip3		
	Pcnx		Hist1h1a		
	Pctp		Hist1h1b		
	Pdcd4		Hist1h1c		
	Pde11a		Hist1h1d		
	Pde1b		Hist1h1e		
	Pde6g		Hist1h2ab		
	Pdgfa		Hist1h2ac		
	Pdk2		Hist1h2ae		
	Pdlim4		Hist1h2af		
	Pdlim5		Hist1h2ag		
	Pdrg1		Hist1h2ak		
	Pdzd2		Hist1h2an		
	Pdzd4		Hist1h2bb		
	Pdzrn3		Hist1h2be		
	Pea15a		Hist1h2bg		
	Peak1		Hist1h2bj		
	Peli3		Hist1h2bk		
	Per3		Hist1h2bl		
	Perm1		Hist1h2bn		
	Pfkfb2		Hist1h3a		
	Pgr		Hist1h3b		
	Phf1		Hist1h3c		
	Phf11d		Hist1h3d		
	Phf20l1		Hist1h3e		
	Phf21a		Hist1h3f		
	Phf21b		Hist1h3g		
	Phka1		Hist1h3h		
	Pid1		Hist1h3i		
	Pigz		Hist1h4b		
	Pik3ip1		Hist1h4c		
	Pik3r5		Hist1h4d		
	Pilrb1		Hist1h4f		
	Pilrb2		Hist1h4h		
	Pkd1		Hist1h4i		
	Pkd1l3		Hist1h4j		
	Pkd2		Hist1h4k		
	Plcb2		Hist2h2ac		
	Plcd1		Hist2h2bb		

	Plcl2		Hist2h3b		
	Plec		Hist2h4		
	Plekha1		Hjurp		
	Plekhm3		Hlf		
	Plekhn1		Hmbs		
	Plp1		Hmga1		
	Plpp6		Hmgb1		
	Plscr2		Hmgb2		
	Plscr4		Hmgb3		
	Plxdc2		Hmgcr		
	Pnisr		Hmgcs1		
	Pnpla6		Hmgn1		
	Pnpla7		Hmgn2		
	Pnpo		Hmgn3		
	Pnrc1		Hmgn5		
	Podnl1		Hmmr		
	Podxl		Hmox1		
	Pogk		Hmx2		
	Pot1b		Hnrnpa1		
	Pou4f1		Hnrnpa1l2-ps2		
	Pou6f1		Hnrnpa3		
	Ppargc1a		Hnrnpab		
	Ppargc1b		Hnrnpd		
	Ppm1h		Hook1		
	Ppm1j		Hormad2		
	Ppp1r13b		Hpdl		
	Ppp1r3d		Hpf1		
	Ppp1r3e		Hrc		
	Ppp2r2c		Hsd17b7		
	Ppp2r5a		Hsf2		
	Ppp3ca		Hsp90aa1		
	Prex1		Hspa12a		
	Prickle3		Hspa2		
	Prkce		Hspa4l		
	Prkcz		Hspb6		
	Prkd3		Htra2		
	Prkx		Hyls1		
	Prr22		Id3		
	Prr5		Idh2		
	Prrt1		Idi1		
	Prss16		Ifng		
	Prss30		Ift46		
	Psd2		Ift80		
	Psg17		Ift81		
	Ptgdr2		Igf1r		
	Ptger3		Igf2bp3		
	Ptges		Igsf23		
	Ptpn4		Iigp1		
	Ptpn9		Ikzf2		
	Ptpre		Il17rd		
	Ptprj		Il1rl1		
	Pvrig		Il1rl2		
	Pxdc1		Il24		
	Pyroxd2		Il2ra		
	Qpct		Il4i1		
	Qtrt1		Il6st		
	Qtrt2		Il7r		
	Rab20		Ildr1		
	Rab27b		Incenp		
	Rab36		Inpp5f		
	Rab6b		Insig1		
	Rabggta		Intu		
	Rap1gap2		Ipo5		
	Rasa3		Ipo7		
	Rasal3		Ipp		

	Rbm20		Iqcb1		
	Rdh5		Iqgap3		
	Reck		Irak1bp1		
	Ret		Irak3		
	Rfx3		Irf4		
	Rfx5		Irf6		
	Rgl2		Irf8		
	Rhbdl1		Islr		
	Rimkla		Itga5		
	Ripor2		Itgae		
	Ripor3		Itgb4		
	Rnf122		Itih5		
	Rnf144b		Itm2a		
	Rnf152		Itpa		
	Rnf166		Itpka		
	Rnf167		Izumo1r		
	Rora		Jag2		
	Rpgrip1		Jcad		
	Rps19		Jph4		
	Rps21		Jpt2		
	Rps24		Jup		
	Rps28		Katnal2		
	Rptor		Kbtbd6		
	Rrp12		Kcna2		
	Rsad1		Kcnb1		
	Rslcan18		Kcnc1		
	Rsrp1		Kcnh3		
	Rtl8c		Kdm8		
	Rtn4rl1		Kif11		
	Rundc3a		Kif14		
	Rundc3b		Kif15		
	Rwdd3		Kif18a		
	Rxra		Kif18b		
	Ryk		Kif20a		
	Ryr3		Kif20b		
	S100a4		Kif22		
	S100a6		Kif23		
	S1pr1		Kif24		
	S1pr4		Kif2c		
	Samd3		Kif4		
	Samd9l		Kif5a		
	Saraf		Kif7		
	Sarm1		Kifc1		
	Sat1		Kifc5b		
	Satb1		Klc3		
	Sbsn		Klf11		
	Scd4		Klf7		
	Scin		Klhdc9		
	Scml4		Klhl23		
	Sdc2		Klhl5		
	Sec31b		Klra1		
	Sema6d		Klra15		
	Sept8		Klra19		
	Sesn1		Klra22		
	Setbp1		Klra3		
	Sez6l2		Klra6		
	Sfxn3		Klrb1f		
	Sgk1		Klri2		
	Sgsh		Kmo		
	Sh2d1b1		Kmt5a		
	Sh2d3c		Knl1		
	Sh3bp5		Knstrn		
	Shank1		Kntc1		
	Shisa5		Kpna2		
	Shpk		Kpna3		

	Sike1		Kras		
	Sirt5		Kremen2		
	Six3		Ksr1		
	Slc11a2		Lacc1		
	Slc12a3		Lad1		
	Slc16a2		Lag3		
	Slc17a9		Lamc2		
	Slc24a3		Lancl2		
	Slc25a27		Larp1b		
	Slc25a45		Lca5		
	Slc25a53		Lclat1		
	Slc26a11		Ldhb		
	Slc26a6		Ldlr		
	Slc26a8		Leo1		
	Slc27a6		Lgalsl		
	Slc31a2		Lif		
	Slc35e4		Lig1		
	Slc36a1		Lin54		
	Slc38a7		Lin9		
	Slc3a1		Lipg		
	Slc41a2		Litaf		
	Slc46a1		Lmf2		
	Slc4a1ap		Lmna		
	Slc4a4		Lmnb1		
	Slc7a4		Lmnb2		
	Slc9a9		Lmtk3		
	Slco2a1		Lnpk		
	Slco3a1		Lonp1		
	Slfn1		Lonrf1		
	Slfn2		Lpar2		
	Smad3		Lpcat1		
	Smarca2		Lpin3		
	Smg1		Lrfn4		
	Smim10l1		Lrmp		
	Smim14		Lrp1		
	Smim27		Lrp8		
	Smim4		Lrr1		
	Smpd2		Lrrc27		
	Smpd5		Lrrc40		
	Smug1		Lrrc59		
	Sntb2		Lrrc71		
	Snx29		Lrrc75a		
	Snx32		Lrrc8b		
	Soat2		Lsm2		
	Socs3		Lsm3		
	Sorbs3		Lsm5		
	Sorcs2		Lsr		
	Sorl1		Lst1		
	Spag1		Ltk		
	Spata13		Ly6a		
	Specc1		Lyar		
	Speg		Lzts1		
	Spns1		Mad1l1		
	Spo11		Mad2l1		
	Spp1		Maged1		
	Sppl2b		Maged2		
	Spr		Magi3		
	Sptbn2		Man1c1		
	Spx		Manf		
	St3gal6		Mansc1		
	Stc2		Maoa		
	Stk32c		Map1a		
	Ston2		Map2		
	Styk1		Map2k6		
	Suco		Map3k19		

	Sulf2		Map3k6		
	Sult4a1		Map3k9		
	Susd4		Map7		
	Susd6		Map9		
	Syt3		Mapk11		
	Syt6		Mapk6		
	Tanc2		Mapkapk2		
	Tas1r3		Marcksl1		
	Taz		Mars		
	Tbc1d10c		Marveld2		
	Tbc1d12		Mast2		
	Tbc1d16		Mastl		
	Tbc1d17		Matk		
	Tbx6		Mb21d1		
	Tcf24		Mbd4		
	Tcn2		Mblac1		
	Tcp11l2		Mboat7		
	Tcta		Mcam		
	Tctex1d4		Mcm10		
	Tdrd7		Mcm2		
	Tdrp		Mcm3		
	Tecpr1		Mcm4		
	Teddm2		Mcm5		
	Tef		Mcm6		
	Tfap2a		Mcm7		
	Tgfa		Mcm8		
	Tgfb1i1		Mctp1		
	Tgm2		Mcu		
	Tgm4		Mdm1		
	Tha1		Me1		
	Thbs1		Me2		
	Thtpa		Med7		
	Tjp1		Megf9		
	Tk2		Melk		
	Tle4		Metrn		
	Tlr12		Mfhas1		
	Tlr4		Mfsd13a		
	Tm6sf2		Mfsd2a		
	Tmc6		Mical2		
	Tmem119		Micall2		
	Tmem140		Milr1		
	Tmem151a		Minpp1		
	Tmem154		Mipep		
	Tmem159		Mis12		
	Tmem176a		Mis18a		
	Tmem176b		Mis18bp1		
	Tmem198		Mki67		
	Tmem42		Mmp11		
	Tmem63a		Mmp14		
	Tmem63b		Mmp15		
	Tmem64		Mms22l		
	Tmem71		Mnd1		
	Tmem8		Mns1		
	Tmem80		Morn1		
	Tmod4		Mpeg1		
	Tmppe		Mpp2		
	Tmtc1		Mpp6		
	Tnfrsf11b		Mpzl1		
	Tnfrsf14		Mpzl2		
	Tnfrsf22		Mrnip		
	Tnfrsf23		Ms4a4a		
	Tnfrsf26		Ms4a4d		
	Tnfsf4		Msh5		
	Tnfsf8		Msh6		
	Tnrc6b		Msmo1		

	Tob1		Mst1		
	Tob2		Mt1		
	Tom1l1		Mt2		
	Tom1l2		Mt3		
	Tpbgl		Mtbp		
	Tpgs2		Mtfr2		
	Tppp3		Mthfd1l		
	Tpst2		Mthfd2		
	Trim16		Mtmr14		
	Trim2		Mutyh		
	Trim26		Mvd		
	Trim65		Mvk		
	Trio		Mxd3		
	Trip4		Mxra8		
	Trip6		Mybl1		
	Trp53inp1		Mybl2		
	Trpc6		Mycl		
	Tspan17		Myef2		
	Tssk4		Myh10		
	Ttc38		Myh7b		
	Ttll3		Myl6b		
	Tub		Mylpf		
	Tulp4		Myo1c		
	Tusc1		Myo1h		
	Tusc2		Myrf		
	Txk		Mzt1		
	Txnip		Naaladl1		
	Uba7		Nab2		
	Ubn2		Nampt		
	Ubr4		Nap1l1		
	Ubxn6		Naprt		
	Unc5a		Nasp		
	Upk1b		Ncapd2		
	Upp1		Ncapd3		
	Usp48		Ncapg		
	Ust		Ncapg2		
	Utrn		Ncaph		
	Uvssa		Ncaph2		
	Vav3		Ncf1		
	Vezf1		Ncf2		
	Vpreb1		Ncmap		
	Vps13c		Ncs1		
	Vps13d		Ndc1		
	Vsir		Ndc80		
	Wars2		Nde1		
	Wdr45		Ndrg2		
	Wdr49		Ndufa4		
	Wdr81		Neb		
	Wdr82		Nebl		
	Wdr95		Necab3		
	Wls		Nectin2		
	Xcl1		Nedd1		
	Xkr6		Neil3		
	Yes1		Nek2		
	Ypel3		Nek6		
	Zbtb20		Nelfcd		
	Zbtb37		Nelfe		
	Zbtb4		Nemp1		
	Zbtb40		Nenf		
	Zc2hc1a		Neu3		
	Zcchc18		Neurl1b		
	Zcchc7		Nfatc2ip		
	Zdhhc1		Nfya		
	Zdhhc17		Nfyb		
	Zfand3		Nid1		

	Zfc3h1		Nlgn2		
	Zfhx2		Nlrx1		
	Zfp12		Nmb		
	Zfp14		Nme4		
	Zfp169		Nme6		
	Zfp235		Nmral1		
	Zfp276		Noct		
	Zfp28		Notch3		
	Zfp287		Noxred1		
	Zfp316		Nphp1		
	Zfp317		Nphp3		
	Zfp369		Nphp4		
	Zfp36l2		Npl		
	Zfp420		Nqo1		
	Zfp456		Nr4a1		
	Zfp458		Nr4a2		
	Zfp493		Nr4a3		
	Zfp512		Nrap		
	Zfp523		Nrbp2		
	Zfp579		Nrg4		
	Zfp595		Nrgn		
	Zfp619		Nrm		
	Zfp623		Nrn1		
	Zfp652		Nrp1		
	Zfp658		Nsd2		
	Zfp661		Nsdhl		
	Zfp738		Nsl1		
	Zfp78		Nsmce1		
	Zfp85		Nt5dc2		
	Zfp871		Ntf5		
	Zfp874a		Ntn3		
	Zfp874b		Nucks1		
	Zfp882		Nuf2		
	Zfp932		Nup107		
	Zfp94		Nup133		
	Zfp945		Nup155		
	Zfp950		Nup160		
	Zfp970		Nup205		
	Zfp971		Nup37		
	Zfp992		Nup43		
	Zgpat		Nup54		
	Zhx2		Nup62		
	Zkscan14		Nup85		
	Zkscan7		Nup93		
	Zmat3		Nupr1		
	Znrf3		Nusap1		
	Zrsr1		Nxt1		
	Zscan26		Nyap1		
	Zswim8		Oaf		
	Zzef1		Odc1		
			Odf2		
			Odf2l		
			Oip5		
			Olfr56		
			Orc1		
			Orc6		
			Osbpl1a		
			Oscp1		
			P2rx3		
			Pabpc1l		
			Pacsin1		
			Pacsin3		
			Padi3		
			Pafah1b3		
			Pak4		

			Palb2		
			Palm		
			Paox		
			Papd7		
			Paqr3		
			Paqr4		
			Paqr8		
			Pard6g		
			Parpbp		
			Pask		
			Paxip1		
			Pbdc1		
			Pbk		
			Pbx4		
			Pcdhgc3		
			Pcdhgc4		
			Pcdhgc5		
			Pcgf5		
			Pck2		
			Pclaf		
			Pcna		
			Pcsk9		
			Pcx		
			Pdcd1		
			Pdgfb		
			Pdgfrb		
			Pdia5		
			Pdik1l		
			Pdk3		
			Pdp1		
			Pdss1		
			Pdzd11		
			Penk		
			Perp		
			Pfas		
			Pfn2		
			Pgm1		
			Pgp		
			Phactr2		
			Phf19		
			Phgdh		
			Phldb1		
			Phtf2		
			Pi4k2b		
			Pianp		
			Pidd1		
			Pif1		
			Pigf		
			Pik3cg		
			Pik3r6		
			Pim2		
			Pimreg		
			Pkib		
			Pkig		
			Pkmyt1		
			Pkn3		
			Pla2g12a		
			Plcb4		
			Plcl1		
			Plek		
			Plekhf2		
			Plekhg2		
			Plekhg4		
			Plekho1		
			Plk1		

			Plk2		
			Plk4		
			Plp2		
			Plpp1		
			Plxna3		
			Plxnb1		
			Plxnb2		
			Plxnd1		
			Pmel		
			Pmf1		
			Pml		
			Pmvk		
			Pnck		
			Pnp2		
			Poc1a		
			Poc1b		
			Pola1		
			Pola2		
			Pold1		
			Pold3		
			Pole		
			Pole2		
			Polh		
			Polq		
			Pomgnt2		
			Pomt1		
			Pop4		
			Pou2f1		
			Ppa1		
			Ppat		
			Ppfibp1		
			Pphln1		
			Ppih		
			Ppil1		
			Ppp1r16b		
			Ppp1r35		
			Ppp2r3a		
			Pradc1		
			Prc1		
			Prcp		
			Prdx4		
			Prelid3a		
			Prelid3b		
			Prickle1		
			Prim1		
			Prim2		
			Primpol		
			Prkch		
			Prpf38a		
			Prps1		
			Prr11		
			Prss41		
			Prx		
			Psat1		
			Psip1		
			Psmc3ip		
			Psmd1		
			Psmg1		
			Pspc1		
			Pstpip2		
			Pter		
			Ptgfrn		
			Ptgir		
			Ptgr1		
			Ptma		

			Ptms		
			Ptpn6		
			Ptprk		
			Ptprs		
			Pxmp2		
			Pycr1		
			Rab26		
			Rab27a		
			Rab33a		
			Rab34		
			Rab39b		
			Racgap1		
			Rad18		
			Rad21		
			Rad51		
			Rad51ap1		
			Rad51b		
			Rad51c		
			Rad54b		
			Rad54l		
			Ralb		
			Raly		
			Ran		
			Ranbp1		
			Rangap1		
			Rapgef3		
			Rapgef5		
			Rarg		
			Rasd1		
			Rasgef1b		
			Rasl2-9		
			Rassf3		
			Rassf4		
			Rb1		
			Rbbp4		
			Rbbp7		
			Rbbp8		
			Rbl1		
			Rbm3		
			Rbm44		
			Rbmx2		
			Rbmxl1		
			Rbpms		
			Rcan3		
			Rcc1		
			Rcn3		
			Rcor2		
			Rdh11		
			Rdm1		
			Recql4		
			Reep1		
			Reep2		
			Reep4		
			Rell1		
			Renbp		
			Rfc1		
			Rfc2		
			Rfc3		
			Rfc4		
			Rfc5		
			Rfwd3		
			Rfx2		
			Rfx4		
			Rgcc		
			Rgl1		

			Rgs8		
			Rhpn2		
			Ribc1		
			Rims3		
			Riox2		
			Ripk3		
			Ripply3		
			Rmi2		
			Rnaseh2b		
			Rnd1		
			Rnd2		
			Rnf157		
			Rnf168		
			Rnf19b		
			Rnf208		
			Rnf216		
			Rnf26		
			Rogdi		
			Ropn1l		
			Rpa2		
			Rpa3		
			Rpp30		
			Rps6ka5		
			Rps6ka6		
			Rrm1		
			Rrm2		
			Rsph1		
			Rtkn		
			Rtkn2		
			Rtn3		
			Rubcnl		
			Runx1		
			Saal1		
			Sae1		
			Samd11		
			Sap30		
			Sapcd1		
			Sapcd2		
			Sass6		
			Scamp1		
			Scarb1		
			Sccpdh		
			Scd1		
			Scpep1		
			Sdf2l1		
			Sectm1a		
			Selenbp1		
			Selenoh		
			Sema4c		
			Sema4g		
			Sema6b		
			Sema7a		
			Sephs1		
			Sept10		
			Serinc3		
			Serinc5		
			Serpinb1b		
			Serpinb6b		
			Serpinb9		
			Serpinf1		
			Sestd1		
			Sfmbt2		
			Sgo1		
			Sgo2a		
			Sh2b2		

			Sh3bp4		
			Sh3rf1		
			Sh3tc1		
			Shcbp1		
			Shmt1		
			Shmt2		
			Shroom3		
			Siah1b		
			Siah2		
			Sik1		
			Siva1		
			Ska1		
			Ska2		
			Ska3		
			Skp2		
			Slamf1		
			Slbp		
			Slc12a8		
			Slc15a1		
			Slc15a3		
			Slc16a1		
			Slc16a10		
			Slc16a11		
			Slc1a4		
			Slc25a1		
			Slc25a10		
			Slc25a13		
			Slc25a25		
			Slc25a40		
			Slc25a43		
			Slc26a10		
			Slc29a1		
			Slc31a1		
			Slc35d3		
			Slc3a2		
			Slc43a1		
			Slc43a3		
			Slc4a11		
			Slc4a7		
			Slc4a8		
			Slc6a13		
			Slc6a9		
			Slc7a1		
			Slc7a3		
			Slc7a5		
			Slc9a5		
			Slc9b2		
			Slfn3		
			Smc1a		
			Smc2		
			Smc3		
			Smc4		
			Smc5		
			Smc6		
			Smchd1		
			Smox		
			Smpdl3b		
			Sms		
			Sms-ps		
			Smtn		
			Snrnp25		
			Snrnp35		
			Snrpd1		
			Snx9		
			Soga1		

			Sowahc		
			Sox12		
			Sox4		
			Spaca1		
			Spag4		
			Spag5		
			Spata24		
			Spats1		
			Spats2l		
			Spc24		
			Spc25		
			Spdl1		
			Spidr		
			Spire1		
			Spock2		
			Spred1		
			Spry1		
			Spry4		
			Sptb		
			Sqle		
			Srl		
			Srsf12		
			Srsf4		
			Ssbp3		
			Ssx2ip		
			St6gal1		
			St6galnac3		
			St6galnac6		
			Stag3		
			Stard10		
			Stard13		
			Stard3nl		
			Stard4		
			Stat1		
			Stbd1		
			Stil		
			Stk38l		
			Stk39		
			Stmn1		
			Stom		
			Ston1		
			Stxbp1		
			Supt16		
			Susd1		
			Suv39h1		
			Suv39h2		
			Suz12		
			Sv2c		
			Syce2		
			Syde1		
			Syngap1		
			Syngr1		
			Syngr3		
			Syngr4		
			Synpo		
			Sypl		
			Sytl3		
			Tacc2		
			Tacc3		
			Taf5		
			Taf6		
			Tank		
			Tarsl2		
			Tbc1d1		
			Tbc1d2		

			Tbc1d24		
			Tbc1d31		
			Tbc1d7		
			Tbc1d8		
			Tcam1		
			Tceal9		
			Tcf19		
			Tcp1		
			Tctex1d2		
			Tdg		
			Tdg-ps		
			Tdp1		
			Tdp2		
			Tedc1		
			Tedc2		
			Terf1		
			Tesc		
			Tet1		
			Tex13d		
			Tex15		
			Tex30		
			Tfdp1		
			Tfr2		
			Tfrc		
			Tg		
			Tgfb1		
			Tgm1		
			Themis2		
			Thnsl2		
			Thoc6		
			Thop1		
			Thrb		
			Tiam1		
			Ticam2		
			Ticrr		
			Tigit		
			Timeless		
			Timm17b		
			Tinf2		
			Tipin		
			Tjp3		
			Tk1		
			Tkt		
			Tlcd1		
			Tlcd2		
			Tln2		
			Tmcc2		
			Tmed1		
			Tmem106a		
			Tmem107		
			Tmem108		
			Tmem120b		
			Tmem121		
			Tmem136		
			Tmem144		
			Tmem2		
			Tmem206		
			Tmem237		
			Tmem243		
			Tmem25		
			Tmem263		
			Tmem40		
			Tmem59l		
			Tmem67		
			Tmem9		

			Tmem97		
			Tmie		
			Tmpo		
			Tnfaip8l1		
			Tnfrsf21		
			Tnfrsf4		
			Tnfrsf8		
			Tnip3		
			Tnni3		
			Tnnt1		
			Tnp2		
			Tns3		
			Top2a		
			Topbp1		
			Tox		
			Tpm2		
			Tpm4		
			Tpmt		
			Tpst1		
			Tpx2		
			Traf4		
			Traip		
			Trat1		
			Trdmt1		
			Trib1		
			Trib3		
			Trim45		
			Trim6		
			Trim7		
			Trip13		
			Troap		
			Trp53i11		
			Trp53inp2		
			Trp73		
			Trpm4		
			Trpv4		
			Tsga10		
			Tspan2		
			Tspan3		
			Tspan6		
			Tspoap1		
			Ttc16		
			Ttc26		
			Ttf2		
			Ttk		
			Tuba1a		
			Tuba1b		
			Tuba1c		
			Tuba4a		
			Tuba8		
			Tubb2a		
			Tubb2b		
			Tubb4b		
			Tubb5		
			Tube1		
			Tubg1		
			Tubgcp2		
			Tuft1		
			Twsg1		
			Txn1		
			Txnl1		
			Tyms		
			Uap1		
			Ube2c		
			Ube2e3		

			Ube2l6		
			Ube2s		
			Ube2t		
			Ubtd2		
			Uchl1		
			Uchl5		
			Uevld		
			Ugp2		
			Ugt1a7c		
			Uhrf1		
			Umps		
			Unc93b1		
			Ung		
			Usp1		
			Usp18		
			Usp2		
			Usp44		
			Usp6nl		
			Utf1		
			Utp14b		
			Uxs1		
			Vat1		
			Vav2		
			Vcl		
			Vdac1		
			Vps37d		
			Vrk1		
			Wdfy4		
			Wdhd1		
			Wdpcp		
			Wdr31		
			Wdr35		
			Wdr62		
			Wdr76		
			Wdr90		
			Wee1		
			Wfikkn2		
			Wipi1		
			Wnt10b		
			Wwc1		
			Wwc2		
			Xbp1		
			Xk		
			Xkr5		
			Xpnpep1		
			Xpnpep2		
			Xpo1		
			Xrcc2		
			Xrcc3		
			Yars		
			Ybx1		
			Ybx2		
			Ybx3		
			Yif1b		
			Ywhae		
			Ywhah		
			Zbed3		
			Zbtb12		
			Zcchc3		
			Zeb2		
			Zfand4		
			Zfp101		
			Zfp280b		
			Zfp318		
			Zfp365		

			Zfp367		
			Zfp382		
			Zfp41		
			Zfp473		
			Zfp52		
			Zfp575		
			Zfp599		
			Zfp608		
			Zfp870		
			Zfp92		
			Zfp948		
			Zgrf1		
			Zranb3		
			Zwilch		